Industrial Chemistry & Materials

ROYAL SOCIETY OF CHEMISTRY

REVIEW

View Article Online
View Journal | View Issue

Cite this: *Ind. Chem. Mater.*, 2024, **2**, 226

Recent progress and challenges in silicon-based anode materials for lithium-ion batteries

Gazi Farhan Ishraque Toki,[a] M. Khalid Hossain,[b] Waheed Ur Rehman,[a] Rana Zafar Abbas Manj,[a] Li Wang*[a] and Jianping Yang *[a]

Anode materials for Li-ion batteries (LIBs) utilized in electric vehicles, portable electronics, and other devices are mainly graphite (Gr) and its derivatives. However, the limited energy density of Gr-based anodes promotes the exploration of alternative anode materials such as silicon (Si)-based materials because of their abundance in nature and low cost. Specifically, Si can store 10 times more energy than Gr and also has the potential to enhance the energy density of LIBs. Despite the many advantages of Si-based anodes, such as high theoretical capacity and low price, their widespread use is hindered by two major issues: charge-induced volume expansion and unreliable solid electrolyte interphase (SEI) propagation. In this detailed review, we highlight the key issues, current advances, and prospects in the rational design of Si-based electrodes for practical applications. We first explain the fundamental electrochemistry of Si and the importance of Si-based anodes in LIBs. The excessive volume increase, relatively low charge efficiency, and inadequate areal capacity of Si-based anodes are discussed to identify the barriers in enhancing their performance in LIBs. Subsequently, the use of binders (*e.g.*, linear polymer binders, branched polymer binders, cross-linked polymer binders, and conjugated conductive polymer binders), material-based anode composites (such as carbon and its derivatives, metal oxides, and MXenes), and liquid electrolyte construction techniques are highlighted to overcome the identified barriers. Further, tailoring Si-based materials and reshaping their surfaces and interfaces, including improving binders and electrolytes, are shown to be viable approaches to address their drawbacks, such as volume expansion, low charge efficiency, and poor areal capacity. Finally, we highlight that research and development on Si-based anodes are indispensable for their use in commercial applications.

Keywords: Lithium-ion battery; Silicon-based anode; Volume expansion; Solid electrolyte interphase propagation; Binders; Composite anode materials.

Received 24th October 2023,
Accepted 27th December 2023

DOI: 10.1039/d3im00115f

rsc.li/icm

1 Introduction

Traditionally, the energy industry worldwide depends on power from the utilization of fossil fuels, which releases a significant amount of carbon dioxide (CO_2) gas and exacerbates the greenhouse effect. Moreover, this energy source is a limited resource that is predicted to be exhausted in the next century as a result of its present excessive dependence. Thus, it is critical to find alternative renewable, eco-friendly forms of energy to power the global enterprises of the future.[1] Furthermore, energy storage technologies that are both efficient and cost-effective are urgently needed given that many types of clean energy (such as wind and solar) are

[a] *State Key Laboratory for Modification of Chemical Fibers and Polymer Materials, College of Materials Science and Engineering, Donghua University, Shanghai, China. E-mail: lw66@dhu.edu.cn, jianpingyang@dhu.edu.cn*
[b] *Institute of Electronics, Atomic Energy Research Establishment, Bangladesh Atomic Energy Commission, Dhaka 1349, Bangladesh*

Gazi Farhan Ishraque Toki

Gazi Farhan Ishraque Toki is a Master's candidate at the College of Materials Science and Engineering, Donghua University, Shanghai, China. He received his Bachelor of Science (B.Sc.) Degree (2019) from the National Institute of Textile Engineering and Research (NITER), which is a constituted institute of the University of Dhaka, Bangladesh. He is presently engaged in research on silicon-based anode materials for lithium-ion batteries under the supervision of Professor Jianping Yang at Donghua University, Shanghai, China.

primarily intermittent.[2] In recent years, the need for high-capacity lithium (Li) batteries has rapidly increased, making their many features and applications common knowledge. Similar to other areas of science and technology, the need for high-tech lightweight batteries was not always the focus. Initially, the study on batteries was insufficient; however, it has recently witnessed a surge in interest because of the growing need for various portable electric devices and electric vehicles. Thus, the battery storage demand is now dominated by refillable lithium-ion batteries (LIBs), which are utilized to power electronic items (cell phones, computers, *etc.*), electric cars, and hybrid electric cars.[3–6]

With the increasing demand for energy storage in electric vehicles, the scientific community expects developing countries to enact legislation prohibiting the manufacture of conventional vehicles after 2050, similar to China, Germany, France, and England.[7,8] Investigations on the energy trends suggest that by 2025, electric vehicles will make up 10% of the growing international automotive market.[9,10] In this case, despite the fascinating expansion of battery technology, its underlying purpose has remained unchanged, *i.e.*, to reduce the shape and size, enhance the cycling lifetime, preserve the reliability, and decrease the cost of the device. Presently, there has been an increase in the use of LIBs with exceptionally high power and energy density because existing LIB techniques cannot keep up with the rapidly increasing needs of electric cars and hybrid electric cars.[11] Graphite carbon (C) is utilized as the anode in standard LIBs, while lithium iron phosphate or lithium oxide (such as $LiCoO_2$) is utilized as the cathode. However, despite the prominent role of graphite (Gr) in existing LIBs, its low theoretical gravimetric capacity of 372 mA h g^{-1} and security concerns make it unsuitable as a future anode material.[12–14] Accordingly, because of the limited lithiation prospects (0.4 V *vs.* Li/Li^+), environmentally friendly nature and higher theoretical specific capacity of 4200 mA h g^{-1} (more than ten-times that of traditional Gr anodes) of silicon (Si), it has emerged as the most capable anode candidate in upcoming LIBs.[15,16] Additionally, tin (Sn), sulfur (S), and lithium–sulfur (Li–S) are also utilized as anode materials in LIBs.[17,18] Among them, Si is the second most abundant element on Earth and its industrialization has advanced greatly over the past few years. However, the excessive volume expansion (up to 300–400%), non-stop formation of a solid electrolyte interface (SEI), relatively low electrical conductivity (10^{-5} to 10^{-3} S cm^{-1}), and poor Li-ion diffusivity (10^{-14} to 10^{-13} cm^2 s^{-1}) of Si materials are major obstacles in expanding their application as viable electrodes.[19,20] Furthermore, these incidents result in problems such as Si pulverization, architecture deterioration, excessive thickness swelling, limited areal capacity, and loss of interaction with the current collectors.[21] Thus, to overcome these obstacles and attain a superior energy density of around 300 W h kg^{-1} together with a driving range per charge of about 500 km, Tesla's Model 3 employs a Gr composite anode composed of 5–10 wt% Si.[22]

Numerous methods have been introduced to deal with the above-mentioned obstacles in recent years and enhance the performance of Si-based anodes in LIBs.[23–27] Several studies focused on improving the electrical conductivity of Si-based anodes by employing carbon sources,[28–41] Sn,[42] Al,[43] Si_3C,[44] Cu_3S,[45] *etc.* over the last few years. Similarly, several structural modifications and the incorporation of other materials such as C, copper (Cu), nitrogen (N), nickel (Ni), graphene, and rGO were adopted to reduce the volume expansion in Si-based anodes impressively,[46–60] enhancing their initial coulombic efficiency (ICE)[45,56,61–66] and cyclic stability[61,65,67–80] to achieve sustainable and affordable Si-based anodes in LIBs. However, all these approaches cannot mitigate the Si pulverization, architecture deterioration, excessive thickness swelling, limited areal capacity, and loss of interaction with the current collector. Thus, it is necessary to make a breakthrough to mitigate the various obstacles encountered in Si-based anodes in LIBs.

In recent years, several reviews have been presented on Si-based anodes focusing on particular features such as their characterization methods,[81] electrochemical mechanisms,[82] eco-friendly reduction,[83] sustainability,[84] anode interactions,[85] surface and interface engineering,[86] and commercial

Li Wang

Li Wang is an Associated Professor in the College of Materials Science and Engineering at Donghua University (China). She received her PhD at the University of Wollongong in 2018, and then worked as a Research Fellow and Postdoctoral Researcher in Monash University and Ludwig-Maximilians-Universität München. Her research interests include the design of two-dimensional functional materials towards energy and environmental applications.

Jianping Yang

Jianping Yang is a Professor and Associate Dean in the College of Materials Science and Engineering at Donghua University (China). He received his PhD in Inorganic Chemistry from Fudan University in 2013, and then worked as a Postdoctoral and Visiting Research Fellow at Tongji University, University of Wollongong and Monash University. His research interests include interfacial design of functional materials for environmental electrocatalysis and sustainable energy systems.

prospects,[87] together with other aspects.[88–90] Alternatively, herein we provide a thorough overview of the recent progress, challenges, and prospects of Si-based LIBs to enhance their outcomes in related studies. Initially, the fundamental electrochemical importance of Si and its application in Si-based anodes in LIBs are discussed. Subsequently, with a foundation in intrinsic electrochemistry, a description of the major difficulties encountered in Si-based anodes is presented, including their significant volume expansion, low electrical conductivity, inconsistent kinetic reactions, and relatively low ICE. After that, according to the critical concerns and challenges regarding the effectiveness of current strategies, the tremendous enhancement in the electrochemical properties achieved by researchers in recent years by means of binders, composites, and liquid electrolytes with remarkable expected outcomes is presented as a solution. Finally, a summary is presented on the prospects of Si-based materials in LIBs for the future commercialization of Si-based anodes.

2 Si-based anodes and their importance in LIBs

Over the years, Li, S, Sn, Gr, antimony (Sb), lithium titanium oxide, and silicon-based materials such as silicon oxycarbide (SiOC) have become common anode elements.[91] Among them, commercial Si or Si nanoparticles are considered some of the best anode materials for next-generation LIBs because of the natural abundance, environmentally friendly nature, and minimal lithiation potential of Si. Accordingly, the electrochemistry of Si and Si-based anodes and their importance in LIBs are discussed in this section.

2.1 Electrochemical behavior of silicon

The electrochemistry of Si has been broadly considered due to its likely application as an anodic material in LIBs. Si has a very high theoretical capacity, which is around 10-times greater than that of the Gr anodic material. Nevertheless, Si also has several drawbacks that need to be overcome before it can be used in commercial LIBs. The key disadvantages of Si are its volume expansion, low electrical conductivity, and inconsistent kinetic reactions. The low electrical conductivity of Si is due to its large bandgap of 1.1 eV. Thus, to use Si as an alternative anodic material, it is necessary to reduce its bandgap to about 0.7 eV. In this case, several approaches can be applied to reduce its bandgap such as doping with group III and group V elements (boron and phosphorous, respectively), alloying with lower bandgap materials such as carbon and germanium, transition metal doping, and hybridization as the most utilized approaches. Fig. 1 illustrates the overall evolution and

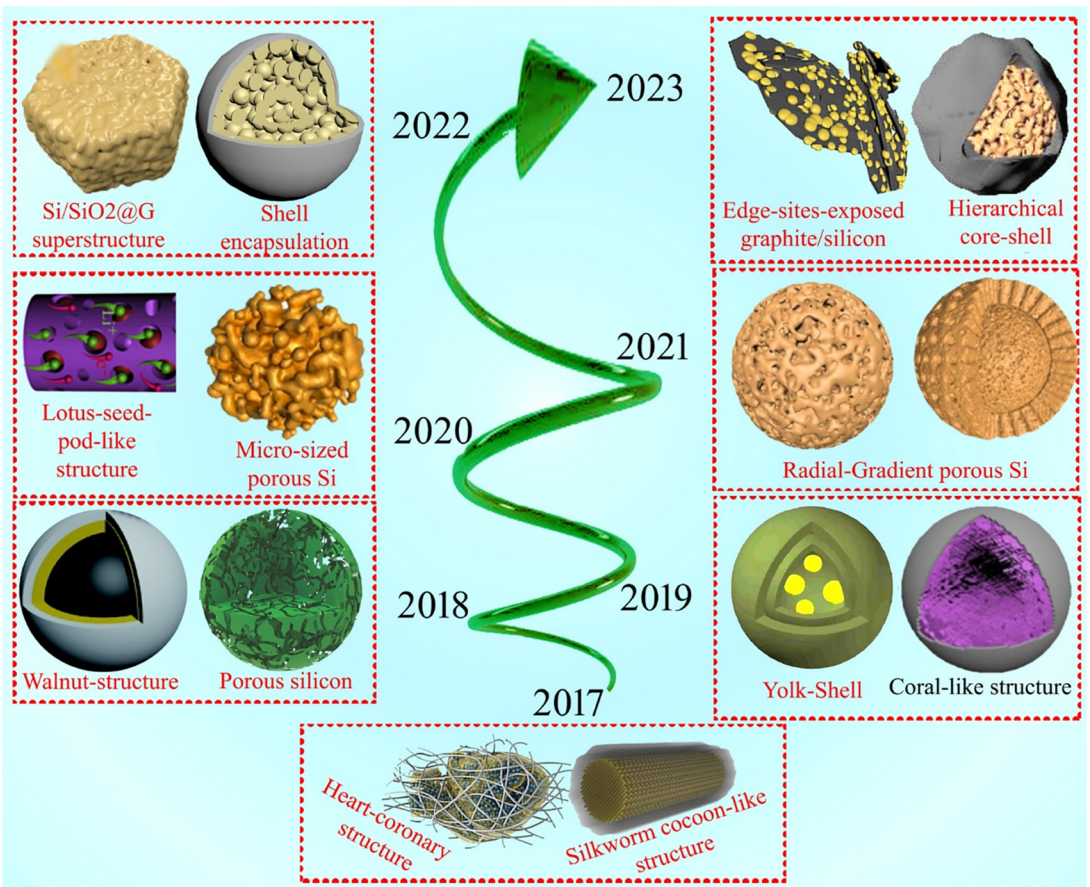

Fig. 1 Development of several types of Si-based anodes in LIBs from 2017 to 2023.

application of Si-based anodes in LIBs. In this period, several novel structures attracted attention such as porous structures to reduce the excessive volume expansion of Si particles, core–shell structures employing carbon, graphene and SiO_2 to stabilize the structure during charging/discharging, and double core–shell structures to further stabilize the structures and secure the performance of Si.[92–104]

2.2 Strategies to improve Si-based anodes

To enhance the performance of silicon-based anodic materials in LIBs, multiple approaches can be employed to address their electrochemical properties, volume expansion, low conductivity, and inconsistent kinetic reactions.[96,105–110] The most common strategy is the use of a protective layer on the Si-based anodic material. The predominant coating employed is carbon coating, where carbon is placed on the silicon anode through the chemical vapor deposition (CVD) technique.[103] Another strategy is the use of a nano-architecture design for the Si anodic material. This can be done by using a small amount of another element, such as phosphorous (P) and boron (B), to dope Si-based anodes.[111,112] Also, surface/interface engineering can be employed to improve the electrical conductivity of Si.[104,113] This can be done using a thin layer of another material, such as gold and platinum, to coat the Si-based anode. Another strategy is the use of binders,[114–123] composites,[95,124–126] and electrolytes[127,128] to improve the cyclic stability of Si-based anodic materials. The broad utilization of the improved outcomes LIBs by employing Si-based anodes requires an understanding of the underlying physics and the degradation mechanism in the system. To date, Si-based LIB systems are well-understood due to the advancement of characterization techniques. The improvements in outputs due to the changes in anode materials can also be understood using similar techniques. Recent advances in characterization techniques have enabled the prediction of the worldwide propagation of reactions and infrastructure breakdown in anodes during cycling and the probing of the chemical environment of elements at the sub-atomic level.[129]

3 Challenges in Si-based anodes

Over the years, LIBs have been equipped with technologies that cannot meet the increasingly growing demands of electronic and hybrid vehicles; consequently, LIBs with extremely significant power and energy densities are urgently needed. The challenges in Si-based anodes that prohibit extreme power and energy density are discussed in this section.

3.1 Massive volume expansion

Due to its unrivalled theoretical gravimetric capacity at a lower voltage and abundance in nature, Si is arguably the strongest candidate to substitute Gr electrode materials. Furthermore, Si has the ability to store more Li-ions than Gr, which is the primary contributor to the significantly higher specific capacity of Si. Gr employs six carbon atoms to host one Li-ion (such as LiC_6), whereas Si can react with many Li-ions ($Li_{15}Si_4/Li_{22}Si_4$).[130–132] However, Si has a high Li-ion facility, which is problematic given that it leads to significant volume expansion of up to 300–400% when completely lithiated, comprising the structural stability of the electrode in several ways.[133] For instance, the huge mechanical strain in Si materials caused by the constant insertion and removal of Li-ions results in Si pulverization and electrode cracking.[134] Consequently, the electrical contact between the surrounding shards of Si is broken, leading to poor conductivity. Also, the devastating electrode swelling caused by volumetric variations can result in structural failure of the electrode and current collectors, drastically reducing the capacity.[135]

3.2 Formation of volatile solid electrolyte interface (SEI)

To date, another major obstacle preventing the widespread use of Si-based anodic materials is the poor stability of their interface with the electrolyte, which is known as the SEI.[136,137] Also, the substantial volumetric fluctuations experienced by silicon-based anodes throughout the discharging/charging process further promote the formation of an undesirable solid electrolyte interface (SEI). The SEI layer, which is primarily composed of inorganic and organic components (such as lithium carbonate (Li_2CO_3), Li_2O, Li alkyl carbonates ($ROCO_2Li$), and lithium fluoride (LiF)), is formed within the first charge/discharge phase as the electrode discharge energy drops below 1 V and the anode material becomes fully lithiated. A properly generated SEI film improves the cycling efficiency by isolating the active constituents from the electrolyte, which prevents adverse reactions with the electrolyte, speeding up the movement of Li ions and functioning as an electronic insulator.

The volume fluctuations of Si throughout the Li extraction/insertion cycle may potentially cause stresses that are too great for the delicate SEI to endure, resulting in unwanted persistent SEI growth.[138,139] In this case, given that the new Si is bare to the electrolyte whenever the SEI is broken during volume expansion, it has several adverse impacts such as enhanced Li-ion diffusion, constant expenditure and reduction of electrolyte, diminished electrostatic field between the Si-based components and current collector because of the thermal insulation by the SEI layer, dramatically decreased rate capabilities and cycling output, and enhanced electrode impedance. Accordingly, industrial-applicable LIBs cannot afford the effects of persistent SEI expansion.[140–143]

3.3 Inadequate kinetic reactions

Besides the above-mentioned problems associated with volume expansion, Si also has a naturally slow kinetic reaction rate. Its poor rate capability and cycling endurance originate from its low electrical conductivity (10^5 to 10^3 S

cm^{-1}) and Li-ion diffusion rate (while diffusion coefficient is in the range of 10^{14} to 10^{12} cm^2 s^{-1}).[144] In the case of related materials such as SiOC, their low electrical conductivity, with values fluctuating from 10^{-5} S m^{-1} to 2 S m^{-1}, depends on the volume of free carbon in the material and its assembly.[145] The Li-ion diffusion in electrochemical devices can be represented by the time constant (τ) according to the following equation:

$$\tau = \frac{L^2}{D}$$

where L denotes the diffusion length and D is the diffusivity. In this case, the vital issue is to reduce the ionic/electron diffusion length (L) and boost the diffusivity (D) of Si-based anodes to speed up the diffusion process and improve the electrochemical behavior of the anode. Intensifying the Li-ion solubility and reducing the electrolyte viscosity through material engineering techniques, for instance, surface coating, doping, and employing conductive agent composites, can increase the conductivity of Si significantly, which can enhance the reaction rate of Si-based anodic materials, allowing for faster Li diffusion.[146] Although Si is an intrinsic semiconductor, these techniques can be used to continuously improve the Li diffusion kinetics.

3.4 Limited initial columbic efficiency (ICE)

An essential indicator of the reversible capacity and longevity of a battery is its charge-to-discharge ratio, which is called the columbic efficiency (CE).[147] Alloy and conversion-type anode materials exhibit a low ICE because of their high initial irreversible performance degradation in comparison to insertion materials. Typically, Si-based anodes have an ICE in the range of 60–80%, which is considerably lower than that required for widespread commercialization. For example, SIOC offers a low CE of 40–70%, specifically during the first cycle, which is comparatively lower than that of Si.[148] The initial irreversible performance reduction primarily results from electrolyte degradation during the development of the SEI layer and Li-ion consumption through side reactions with the electrolyte.[149,150] Also, the magnitude of capacity loss is affected by factors such as the size, shape, volume expansion, and electrolyte content of the anode material.

4 Recent progress on Si-based LIBs

To overcome the barriers in improving the performance of LIBs, researchers have been continuously trying to achieve the theoretical assumptions by adopting several strategies, including the addition of binders, construction of composites, and utilization of liquid electrolytes over the last few years (2017–2022), as highlighted in Fig. 2.[151–157]

4.1 Addition of binders

To improve the performance of Si-based anodic materials, several types of binders such as linear, branched, crosslinked, and newly dynamically crosslinked binders have been discussed.[158–171] A summary of the binders utilized over the last few years (2017–2022) is presented in Table 1. All the binders are classified into four categories, as listed below.

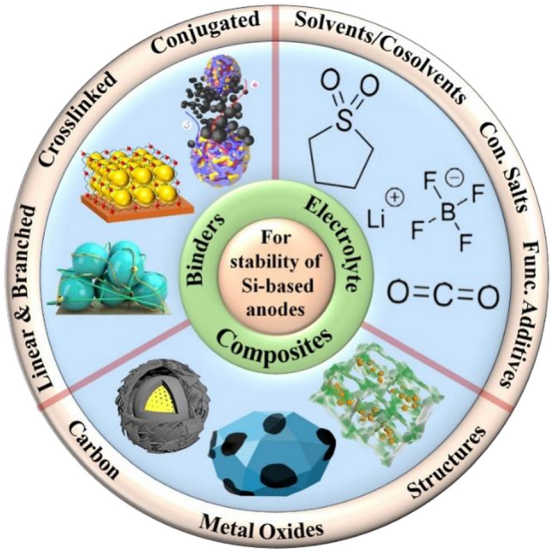

Fig. 2 Recent progress in Si-based anodes in LIBs.

4.1.1 Linear polymer binders. With an increase in the crystallinity of the binder, the molecular weight (M_W) and different pendant groups such as hydroxyl (–OH) and carboxyl (–COOH) play a role in the functional properties of linear polymer binders, impacting the electrochemical outputs of Si-based anodes.[172] Several techniques including copolymerization, blending, and modification are employed to boost the adhesive characteristics of linear adhesives. Typically, linear polymers such as alginate (Alg), chitosan (CS), and carboxymethyl cellulose (CMC), or synthetic polymers such as polyvinyl alcohol (PVA) and polyacrylic acid (PAA) are employed as binders in Si-based electrodes.

Water-based CMC emulsion polymerization can be employed to create conductive polymers suitable for slurry mixing and anode coating, while saving time and energy, making Si-containing electrodes inexpensive and environmentally friendly.[199] Homogeneous electrodes with an identical Si and C particle distribution could be created employing PAA and CMC/citric acid (CA) binder formulations. Karkar *et al.* showed that CMC/CA seems to be more proficient than PAA at lower binder concentrations because CMC has higher bridging effectiveness than PAA, resulting in a greater areal density of bridging chains for interparticle interactions and CA acts as an artificial SEI layer element. Moreover, PAA outperformed CMC/CA at a higher binder content due to its mass transfer durability.[200] Fig. 3a demonstrates the mechanism of the potassium triphosphate (PTP) interaction with Si materials. This Si@PTP electrode exhibited long-term cycling efficiency when subjected to a current density of 800 mA g^{-1}, which exhibited a charge capacity of 1279.7 mA h g^{-1} even after undergoing 300 cycles, indicating a notable capacity maintenance of 72.7%

Table 1 The binders used in the last few years in Si-based anodes (2017–2022)

Authors (year)	Anodic Si type	Binder	Binder ratio	Cyclic performance	Current density (mA g^{-1})	Areal loading (mg cm^{-2})	Ref.
Wang *et al.* (2017)	SiNPs	Stretchable conductive glue	10%	1500 mA h g^{-1} after 700 cycles	840/0.2C	1%	173
Sunghun *et al.* (2017)	SiMPs (~2.1 μm)	Slide-ring PR-PAA	10%	91% capacity retention after 150 cycles	(0.64 mA cm^{-2})	1.07	174
Lei *et al.* (2018)	SiNPs (50 nm)	PDA-PAA-PEO	20%	1597 mA h g^{-1} after 200 cycles	0.5C	~0.4	175
Songtao *et al.* (2018)	Si@SiO_2 (40–100 nm)	Konjac glucomannan	25%	1278 mA h g^{-1} after 1000 cycles	2000	0.2–0.3	176
Xingyu *et al.* (2018)	SiNPs	Crosslinked PAM hydrogel	10%	2843 mA h g^{-1} after 100 cycles	0.1C	1.0–1.1	177
Guangzhao *et al.* (2018)	SiNPs (~70 nm)	PAA-Upy supramolecular	20%	2638 mA h g^{-1} after 110 cycles	2100/0.5C	0.4–0.6	178
Nelsihan *et al.* (2018)	SiNPs	PEG grafted PFP	10%	605 mA h g^{-1} after 1000 cycles	C/3	0.6	179
Hui *et al.* (2018)	Si-alloy particles (1 μm)	Pyrene-based (PPyMADMA)	10%	~800 mA h g^{-1} after 100 cycles	0.1C	~0.5	180
Chul *et al.* (2019)	SiNPs (50 nm)	PAA	20%	1500 mA h g^{-1} after 500 cycles	1000	0.7–1.2	181
Pengcheng *et al.* (2019)	SiNPs	MA H crosslinked CMC	20%	996 mA h g^{-1} after 120 cycles	1000	~1	182
Peng *et al.* (2019)	SiNPs (<100 nm)	CS-CG + GA	20%	~2144 mA h g^{-1} after 100 cycles	—	0.40	183
Tsung *et al.* (2019)	SiNPs (≤50 nm)	Crosslinked PU elastomer	20%	2414 mA h g^{-1} after 100 cycles	0.2C	0.55	184
You *et al.* (2019)	SiNPs (~50 nm)	Metallopolymer	15%	81.9% capacity retention after 350 cycles	1500/1C	0.7	185
Wang *et al.* (2020)	SiNPs	Pectin/PAA	20%	2386 mA h g^{-1} after 100 cycles	0.2C	0.5–0.7	186
Zeheng *et al.* (2020)	SiNPs (100 nm)	Partially lithiated PAA and Nafion	10%	2143 mA h g^{-1} after 100 cycles	0.2C	0.7–1.0	187
Xuejiao *et al.* (2020)	SiNPs	Glycerol-crosslinked PEDOT:PSS	27%	1951.5 mA h g^{-1} after 200 cycles	500	~0.7	188
Jaebin *et al.* (2020)	SiNPs (~50 nm)	Self-healing PAU-*g*-PEG	20%	1450.2 mA h g^{-1} after 350 cycles	0.5C	0.5–0.6	189
Hyungsub *et al.* (2020)	SiMPs (1–5 μm)	(Fe^{3+})-crosslinked ($PANa_{0.8}Fe_y$)	20%	~1400 mA h g^{-1} after 400 cycles	1790	0.8	190
Jaebin *et al.* (2021)	SiNPs (<50 nm)	PEG-crosslinked-GCS	20%	2141 mA h g^{-1} after 150 cycles	0.5C	~0.5	191
Linlin *et al.* (2021)	SiNPs	Gradient hydrogen-bonding binder	10%	1583 mA h g^{-1} after 700 cycles	1C	0.5 mg cm^{-2}	192
Zhe *et al.* (2021)	SiNPs (~50 nm)	Organic binder (PVDF)	20%	1154 mA h g^{-1} after 100 cycles	300 mA g^{-1}	≈0.6 mg cm^{-2}	193
Chao *et al.* (2021)	SiOx	PAA (4A-PAA) homopolymer binder	10%	558.1 mA h g^{-1} after 200 cycles	0.16 A g^{-1}	2.2–2.6 mg cm^{-2}	194
Zechen *et al.* (2022)	SiNPs (80–100 nm)	Natural sesbania gum (SG)	20%	1621.1 mA h g^{-1} at after 100 cycles	1000	4.5	195
Zhibo *et al.* (2022)	SiNPs (~50 nm)	Polyfluorene-type conductive terpolymer (PFPQDA)	10%	Capacity retention of 80% after 200 cycles	0.4 A g^{-1}	0.8 mg cm^{-2}	196
Ming *et al.* (2022)	SiNPs (~50 nm)	Cross-linked γ-PGA-PAA binder	10%	Capacity retention of 72.5% after 400 cycles/92.0% after 50 cycles	2940 mA g^{-1}/420 mA g^{-1}	0.7–0.9 mg cm^{-2}/1.1 mg cm^{-2}	197
Shichao *et al.* (2022)	Nano Si	Cross-linked CMC/EDTA-Ca^{2+}	15%	80.7% (602 mA h g^{-1}) after 380 cycles	1 A g^{-1}	—	198

compared to its initial charge capacity (Fig. 3b). Furthermore, it exhibited a notable rate property, as evidenced by the high charge capacities achieved at various current densities (400, 800, 1600, 3200, 6400, and 400 mA g^{-1}). These charge capacities, as depicted in Fig. 3c, were measured to be 1980.5, 1664.5, 1353.6, 1028.4, 648.8, and 1700.0 mA h g^{-1}, respectively, based on the fifth cycle for each rate. Also, according to the thickness observed in the cross-sectional SEM image of the Si@PTP electrode, it had a density of 0.631 g cm^{-3}, which was substantially greater than that of the Si@PVDF electrode (0.419 g cm^{-3}) (Fig. 3d). Fig. 3e presents a schematic diagram of the long chain and short-chain polymer lithiation/delithiation of this binder.[201] A coating slurry of polyamic acid (PAA) and Si was heat-treated *in situ*

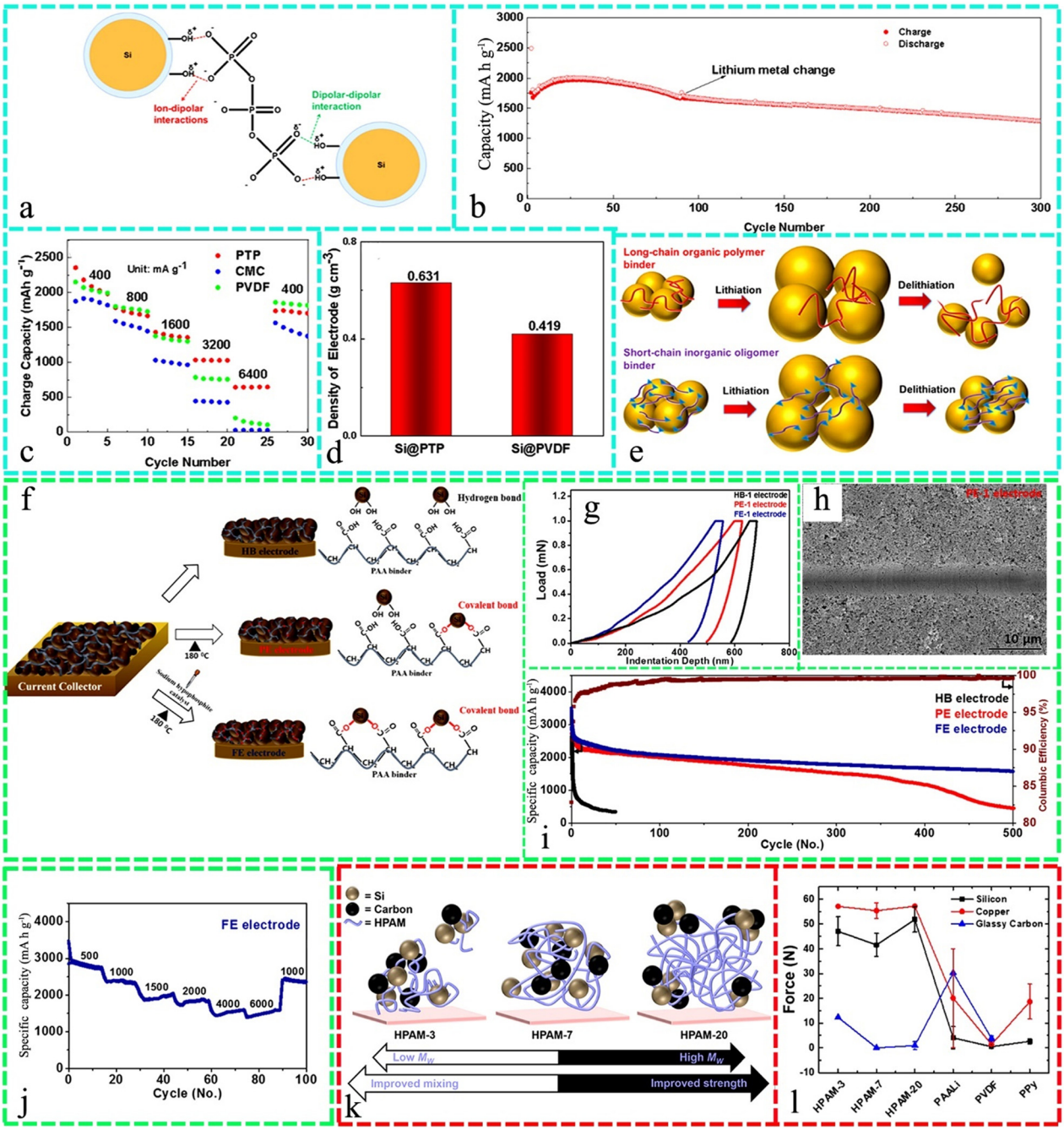

Fig. 3 (a) Mechanism of robust interfacial interactions between the PTP binder and Si active materials. (b) Rate capability of Si@PTP, Si@PVDF, and Si@CMC electrodes and (c) long-term cycle performance of the Si@PTP electrode at 800 mA g^{-1}. (d) Density of the Si@PTP and Si@PVDF electrodes. (e) Schematic representation of lithiation/delithiation of Si anodes using a long-chain polymer binder and a short-chain inorganic oligomer binder. Reproduced with permission from ref. 201 Copyright 2021, the American Chemical Society. (f) Graphical representation of the preparation of three types of Si anodes (HB, PE, and FE electrodes) and chemical interactions between Si NPs and PAA binder. (g) Nano-indentation profiles for HB-1, PE-1, and FE-1 electrodes, (h) friction coefficient obtained by the nanoscratch test, and SEM images after the scratch test for PE-1; (i) long-term cycling stability of HB, PE, and FE electrodes at the current density of 500 (1 cycle)–1000 mA g^{-1} (subsequent cycles); and (j) rate capability of FE electrode from 500 to 6000 mA g^{-1}. Reproduced with permission from ref. 181 Copyright 2019, the American Chemical Society. (k) Schematic diagram of high M_W HPAM polymeric binder and the electrode stability and performance, (l) force required to pull apart silicon (black square), copper (red circle), and glassy carbon (blue triangle) substrates using various binders dried at 70 °C under vacuum. Reproduced with permission from ref. 203 Copyright 2019, the American Chemical Society.

to prepare the Si/C/polymer hybrid composite anode. This construction method provides cohesion and C dispersion in the hybrid electrode and LIB anodes benefit from its high electrical conductivity and binding force.[202]

Fig. 3f shows the fabrication of three Si electrode types, *i.e.*, hydrogen-bonded (HB), PE (partly esterified), and FE (completely esterified). Fig. 3g demonstrates the load vs indenter deformation statistics for these three electrodes under 1000 μN force, which the nano-indentation force increase in the order of HB-1, PE-1, and FE-1. Moreover, the SEM pictures of the electrodes after the nanoscratch assessment showed that the PE-1 electrode had an even track with partial cracks (Fig. 3h). When subjected to 500 cycles at a current density of 1000 mA g^{-1}, the produced Si-based anode retained a capacity of 1500 mA h g^{-1} (Fig. 3i). The rate capability of the FE electrode with a variation in the current density from 500 to 6000 mA g^{-1} is illustrated in Fig. 3j. In the 10th cycle at each current density, the reversible capacity was 2750, 2333, 2046, 1845, 1574, and 1550 mA h g^{-1}.[181] Fig. 3k highlights the relationship between high M_W (varying from 3 to 20 × 10^6 g mol^{-1}) hydrolyzed polyacrylamide (HPAM) binders and electrode stability and performance. Fig. 3l demonstrates the force needed for pulling Si, copper, and carbon utilizing several binders, where it can be found that the adhesion between the HPAM binders and carbon is relatively weak, potentially due to the hydrophobic characteristics of the carbon substrate.[203] The volume expansion of Si-based anodes could be effectively inhibited by modifying natural polysaccharides, causing the (–COOH) and acetyl units in the polymeric chain to be uniformly circulated. Even after being exposed to 200 cycles at a current density of 1 A g^{-1}, the capacity remained at 1138 mA h g^{-1}.[204] PAA bonds high-capacity Si anodes in LIBs, and the pre-lithiation of the carbo groups in PAA aids lamination, especially for large-scale production. Nevertheless, this treatment affects several physicochemical features of the PAA binder, hindering electrode cycling.[205]

4.1.2 Branched polymer binders. The stress produced by volume expansion can be alleviated and the integrity of the anode can be preserved by using branched-chain binders, which typically have an extended core chain and are divided by functional side chains to enhance the connection strength with the active materials or the electrical conductivity.[206]

Using glycol chitosan (GC) as the core chain and Li-PAA as the adjacent chain, Cao *et al.* developed a graft copolymer. The capacity loss experienced by Si-based anodes can be mitigated by using a binder that is both water-soluble and made of Si. When the graft density was maximized, a stable cycling performance was achieved, while the ICE was 90.3%, and after 100 cycles, the capacity dropped to 495 mA h g^{-1}.[206] Radical polymerization creates ultra-high-catechol poly(*N*-methacryloyl-3,4-dihydroxy-L-phenylalanine) (PMDOPA) Si anode binders. The ultra-high catechol content in PMDOPA outweighs the (–COOH) groups in PAA. With an increase in M_W, the PMDOPA binders become more flexible, solvent-resistant, and sticky, minimizing electrode pulverization and extending the battery life. PMDOPA-20 exhibited the maximum cycle life of 665 cycles at 840 mA g^{-1}.[207]

Jiang *et al.* demonstrated the architectures of branched PAA polymers, branched by ether chains, as shown in Fig. 4a. The advantages of this design are as follows: when the ether content is kept low, PAA remains the dominant component, retaining its benefits such as adhesion to Si NPs through bonding between the carboxylic acid and silanol (Si–OH) groups on their surface. The PEG chains can also increase the ionic conductivity of Li, which is a beneficial feature to achieve an improved performance. As shown in Fig. 4b, the conductivity increased with an increase in the content of tetra(ethylene glycol)diacrylate (TEGDA), confirming our hypothesis that the ether moiety enhances the Li ionic conductivity. According to Fig. 4c, it is promising that anodes containing branched PAA binders exhibit enhanced electrochemical effectiveness, where the synthesized binders, except for bPAA-1, exhibited an enhanced initial capacity and retention compared to linear PAA binders, with a greater improvement with an increase in the content of TEGDA. The best-performing bPAA-3 cell exhibited an initial capacity of 752 mA h g^{-1} and capacity retention of 76%, which are significantly greater than that of the linear PAA cell (678 mA h g^{-1} and 45%, respectively).[208] Moreover, binders for Si-based anodes that include peptoids with the ability to tailor –OH and –COOH are viable options. Long-term cycling showed no visible cracks because the quantity and spacing of the –OH and –COOH groups were carefully managed to improve the structural and chemical stability.[209]

Li hydroxide solvent deactivated the Li-PAA binder, buffering the Si volume expansion, reducing the surface fractures, and improving the anode crystal integrity. The NCA/SiOx/C cell with a single-sided anode electrode density of 11.5 mg cm^{-2} exhibited 90.9% capacity retention (*vs.* 0.1C) at 1C rate and 90.8% after 100 cycles, which supports building 300 W h kg^{-1} cells with 20 Ah capabilities.[210] The Si anode shown in Fig. 4d was composed of NaPAA and PAA-PDA-1-1 binders, while the PAA-PDA-1-1 homogeneous distribution and improved coating ensured the particle integrity and good contact of Si with the current collector. To evaluate the electrochemical performance of the sample, 500 cycle tests were conducted (Fig. 4e), where the diminishing pattern of the battery with PAA-PDA-1-1 binder slowed with an increasing number of cycles. The specific capacity of the battery decreased to 1410 mA h g^{-1} after 500 cycles, with a retention rate of approximately 56%. The homogeneous coating on the NaPAA and PAA-PDA-1-1 binder-based anodes was observed by their close stripping force and displacement (Fig. 4f). The FE-SEM images of the Si anodes with PAA-PDA-1-1 binder before cycling are shown in Fig. 4g, where after 200 cycles, the electrodes with PAA-PDA-1-1 binder exhibited a flatter surface shape.[211]

An amphiphilic binder for Si anodes was created using thermal renatured DNA (reDNA) and alginate (ALG), as shown in Fig. 5a. ALG prefers to bind with hydrophilic Si particles, while reDNA and its heterocyclic aromatic components bind with hydrophobic carbon conductive agents and graphite in mixed electrodes. The adherence of the matching Si electrodes is significantly affected by various binder conformations. Si anodes were made using a weight ratio of

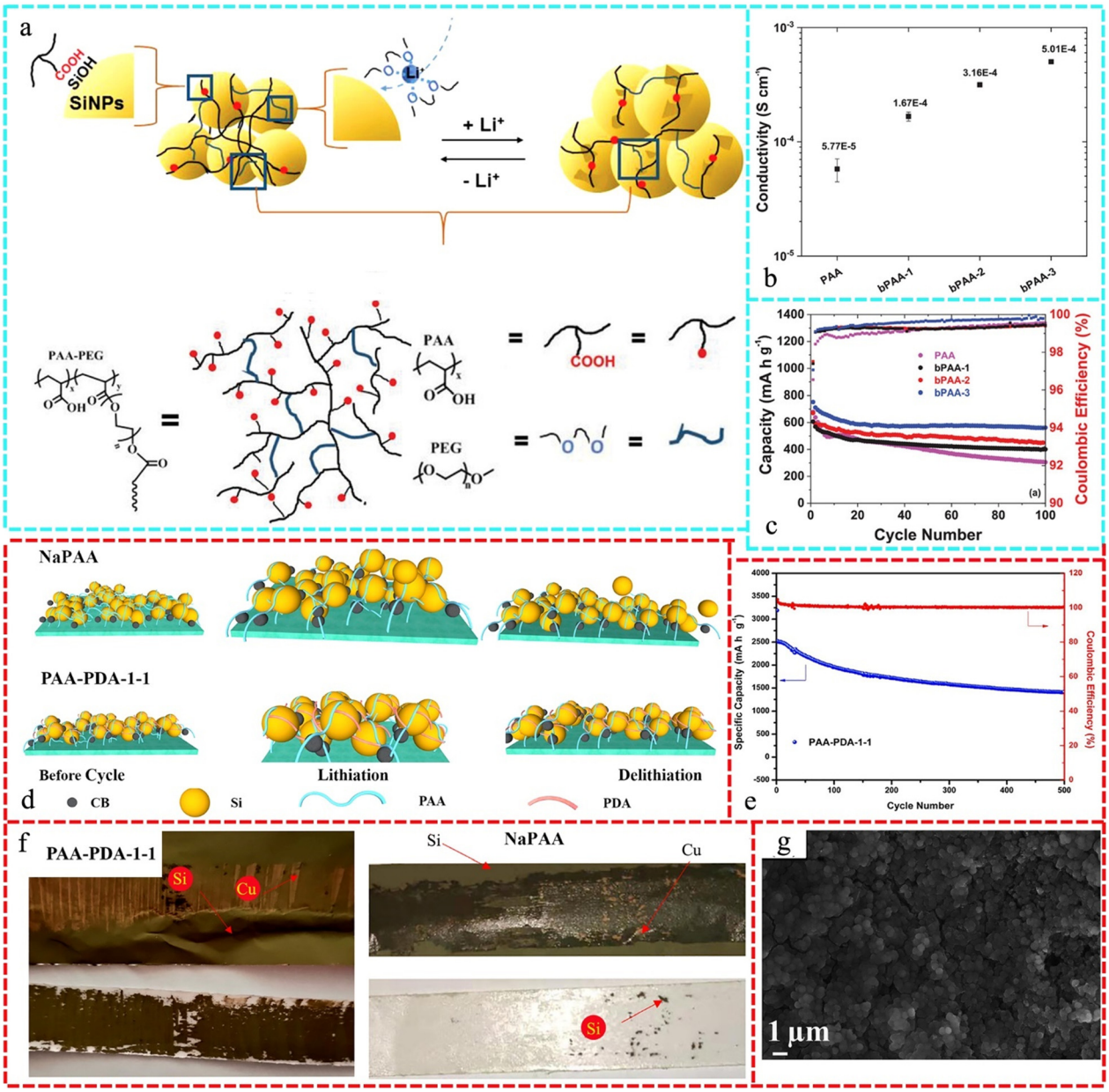

Fig. 4 (a) Schematic structure of branched PAA binder and the design strategy of the branched PAA binder: adhesion between Si NPs promoted by the interaction between the carboxylic acid of PAA and the Si–OH group on the SiNP surface, Li^+ conductivity facilitated by ether chains, and electrode integrity enhanced by the branched polymer chains, respectively. (b) Li ionic conductivity of each binder. (c) Electrochemical characterization of half-cells containing Si–Gr electrodes fabricated using branched PAA binders. Specific delithiation capacity profiles (left) and coulombic efficiency profiles (right). Reproduced with permission from ref. 208 Copyright 2020, WILEY-VCH. (d) Possible working illustration of the structure and schematic features NaPAA and PAA-PDA-1-1, (e) cycling performance test with 500 cycles of PAA-PDA-1-1, (f) photos after the 180° peeling experiments of Si active material with NaPAA and PAA-PDA-1-1 binders and (g) FE-SEM images of Si anodes with different proportion of binders after 200 cycles of PAA-PDA-1-1. Reproduced with permission from ref. 211 Copyright 2021, Elsevier.

Si : binder : super-P = 6 : 2 : 2, and subsequently a 180° peeling test was carried out to assess the adhesion. As the 3M tape peeled off from the Si electrodes, the stress profiles on the electrodes with various polymeric binders varied (Fig. 5b). Fig. 5c depicts the after 300 cycles at 3C (1C = 3500 mA g^{-1}), Si-reDNA/ALG preserved 84.6% of its initial capacity. Si-reDNA/ALG exhibited higher interfacial stability in the SEM images obtained before and after 160 cycles (Fig. 5d).[212] PAA binders with different M_W were added to Si/Gr composite anodes (15 wt% Si) to improve their cyclability. The M_W affected the PAA binder solution viscosity and cycle performance, which is likely due to the changes in cohesion. Despite the large volumetric changes in the Si alloy, an M_W in the range of 24–150 kDa minimized the capacity reduction and maintained the electrode matrix cohesiveness.[213] Water-soluble glycinamide-modified PAA (PAA-GA) polymer binder

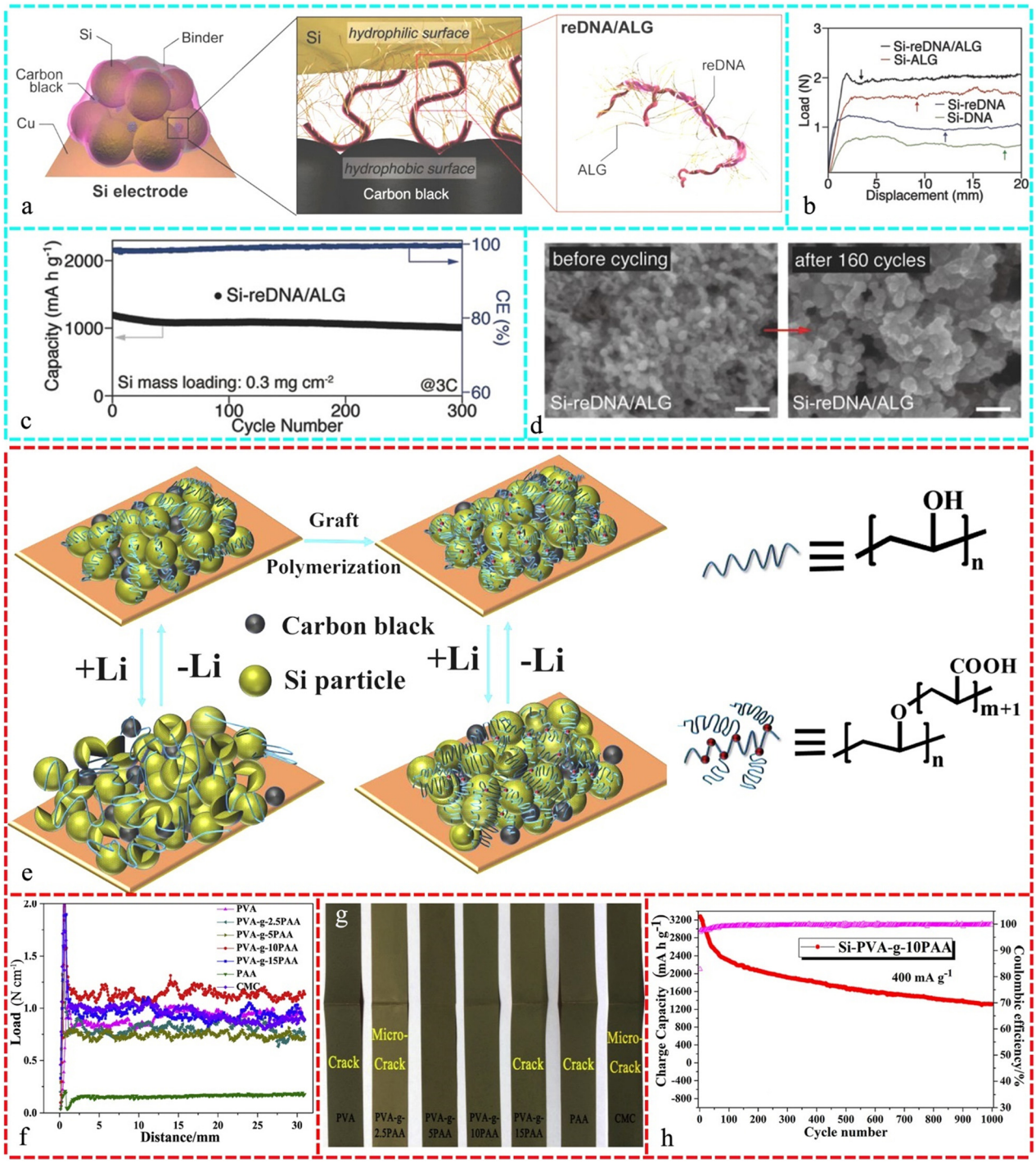

Fig. 5 (a) Proposed reDNA/ALG hybrid binder at Si/carbon interface in the electrode. (b) Binder effect on the adhesion of the electrode: 180° peeling test results of Si electrodes based on reDNA/ALG, reDNA, DNA, and ALG binders. c) Cycling performance of Si-reDNA/ALG at 3C, together with its CEs (right *y*-axis). (d) SEM images of Si electrodes before and after 160 cycles: Si-reDNA/ALG. Reproduced with permission from ref. 212 Copyright 2018, WILEY-VCH. (e) Schematic illustration of grafted PVA-*g*-PAA binder with the formation of strong interactions between its carboxylic/hydroxyl groups and the hydroxylated Si surface upon cycling, together with linear PVA for comparison. (f) Peeling profiles of Si electrode and (g) after repeated folding test with different binders (PVA, PVA-*g*-10PAA, PVA-*g*-15PAA, PAA and CMC). (h) Cycling performances of Si electrode with PVA-*g*-10PAA binder for 1000 cycles at a current density of 400 mA g^{-1}. Reproduced with permission from ref. 216 Copyright 2018, Elsevier.

reduced the volume change in the Si anode. PAA-carboxyl GA and double amide groups can form H-bonds with an Si hydration layer, and interchain cohesion can form double H-bonds. The PAA-GA Si electrodes exhibited reliable cycling and coulombic efficiency.[214] The EDTA PAA-binder system was tested for LIBs composed of high-performance Si-based anodes. The interaction of EDTA and COOH with the SiO_2 layer of SiNPs creates a mechanically robust network.[215]

Fig. 5e illustrates the design of the Si-PVA-*g*-10PAA electrode during cycling with substantial volume fluctuations in the Si particles. To ensure electrical integrity, a standard Si electrode with a linear binder such as PVA binds the active material and conducting carbon black particles and sticks them to the current collector before cycling. However, prolonged cycles can cause pulverization and fracture of the Si particles due to internal stress, causing the degradation of the material. The mechanical properties of the Si-PVA-*g*-PAA electrode were examined by peeling and folding tests, including adhesion strength and flexibility, as shown in Fig. 5f and g, respectively. After graft-polymerizing the appropriate length of PAA on the PVA backbone, Si-PVA-*g*-10PAA had much higher binding capability (1.14 N cm^{-1}) and flexibility (without cracks, Fig. 5g) during peeling and folding measurements compared to the other studied materials. Si-PVA-*g*-10PAA retained a charge capacity of 1315.8 mA h g^{-1} and capacity retention of 40.3% after 1000 cycles at 400 mA g^{-1} (Fig. 5h), with a very low capacity fading of 0.06% in each cycle.[216]

4.1.3 Cross-linked polymer binders. Cross-linked binders have the ability to generate a more robust network structure than both linear and branching binders. The following are two types of cross-linking that can be distinguished by their underlying mechanism.

4.1.3.1 Covalently cross-linked polymer binder. Schiff base reaction, esterification, hydroformylation, *etc.* are common methods of crosslinking polymerization for covalently cross-linked monomers. Covalent bonding endows the binder with increased mechanical strength, which helps to reduce the volume variations in the Si-negative electrode and keeps the electrode stable.[217] CMC, PVA, and poly(ethylene imine) (PEI) are a few of the various monomers that are typically polymerized with PAA to create cross-linking polymers.[217] To increase the lifespan of the electrode, an *in situ* cross-linked CMC-polyethylene glycol (CMC-PEG) binder was applied to the Si anode. Following drying of the electrode, *in situ* cross-linking created the cross-linked CMC-PEG binder. The cross-linked CMC-PEG binder improved the active material adhesion and cohesion. The cross-linked CMC-PEG binder Si-based anode exhibited a capacity of 2000 mA h g^{-1} and could undergo 350 cycles at 0.5C.[218]

A unique gel binder, in conjunction with a three-dimensional network structure created through the crosslinking of CMC and sodium borate, successfully mitigated the volume expansion in a silicon anode, as illustrated in Fig. 6a. Fig. 6b shows that the gel-bound Si anode exhibited a good cycle lifespan (1211.5 mA h g^{-1} after 600 cycles) with high ICE (88.95%) and Fig. 6c presents a schematic diagram of its structure.[219] Fig. 6d demonstrates that the crosslinker with boronic acid forms a network-like polymer structure by covalently connecting two boronic esters without extra driving factors. Also, boronic-crosslinked (BC) guar (BC-g) binder exhibited great mechanical strength due to the balanced mix of secondary contacts and covalent bonding across the polymer network. The crosslinked natural polymer binder for Si anodes features BC, which spontaneously forms covalent bonds between the vicinal alcohols of Guar gum and boronic acid group conjugated to a stiff polystyrene backbone (Fig. 6e). Fig. 6f shows that the BC10-g electrode greatly outperformed the BC5-g and guar electrodes during 300 cycles. The strong covalent interactions and absence of ionic conduction groups in the binders caused the performance of the guar electrode to deteriorate quickly. Alternatively, the adhesive strength of the BC-g electrodes was higher than that of bare guar due to the incorporation of covalent bonds in the hydroxyl-enriched polysaccharides, which delocalized the stress to multiple side chains (boronic ester groups) and enhanced the overall strength, as shown in Fig. 6g. Fig. 6h highlights that the addition of polyethylene oxide (PEO) groups to the BC material enhanced the lithium-ion conductivity of the BC-g binders.[220]

Si anodes using PAA-PEGPBI polymer binders, while physiological crosslinking with acid-base interactions between PAA and PBI, together with the ion-conducting PEG group yielded material characteristics for PAA-PEGPBI-based anodes, including 1600 mA h g^{-1} at 2C after 100 cycles.[221] The cross-linked hyperbranched PEI acts as a generally feasible, ecologically, water-soluble polymer binder for Si anodes in LIBs. The cross-linked 3D structure limits the mobility of the SiNPs, preserving the properties of the anode. Adjusting 1,4-butanediol diglycidyl ether to balance the binding reversibility and mechanical properties of PEI yielded a cross-linked Si/PEI anode with a specific capacity of 2180 mA h g^{-1} at 500 mA g^{-1} over 100 cycles.[222] Poly(ether urethane) (PEU) bonded the Si anodes *in situ*, while gallic acid cross-linked PEU from methylene di-*p*-phenyl diisocyanate and PEG. At C-rates of 0.1, 0.2, 0.5, 1, and 2C, the Si-based anode with the cross-linked binder exhibited a capacity of 3628, 3490, 3156, 2838, and 2491 mA h g^{-1}, respectively. The Si-based anode with the *in situ* cross-linked PEU binder exhibited an excellent cycle lifespan and specific charge capacity of 2414 mA h g^{-1} after 100 cycles at 0.2C.[184] Esterification of PAA and sodium alginate (SA) provided a cross-linked polymer binder for electrodes. Commercialized submicron-sized Si particles performed better electrochemically with cross-linked polymer binders than SA. The cross-linked polymer binder electrodes had an initial specific discharge capacity of 2471 mA h g^{-1} compared to that of 2371 mA h g^{-1} with SA. After 110 cycles at 200 mA g^{-1}, the cross-linked polymer binder electrode exhibited a discharge capacity of 945 mA h g^{-1} with 38.2% capacity retention, outperforming the SA electrodes.[223]

The crosslinking of strands of PAA binder with borax could influence the crosslinking and binding physicochemistry, where up to 5 wt% of borax crosslinker could increase the polymer network modulus and Si electrode endurance. In this study, Si microparticles with an electrode density of 1.25 g cm^{-3} yielded 2470 mA h g^{-1} (3.1 mA h cm^{-2}). Furthermore, after 50 cycles, it exhibited the capacity retention of 91.2% and 1000 mA h g^{-1} after 500 cycles.[224] The dual-cross-linked structure of cxPAA-PEI(*x*) was created by combining PAA with minor amounts of

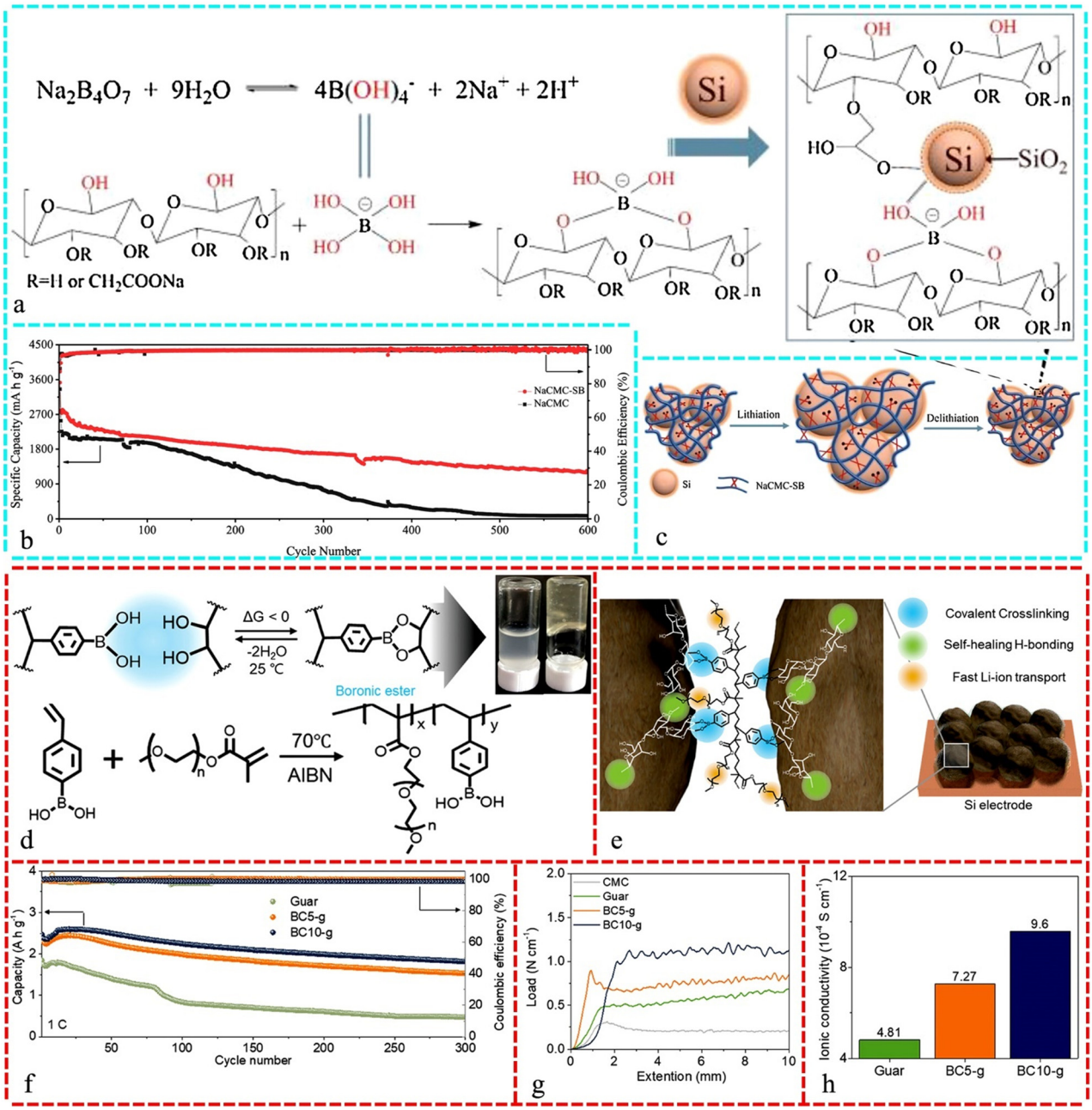

Fig. 6 (a) Chemical structure and illustrative interaction among sodium carboxymethyl cellulose, sodium borate, and Si NPs. (b) Capacity and Coulombic efficiency of the NaCMC-SB binder and NaCMC. (c) Graphical representation of Si/NaCMC-SB configurations during lithiation/delithiation process. Reproduced with permission from ref. 219 Copyright 2018, Elsevier. (d) Spontaneous crosslinking reaction of boronic acid and vicinal alcohol at room temperature together with pictures of guar (left) and BC-g binders (right) and the synthesis process of BC. (e) Schematic of BC-g binder in a Si electrode, showing the formation of a covalent bond from BC, self-healing ability of abundant hydroxyl groups with PEO and boronic ester, and fast Li-ion transport through PEO groups. (f) Long-term stability results of guar and BC-g electrodes at 1C for 300 cycles. (g) Peel off test results for Si electrodes based on CMC, guar, and BC-g binders. (h) Ionic conductivity results of guar and BC-g binder films. Reproduced with permission from ref. 220 Copyright 2020, WILEY-VCH.

hyperbranched PEI (x: wt% of PEI, x = 1, 3, and 5), which was demonstrated to be an outstanding binder for Si anodes in LIBs. In addition to mechanical strength, the –COOH and NH_2 functional groups in cxPAA-PEI(x)s provided strong interfacial adhesion forces towards the anode components (*e.g.*, Cu current collector). The cross-linking density and hydrogen (H) bond interaction forces were responsible for the delicate mechanical strength-adhesive force balance. cxPAA-PEI (3) was employed to form an Si-based anode, which exhibited a high ICE and outstanding specific capacity after 100 cycles of 2602 mA h g^{-1} at 0.2C and after 300 cycles of 1230 mA h g^{-1} at 1C.[225]

Cross-linked dextrin is an affordable, aqueous binder for Si-based LIB anodes, while aldolization between glutaraldehyde and dextrin (–OH) groups creates a 3D network. Polyvinylidene

fluoride (PVDF), CMC, and pure dextrin binders perform worse electrochemically than this inter-waving structure, which reduced the Si anode volume change during cycling. Over 150 cycles under 0.1C, the capacity was reduced to 1000 mA h g^{-1} from 3276 mA h g^{-1} with 88.79% CE. The cycling efficiency increased to over 1700 mA h g^{-1} after 150 cycles at 0.1C and about 1000 mA h g^{-1} under 0.5C by adding 20 wt% fluoroethylene carbonate (FEC) to the electrolyte.[226] *In situ* cross-linked corn starch was bonded with Si composite anodes to stabilize LIB cycles. Maleic anhydride cross-linked the maize starch binder during the formation of the Si anode. The cross-linked corn starch binder enhanced the adhesion of the Si/conductive C composite to the Cu current collector. The Si composite cathode with cross-linked maize starch binder exhibited a specific capacity of 3720 mA h g^{-1} and increased cycling stability.[227] Shi *et al.* observed that direct cross-linking of PAA and branching PEI substantially reduced the solubility of the polymer and made it relaxed to precipitate, but a chemical switch (ammonia, NH_3) could prevent this. PAA did not react with PEI in the slurry due to the presence of NH_4OH. Additionally, to eliminate NH_3 and initiate crosslinking, the ammonium carboxylate group was cleaved during drying. PAA-PEI-i (ionic crosslinks) was created in the first step, while PAA-PEI-c (covalent crosslinks) was designed in the following step at a temperature above 130 °C. In the half-cell assays, PAA-PEI-c helped to retain the capacity of 67%, which was better than PAA.[228]

Li *et al.* used epichlorohydrin (ECH) and peach gum (PG) with varying M_W to create a cross-linked adhesive with good mechanical capabilities, benefiting from covalent bonding and H-bonding, as displayed in Fig. 7a. As shown in Fig. 7b, the peel test revealed that the enhanced adhesion strength of PG-*c*-ECH was attributed to its strong interfacial adhesion and mechanical qualities. This resulted from the covalent contacts between the crosslinking chains and PG, as well as the hydrogen bonding interactions. The Si@PG-*c*-ECH electrode exhibited a consistent and durable cycling performance. It maintained a discharge capacity of 1678 mA

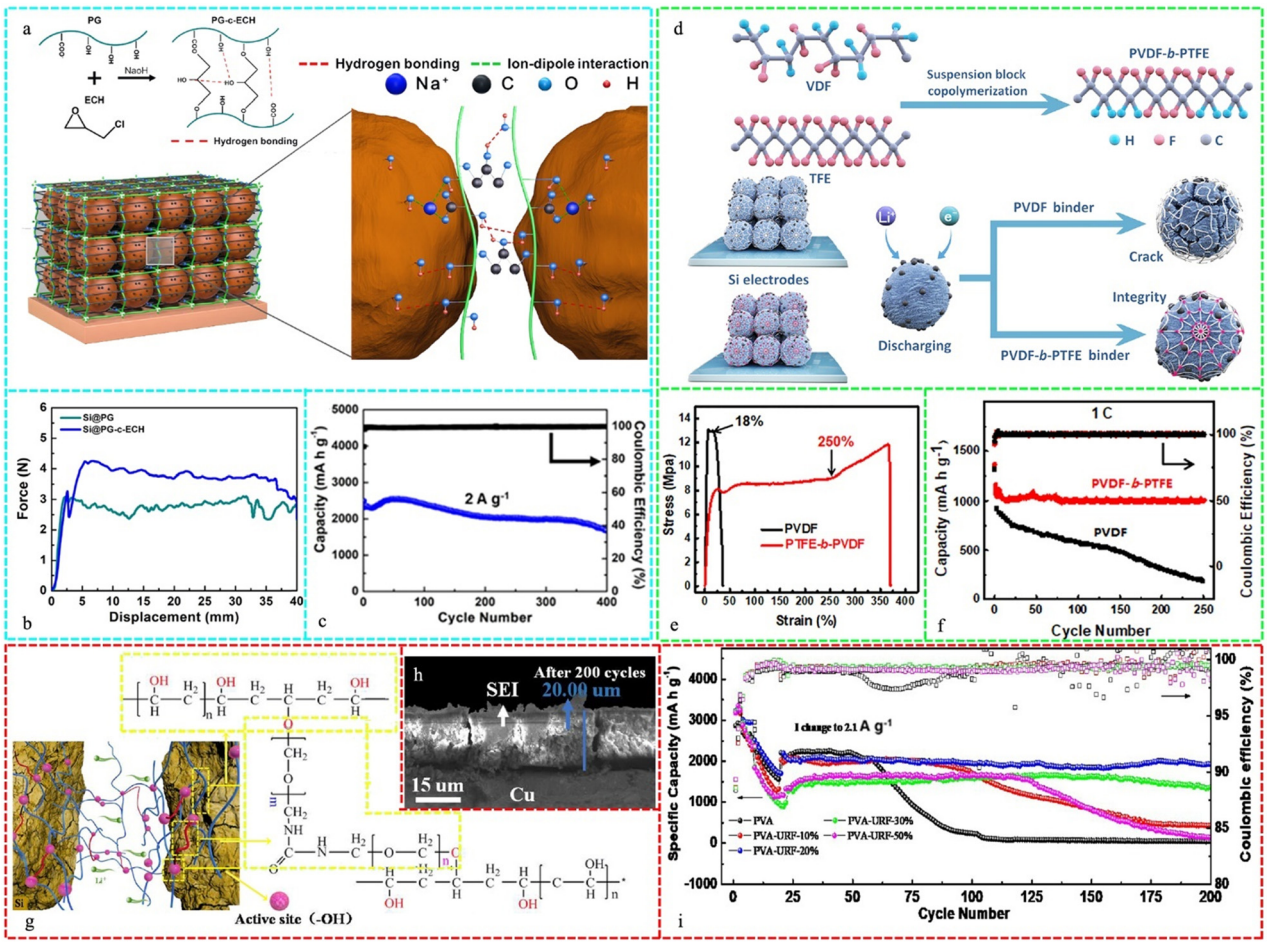

Fig. 7 (a) Schematic illustration of the Si anode using PG-*c*-ECH as a binder; (b) 180° peel test results of Si electrodes with different binders; (c) long-term cycling performance and Coulombic efficiency of the Si@PG-*c*-ECH electrode at 2 A g^{-1}. Reproduced with permission from ref. 229 Copyright 2021, Elsevier. (d) Material synthesis and working mechanism of Si electrodes. (e) Strength–strain curves of PVDF and PVDF-*b*-PTFE and (f) long cycling stability of batteries. Reproduced with permission from ref. 230 Copyright 2020, WILEY-VCH. (g) Mechanism of PVA-UFR binder in Si anode, (h) SEM cross-section images of Si anodes for PVA-UFR binder after 200 cycles and (i) cycling performance of Si anodes with PVA-UFR binders with different UFR grafting contents. Reproduced with permission from ref. 231 Copyright 2021, Elsevier.

h g^{-1} in the 400th cycle, indicating a capacity retention of 72.3% compared to the 2nd cycle at 2 A g^{-1} (Fig. 7c).[229] Wang *et al.* reported the synthesis of PVDF-*b*-PTFE powder *via* the block copolymerization of TFE and VDF solution. Its robust cobweb network kept the crushed Si particles consolidated during battery cycling, maintaining the electrode shape and SEI stability (Fig. 7d). Fig. 7e displays the strength–strain curves of the two dried films. Compared to PVDF, which has weak mechanical properties, the PVDF-*b*-PTFE film showed more than 250% deformation strain and better deformation performance. The battery with the block copolymer binder showed a significant increase in capacity and a CE of ~100% after the second cycle. In the first and second cycles, the electrodes had discharge capacities of 1395 and 1155 mA h g^{-1}, respectively, with an initial CE of 82.7%, which was much greater than that of the PVDF-based electrode (69.5%) (Fig. 7f).[230]

Fig. 7g illustrates the function of the PVA-UFR binder, where the Si anode with the PVA-UFR binder achieved a significantly improved electrochemical performance. The resistivity of the PVA-UFR-based electrode exhibited a slight increase and was significantly lower compared to that of the PVA-based electrode, which is consistent with the considerably thinner electrode, as depicted in Fig. 7h. Fig. 7i displays the cycling performance of the Si anodes with various binders at a current density of 2.1 A g^{-1}, where the PVA-based anodes exhibited a rapid capacity decline after 50 cycles and nearly zero after 100 cycles, which is mostly due to the weak binding ability. However, the PVA-UFR-based anodes exhibited a dramatically enhanced cycle stability. The Si anode with PVA-UFR-20% binder exhibited the highest cycling stability, delivering over 2000 mA h g^{-1} after 200 cycles.[231] In addition to a robust branching network, CMC was covalently cross-linked with PA, which possesses an abundance of sites that can establish stable H-bonds with Si, hence considerably reducing the probability of the cracking of SiNPs. The capacity retention of the complete cell using $LiFePO_4$ as the positive electrode was 88.4% after 100 cycles and the stability of the SEI film was preserved throughout the cycling.[232] A one-pot method was employed to synthesize polyimides (PI) with variable-molecular-weight PEG segments formed by esterifying PEG segments on TMAC and 4,4′-methylenedianiline, and the PI-200 (polyimide copolymerized with PEG-200)-based Si electrode exhibited a high discharge capacity of 2989.7 mA h g^{-1} and maintained 2235.5 mA h g^{-1} during 200 cycles at 0.1C (420 mA g^{-1}).[233] The superior mechanical strength of the 3D-link structure of cross-linked CMC and iminodiacetic acid (IDA) generated by modest *in situ* thermal shrinkage and reaction could effectively control the movement of the SiOx particles and the volume change throughout intercalation and delithiation. The stronger adhesion to an abundance of contact sites allowed the electrode to sustain decent contact with the current collector and the active material, leading to an excellent electrochemical performance. Even after 200 cycles at a current density of 1 A g^{-1}, 70.2% of the original capacity was retained.[234] Cai *et al.* combined furan-modified corn viscose branching arabinoxylan (CFG) with maleimide-PEG to create the CFG-PEG (CFG: corn fiber gum) hydrogel binder. The high concentration of (–OH) and (–COOH) groups in CFG created an abundance of binding sites and improved the adherence of CFGPEG. PEG enhanced the diffusion of Li-ions in the Si particles. This sturdy 3D system infrastructure could efficiently alleviate the volume expansion of Si and keep the electrode intact because of the high mechanical strength of the CFG-PEG binder. Furthermore, after 200 cycles at a current density of 2 A g^{-1}, the reversible capacity was 1500 mA h g^{-1}.[235]

Si anodes containing Alg binder cross-linked with Ca, Ni, Cu, and Fe were compared electrochemically. Although these Alg frameworks bridged *via* transition metal cations constrained the volume expansion of the Si particles, the extended-life cycling efficiency of the anodes differed. Among them, the Si-based anode containing Ni cation-cross-linked Alg exhibited the best reversible capacity, cycle ability, and rate capability.[236] The first reported $Li_4Ti_5O_{12}$ (LTO) electrodes containing SA binder were operated in glyme-based electrolytes and had a significant active material content. The electrodes possessing 87% LTO and 3% SA binder worked better with an outstanding rate capability and great cycling stability for 600 cycles at 1C in the electrolyte.[237] By adding dual-crosslinked Alg with polyacrylamide, the electrochemical performance of the binder improved dramatically. The polyacrylamide adhesive in the electrode prevented the penetration of the organic electrolyte. Furthermore, the ionic and covalent crosslinking in the binder preserved their inherent excellent binding characteristics and improved the Li-ion diffusion. The dual-crosslinked binder helped avoid the volume expansion beyond the inevitable value induced by the active materials in the electrodes during cycling. Thus, after 100 cycles, the Si/C (1/3) electrode retained a high capacity of approximately 840 mA h g^{-1} with exceptional cycle ability.[238]

4.1.3.2 Dynamically cross-linked polymer binders. The distinctive self-healing ability of dynamically cross-linked binders allows for improved force dispersion once the framework is exposed to enormous stress fluctuations and their dynamic reversible bonds can heal fractures, ensuring that the structural integrity of the anodes and Si particles is preserved. Thus, a good cycle performance can be achieved by using a dynamically cross-linked binder that has been reasonably designed to facilitate the volume change in Si particles, while sustaining their integrity.[239]

With the help of H-bonding, Li *et al.* built a soft/hard balanced trifunctional network binder (N–P–LiPN) with mechanical characteristics, good adhesion, and ionic conductivity, which greatly enhanced the electrochemical outputs of Si-based anodes in LIBs, exhibiting the maximum ICE of 93.81% and areal capacity of 49.59 mA h cm^{-2}.[187] CS-*grafted*-polyaniline copolymers (CS-*g*-PANIs) act as innovative electrically conductive, water-soluble, and mechanically strong Si-based anode binder components. Due to its

excellent mechanical qualities and electrical conductivity, the copolymer made of 50% PANI and 50% CS performed the best in the cells. In the 200th cycle, its specific capacity was 1091 mA h g^{-1} and its CE was 99.4%.[239]

Because of its many H-bonds, the unique self-healing poly(ether-thioureas) (SHPET) binder developed by Chen *et al.* completely repaired itself after shearing within just one minute. In this case, given that the Si anode binder could keep the electrode intact, cracks were not formed during the cycling of the battery and the anode exhibited a high rate capability and stable performance across several charges.[240] Polymerization of *N*-acryloyl glycine (NAGA) monomers, which include bisamide functional groups, resulted in the formation of supramolecular polymers with a high number of amide H-bonds and excellent mechanical characteristics. A good cycling performance was demonstrated, with 84% capacity retention after 100 cycles at a current density of 420 mA g^{-1} and 1942.6 mA h g^{-1} after 400 cycles at a current density of 1260 mA g^{-1}. Because of its high H-bonding density, it exhibited excellent mechanical capabilities, and thus effectively limit the volume expansion of Si particles during Li alloying, resulting in the formation of a stable, ultrathin SEI layer.[241]

Mazuozi *et al.* enhanced the mechanical strength of electrodes by utilizing CMC and citric acid, which coordinated with the Cu^{2+} ions migrating from the current collector over the electrode thickness. These cations produced structurally cross-linked connectivity with elastic and self-healing capabilities with the carboxylate groups of the CMC and CA binders. The cyclability of the fully mature electrode was greatly improved compared to the unmatured ones due to their better structural rigidity.[242] A water-soluble polymer binder, PAA-poly(2-hydroxyethyl acrylate-*co*-dopamine methacrylate) was created, which exhibited superior hydrophilicity to liquid electrolytes than PAA. Its sophisticated network architecture with rigid-soft chains and links and *in situ* self-healing reduced the volume change strain in SiMPs. Under a large reversible capacity or electrode loading, the cyclability and rate performance were improved dramatically.[243]

An rGO substrate was employed to construct a high-performance Si adaptable anode for LIBs using graphene and Ca^{2+}-crosslinked SA. This unique method allowed the Si versatile electrode to be self-supported by C materials (rGO and CNTs) and preserved the SiNPs by the crosslinked binder SA. It exhibited good ductility, large capacity, and good cycle stability compared to Si flexible electrodes.[244] Hydrogel Alg binders (M-Alg, M = Mn, Ba, Al, Zn) for Si anodes of LIBs were made by coordinating the chains in the Alg molecule with various cations. Al-Alg and Ba-Alg were the only M-Alg binders with a Vickers hardness of more than 32.0 HV. Unlike the other M-Alg binders, the Ba-Alg binder exhibited a viscosity of 30 270 mPa s. The Si-based anodes with Ba-Alg or Al-Alg exhibited a capacity of approximately 2100 mA h g^{-1} at 420 mA g^{-1} after 300 cycles, while that of the anodes with the other M-Alg binders was around 1500 mA h g^{-1}.[245]

4.1.4 Conjugated conductive polymer binder. Given that Si has poor conductivity, it is commonly mixed with carbonaceous constituents to create Si/C-based composites or other conductive additives to boost its conductivity. Conductive polymer binders not only have superior adherence to traditional binders but can also increase the cycle performance of Si-based anodes by serving as electron or ion transport channels, keeping the overall conductivity of the electrode constant.[246,247]

In Si-based LIBs, polyvinyl pyrrolidone/polyaniline (PVP/PANI), which is a new co-polymer conductive binder, combines the conductivity of PANI with the robustness of PVP. This binder improved the conductivity, adhesion, and stability of the Si anode and LIB electrochemical performance through the intermolecular H-bonds and conductive connection established between PVP and PANI to attain greater bonding, chemical stability, and solubility of the copolymer.[247] Fig. 8a presents a schematic of the fabrication of the Si@SiOx/PANI integrated anode design, where the pre-annealing of commercial Si NPs to form a thin Si–O layer on Si particles is crucial for forming hydrogen bonds between phosphoric acid groups ($-H_2PO_4$) from PA and the surface Si–O layer, enhancing the contact between PANI and the Si@SiOx active particles. As a dopant, PA reacts with PANI, forming a 3D conductive network, which improves the electrochemical reaction kinetics and Li storage in the Si@SiOx/PANI anodes. After 500 cycles at 1 A g^{-1}, the Si@SiOx/PANI-100 electrode exhibited a reversible capacity of 1137 mA h g^{-1}, with a minor capacity loss of 0.072% in each cycle. After 500 cycles, the Si@SiOx/PANi-50 and -200 electrodes exhibited specific capacities of 514 and 674 mA h g^{-1}, respectively (Fig. 8b). Furthermore, the Si@SiOx/PANi-100 and -200 electrodes exhibited a greater rate performance than Si@SiOx/PANi-50. Given that PANi was the only conductive substance, a higher level of PANi enhanced the electronic conductivity and electrochemical reaction kinetics of the Si@SiOx/PANi anode (Fig. 8c).[248]

Fig. 8d demonstrates polymers incorporating 2,2-dimethyl-1,3-dioxane-4,6-dione (Meldrum's acid or MA) and thermally-induced ketene reactions for silicon crosslinking and bonding. After 600 cycles of charge/discharge, the specific capacity of the Si anode was 1,785 mA h g^{-1} with the capacity retention of 58% (Fig. 8e).[249] Plasma-created nano-Si with a specific structure and polymer binder improved the LIB durability and avoided the volume expansion, while coated-c-SiNPs and a new polymer binder decreased the volume variation during anode lithiation/delithiation, resulting in good electrochemical characteristics of 2120 mA h g^{-1} for 400 mA g^{-1} after 100 cycles.[250] Poly(aniline-*co*-anthranilic acid) PAAA, a new Si anode binder, was shown to be electrically conductive and structurally stable. The copolymer with the best electrical conductivity and physical properties had a specific capacity of 1946 mA h g^{-1} in the 50th cycle, keeping 81.6% of its initial capacity on a 1.5 mg cm^{-2} high mass-loaded electrode.[251]

A polyisoindigo derivative (P(iso)) was reported as a novel conductive binder in LIB electrode compositions with C-coated SiNPs (Si@C). The SEI carbon shell stabilized the nanoparticles

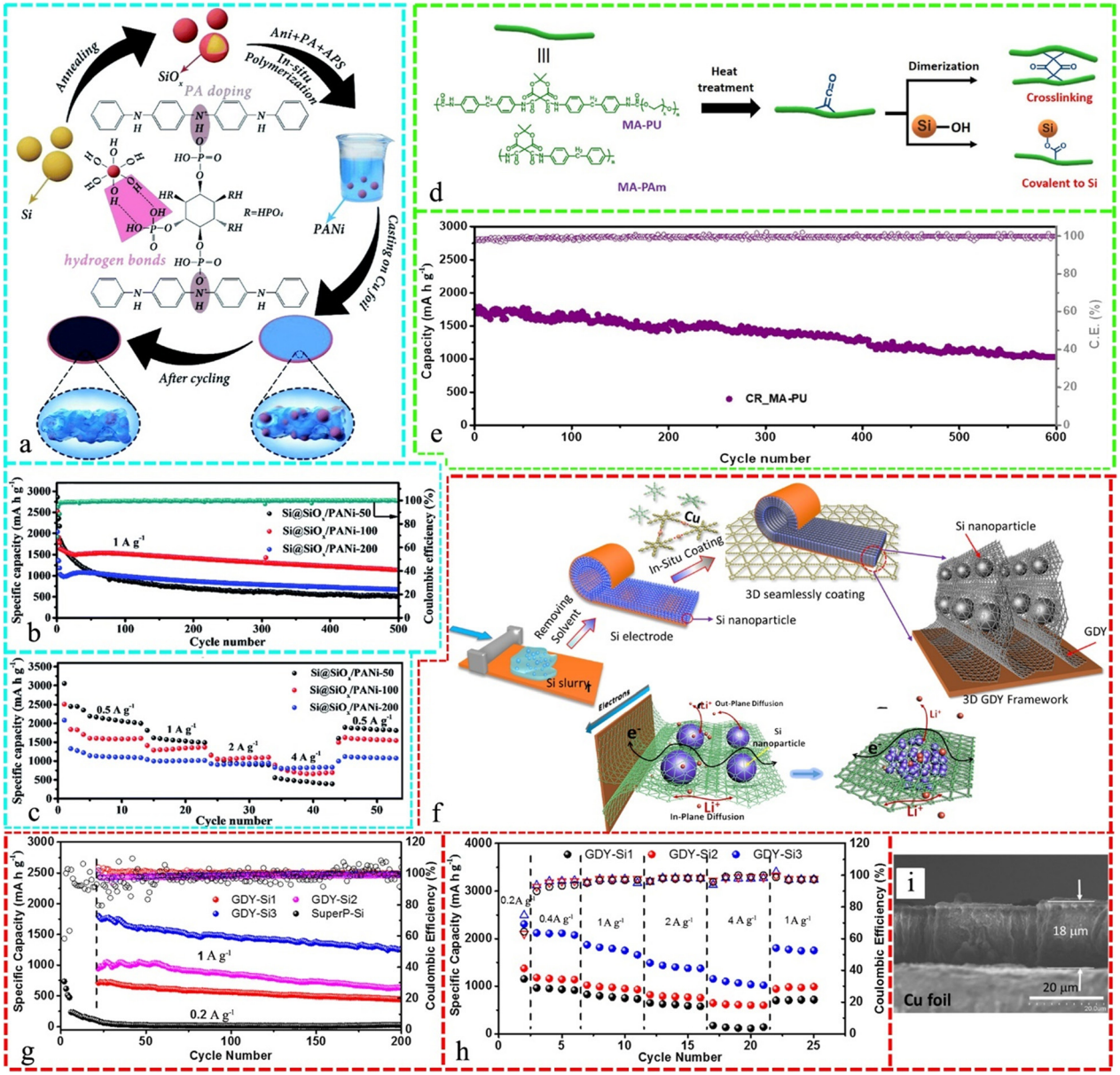

Fig. 8 (a) Schematic of the fabrication of Si@SiOx/PANi-integrated anode and the corresponding electrode stability after cycling. (b) Cycling properties at 1 A g^{-1} and the corresponding CEs of Si@SiOx/PANi electrodes and (c) rate capability of different Si@SiOx/PANi anodes. Reproduced with permission from ref. 248 Copyright 2020, The Royal Society of Chemistry. (d) MA-containing polymers and their thermally-induced ketene-based reactions for crosslinking and bonding to silicon. (e) Long cycling life of CR_MA-PU/Si electrode for 600 cycles at a high current density of 3000 mA g^{-1} (0.8C). Reproduced with permission from ref. 249 Copyright 2021, Elsevier. (f) Schematic representation of the preparation of Si anode seamlessly coated *in situ* by GDY nanosheets, representation of 3D GDY frameworks that seamlessly support and strongly bind SiNPs on the current collector, photographs of a large-scale Si anode before and after *in situ* coating of GDY nanosheets, and double-sided Si anode prepared using this method. (g) Variations in the specific capacity of GDY-Si anodes at various current densities. (h) Long-term cycling stability of GDY-Si and super P-Si anodes at a charge/discharge rate of 1 A g^{-1}. (i) SEM images of the GDY-Si3 anode after long-term cycling tests. Reproduced with permission from ref. 255 Copyright 2018, Elsevier.

and prevented their cracking due to the volume variations during lithiation. The P(iso) conducting polymer can replace carbonaceous additives as a structural binder and n-type conductor. Also, this conductive polymer can replace polymeric binders with carbonaceous additives due to its capacity of 1400 mA h g^{-1} and stability for 500 cycles.[252] Zhao *et al.* synthesized a novel copolymer PFPQ-COONa binder by incorporating 10% phenanthrenequinone (PQ) in the PF-COONa polymer chain. PFPQ-COONa exhibited a remarkable rate capability and cycling performance, maintaining a high reversible capacity of 901 mA h g^{-1} after 400 cycles at a current density of 0.5C.[253]

Poly(1-pyrene methyl methacrylate) and polybutadiene (PPy-*b*-PB) were used to create an n-type conductive binder. Despite the shortage of polar groups and self-assembling

units in PB, the PPy-*b*-PB electrode exhibited greater mechanical integrity than the PPy electrode due to its wider adhesion length scale and reduced stress. The PPy-*b*-PB/Si anode exhibited an excellent ICE of 77.9%, high reversible capacity (2274 mA h g^{-1}), and high capacity retention (87.1%) at 0.2C (0.84 A g^{-1}) over 200 cycles.[254] The ultrathin graphdiyne nanosheet growth method is scalable for the *in situ* formation of 3D all-C mechanical and conductive networks and chemically connecting the current collector with Si anode (Fig. 8f). The well-supported GDY-Si3 sample exhibited a remarkable specific capacity of 2307 mA h g^{-1}, which is equivalent to that of expensive graphene-coated materials (Fig. 8g). Furthermore, after 200 cycles at a current density of 1 A g^{-1}, the GDY-supported silicon anodes, specifically, GDY-Si1, GDY-Si2, and GDY-Si3, maintained strong capacities, reaching as high as 448, 632, and 1250 mA h g^{-1}, respectively (Fig. 8h). Compared to before cycling, the electrode thickness grew by roughly 80% (Fig. 8i), indicating a volumetric increase of more than 80%. The substantial volumetric increase was attributed to the high Si NP content on the anode.[255] The abundant carboxyl groups in the polymer chains bind SiNPs and its n-type polyfluorene backbones ((sodium poly(3,3′-(9*H*-fluorene-9,9-diyl) dipropionic acid) denoted as PF-COONa)) boosted the electronic conductivity in the anodes under a reducing environment, maintaining the electronic integrity during lithiation/delithiation cycles. The polymer without conductive additive in the as-assembled batteries exhibited a reversible capacity of 2806 mA h g^{-1} at 420 mA g^{-1} and cycle stability with 85.2% capacity retention over 100 cycles.[256]

4.2 Constructing composite anode materials

In LIBs, several Si-materials such as nanoparticles (NPs) and microparticles together with various sources of Si have been integrated with many composites such as carbon and its derivatives,[257–259] metal oxides, MXene,[260–262] and other composites such as SiO (ref. 263) to tune the anode materials to enhance their performance in the last few years, which are discussed below sequentially.

4.2.1 Carbon-based composites and its derivatives. The addition of Si to the carbon matrix improves the structural and electrical integrity of Si–C composites. Specifically, carbon-coated Si structures with abundant void spaces between the inner Si core and the outer carbon shell can accommodate the large volume expansion of Si particles, keep the carbon shell intact, and maintain the structural integrity of the electrode during cycling to buffer mechanical stress. Stabilizing Si with carbonaceous materials is the best option because rational structural design may improve the electrochemical performance of Si/C anodes. Carbon coatings can be functionalized as a buffer to tolerate the severe volume change in Si after the electrochemical Li alloying reaction. Also, the ionic and electronic conducting ability of the Si anode can be greatly enhanced, enhancing the electrochemical reaction kinetics of Si with Li. A carbon layer over the external surface of Si can interrupt the direct development of SEI layers on Si and stabilize the electrode/electrolyte interface.

Fig. 9a depicts the synthesis of a peanut-shaped structure, involving the preparation of B-doped Si/C NPs (Si@B–C) through a sol–gel process, followed by thermal reduction. In the HRTEM image, the Si NPs are surrounded by a homogeneous amorphous carbon layer with a thickness of 10 nm (Fig. 9b). The Si@B–C electrode, which resembles a peanut, exhibited exceptional cyclability of 534 mA h·g^{-1} even after 1000 cycles at a high current density of 1000 mA·g^{-1} (Fig. 9c).[264] Fig. 9d presents the successful utilization of ferrocene as the exclusive source of Fe_3O_4 and C in the synthesis of a core–shell-structured Si@Fe_3O_4@C composite. This was achieved through the application of hydrothermal action to wrap an Fe_3O_4@C layer on the surface of Si. In the high-resolution transmission electron microscopy (HRTEM) image (Fig. 9e), two sets of lattice stripes (111) of Si and (220) of Fe_3O_4 are visible, with a carbon layer covering the surface. The development of Fe_3O_4 and carbon coating was influenced by the thermodynamics. The Si@Fe_3O_4@C composite synthesized in this study demonstrated remarkable cycling stability, with a capacity retention of 1026 mA h g^{-1} after 500 cycles at a current density of 1 A g^{-1} (Fig. 9f).[265] Fig. 9g demonstrates the core–shell structured Si@Cu_3Si–Cu NPs, which are enveloped by N-doped C (Si@Cu_3Si–Cu@NC), developed and produced using a two-stage thermal reduction technique. The HRTEM image in Fig. 9h clearly displays the crystal lattice fringes of Si@Cu_3Si–Cu@NC, where the thickness of the NC is around 8 nm, but the thickness of the Cu layer is merely 1 nm. Fig. 9i demonstrates that the integrity of the material structure remained unchanged during the rate performance test. The good mechanical properties of the double shell are responsible for maintaining the structural stability.[266] Polymerization and carbonization created yolk–shell and dual-shell hollow SiNPs@C composites as good LIB anodes given that the SiNPs were homogeneously distributed in the carbon support. The Li-ion anodes constructed using 46 wt% dual-shell SiNPs@C, 46 wt% Gr, 5 wt% acetylene black, and 3 wt% CMC with an areal loading of 3 mg cm^{-2} exhibited a specific capacity of 600 mA h g^{-1}, which was over 100% higher than that of the pure Gr anode.[267]

A hierarchical micro/mesopore smart architecture (Si@void@C@TiO_2) was created *in situ*, with Ti–O–C bond adhesion and protection (Fig. 10a). The TEM images confirmed the carbon coating on the Si@void@C structures, as evident in Fig. 10b. The rate capabilities of Si@void@C (SvC) and Si@void@C@TiO_2 (SvCT) at varying density currents ranging from 0.2 A g^{-1} to 2 A g^{-1} are displayed in Fig. 10c. SvCT performed better than SvC, as predicted, further highlighting the superiority of the unique structure. The SvCT anode showed improved cycling stability, with a specific capacity of 774 mA h g^{-1} for up to 300 cycles. However, the specific capacity of SvC decreased with cycling, particularly after 123 cycles (Fig. 10d).[268] Polymer pyrolysis

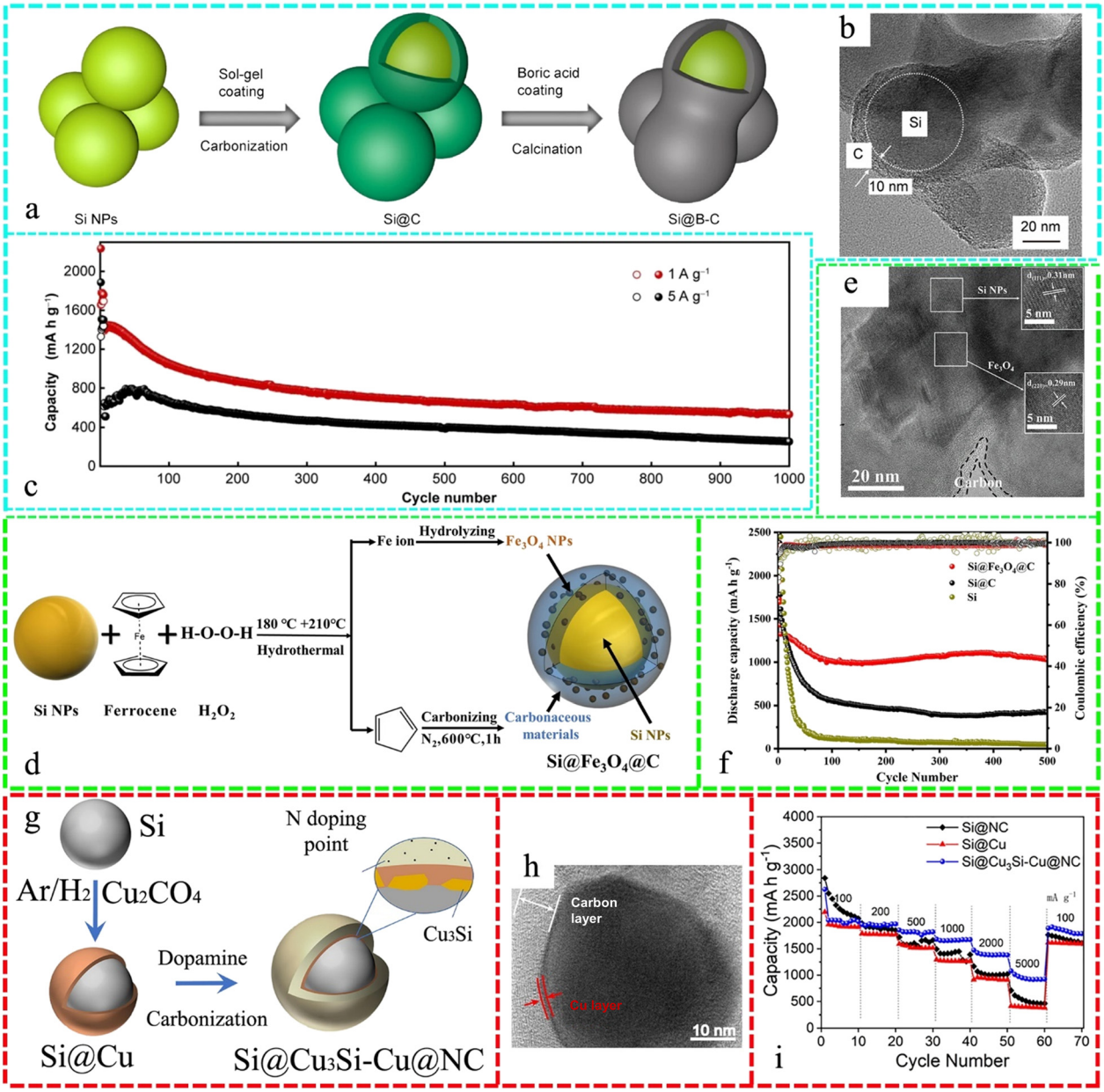

Fig. 9 (a) Schematic illustration of the fabrication process of Si@B–C peanut-like nanostructure. (b) HRTEM images of Si@C nanostructure. (c) Long-term cycling performance of Si@B–C at a high current density of 1000 and 5000 mA g^{-1}. Reproduced with permission from ref. 264 Copyright 2022, Springer. (d) Schematic illustration of the synthesis of Si@Fe_3O_4@C composite. (e) HRTEM images of the Si@Fe_3O_4@C composite, and (f) cycling performance at a high current density of 1 A g^{-1}. Reproduced with permission from ref. 265 Copyright 2023, Springer. (g) Schematic diagram of core–shell Si@Cu_3Si–Cu@NC. (h) HRTEM images of Si@Cu3Si-Cu@NC. (i) Rate performance of Si@NC, Si@Cu, and Si@Cu3Si–Cu@NC. Reproduced with permission from ref. 266 Copyright 2022, Elsevier.

instead of template etching provided a porous structure that accommodates Si volume expansion and promotes ion transport in an Si/C composite. Interwoven CNTs and branch-like carbon black (CB) constituted the conductive framework. The Si/C microsphere anode showed exceptional cycle stability (1325 mA h g^{-1} after 60 cycles with a retention rate of 86.94%) and increased rate capability (925 mA h g^{-1} at 5 A g^{-1}).[269]

A ferrosilicon (Fe–Si)/C nanocomposite (NC) was stable in multiple charge/discharge cycles due to the reduced volumetric expansion of the Fe–Si alloy cores and the outer carbon shell stable contact during the lithiation process. Experimentally, the Fe–Si/C composite anode exhibited a high reversible capacity of 1316.2 mA h g^{-1}, effective mass utilization of 82.6%, long-term cycle durability of over 1000 cycles even at 2.0 A g^{-1}, and high cycling CE of 99.7%.[270] The hierarchical porous structure in the Si core and the abundant void spaces in the CNT arrays permitted Si volume expansion, Li^+ diffusion, and Si utilization in the LIB anode made from NCNTs-Ni_2Si@Si, as illustrated in Fig. 10e. It exhibited remarkable long-term stability over 600

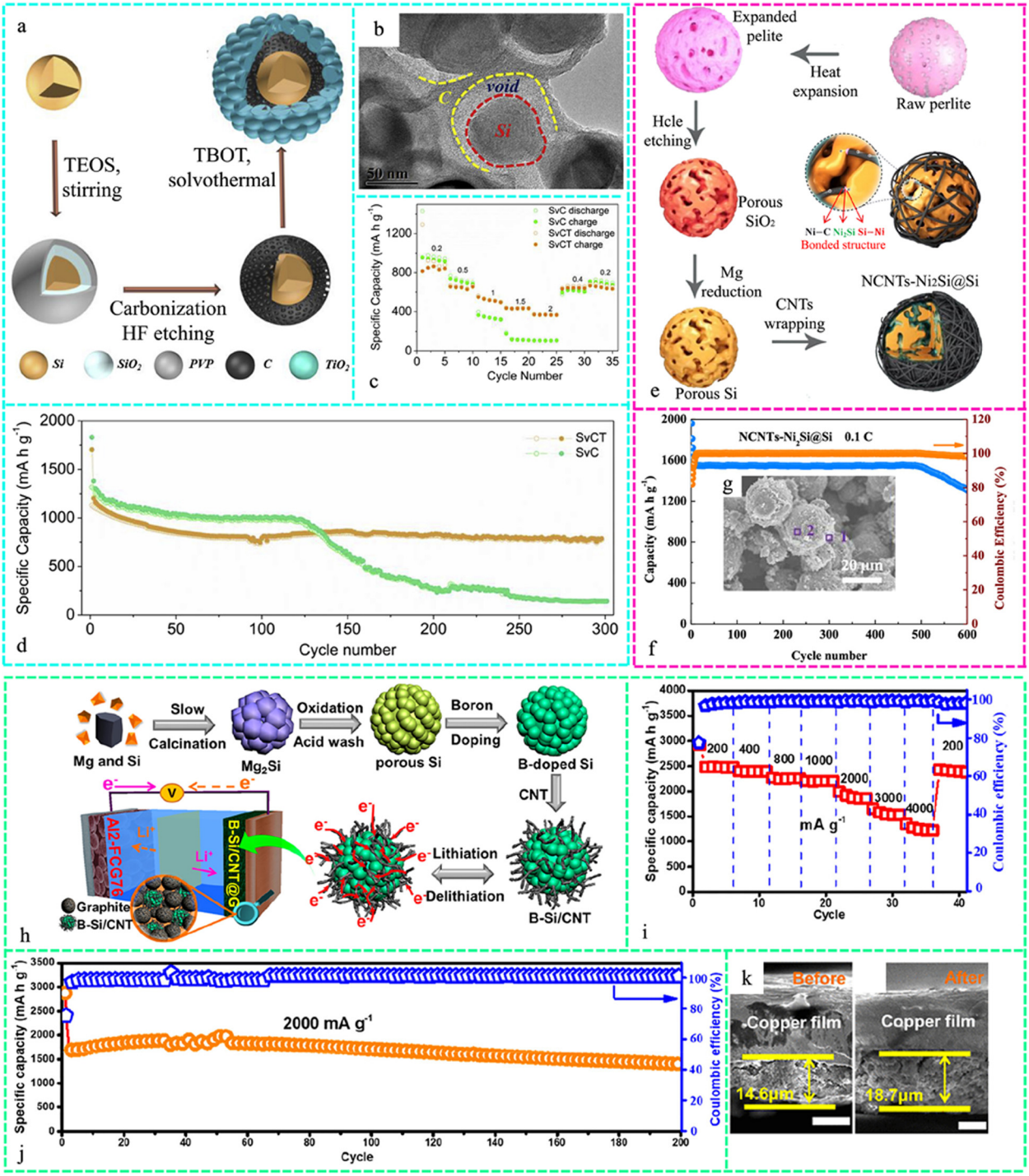

Fig. 10 (a) Schematic illustration of the synthesis and architecture of Si@void@C@TiO_2. (b) TEM images of Si@void@C. (c) Rate capabilities at different densities. (d) Long-term cyclic behaviors of SvC and SvCT. Reproduced with permission from ref. 268 Copyright 2019, Elsevier. (e) Synthesis of NCNTs-Ni_2Si@Si, (f) cycling performance of the NCNT-Ni_2Si@Si electrode at a current density of 358 mA g^{-1} over 600 cycles and (g) SEM images of NCNTs-Ni_2Si@Si. Reproduced with permission from ref. 271 Copyright 2019, the American Chemical Society. (h) Schematic illustration of the synthesis of B–Si/CNT. (i) Rate performance of B–Si/CNT at various current densities. (j) Long cycling performance of B–Si/CNT at 2000 mA g^{-1}. (k) Cross-sectional SEM images of the B–Si/CNT anode. Reproduced with permission from ref. 273 Copyright 2019, the American Chemical Society.

cycles, with a high reversible capacity of 1547 mA h g^{-1} in the first 500 cycles. Even after 600 cycles, the latent capacity remained at 1311 mA h g^{-1} (Fig. 10f). Fig. 10g highlights the SEM image of the NCNT-Ni_2Si@Si anode.[271] Si interacts with Li hexafluorophosphate ($LiPF_6$) to form Li_2SiF_6 aggregates during the cycle. The nanocarbon on Si causes adverse reactions, while

SiC is placed between the Si and carbon layers to inhibit the formation of Li_2SiF_6. The side reaction rate decreased considerably due to the higher reaction activation energy and the Si@SiC@C anode retained a capacity of 980 mA h g^{-1} at 1 A g^{-1} after 800 cycles with an ICE of over 88.5%.[272]

Developing improved Gr electrodes by combining modified Si with the Gr framework can support heavy loading, whereas the customized nano/micro-structured Si with B doping with CNT wedging (B–Si/CNT) can increase the stability, as shown in Fig. 10h. The silicon anode with nano/microstructures also exhibited an excellent rate capability, as revealed in Fig. 10i. Significantly, it could regain a capacity of 2390 mA h g^{-1} after the current density reverted to 200 mA g^{-1}, further showcasing its exceptional ability to handle high charging rates. The cycling performance at a high current density of 2000 mA g^{-1} demonstrated a remarkable capacity of 1415 mA h g^{-1} after 200 cycles, with a cycling retention rate of 88.2% (Fig. 10j). Also, the structure stability was tested *via* SEM images of the anode before and after cycling (Fig. 10k).[273] Compared to alternative deposition methods such as sputtering and CVD, the electrodeposition process is straightforward and cheap to scale up. A flexible Si/CNT composite outperformed Si-based flexible electrodes in the active layer and current collector volumetric capacities. Prelithiation treatment could enhance the poor ICE of the Si/CNT composite, and a complete pouch cell with a flexible Si/CNT anode could light a commercial red LED in the flat or bent state.[274]

Also, 90% Si and 10% Mn/C hybrid electrodes exhibited good cyclability with 82.3% capacity retention after 100 cycles and great rate capability with 880.6 mA h g^{-1} even at 13 A g^{-1}. The excellent performance of the 90% Si and 10% Mn/C electrode was attributed to the inactive Mn_4Si_7 alloy in the composites, which was largely distributed among the nano-Si particles or on their surfaces to connect them and improve the electrode material structure and electrode/electrolyte interface.[275] Spherical Si–C hybrid composite particles were prepared using a simple and scalable microemulsion process, as shown in Fig. 11a. Further investigation of the cycled SN-MCB anode microstructures was conducted utilizing TEM, where the large volume variations of Si particles partially demolished the amorphous carbon layer (Fig. 11b). Fig. 11c shows the exceptional long-term cycling stability of the anode, retaining 80% capacity over 500 cycles and maintaining a high CE of 99.8% throughout regular cycling tests at 0.2C. As illustrated in Fig. 11d, the SN-MCB anode showed rapid charge–discharge up to 10C, retaining 76% capacity at 0.1C (1150 mA h g^{-1} *vs.* 1530 mA h g^{-1}).[276]

By combining graphene oxide-encapsulated SiNPs and soldering with PVDF-derived carbon at the temperature for carbonization, a novel hybrid material (C–Si@G) was created. The 3D conductive graphene network wrapped 50 nm amorphous carbon-coated SiNPs. C–Si@G NC exhibited an Li-storage capacity of 2883.1 mA h g^{-1} at 0.1 A g^{-1}. Also, it showed continuous cyclability with a specific capacity of ~752 mA h g^{-1} after 270 cycles at 5 A g^{-1}.[277] Silane was employed to join Si particles with exfoliated graphite oxide (EGO) sheets and amorphous carbon to create silylated-functionalized EGO/Si@amorphous carbon (3-APTS-EGO/Si@C). 3-Aminopropyltriethoxysilan resulted in covalent bonding between the EGO sheets and SiNPs. Due to the strong covalent interaction and synergistic effect among Si, EGO sheets, and amorphous carbon, the 3-APTS-EGO/Si@C composite retained 97% of its capacity after 450 cycles at 0.4 A g^{-1}.[278]

4.2.1.1 Graphite and graphene-based composites. Graphene exhibits outstanding electronic conductivity, versatility, high Li^+ diffusion efficiency (10^{-8} cm^2 s^{-1}), and a significant conceptual specific area (2630 m^2 g^{-1}), making it an ideal carbon matrix to address the drawbacks of Si anodes. Also, because of its high electronic conductivity, wide specific surface area, structural flexibility, and surface-to-volume ratio, it is a hot topic in energy conversion. Coating Si with graphene and rGO is desirable due to their mechanical flexibility for significant volume expansion.

A simulated macropore-coordinated Gr–Si composite reduced electrode swelling in industrial electrode production. Following 100 cycles in the full-cell configuration, this hybrid anode exhibited a higher volumetric capacity (493.9 mA h cm^{-3}) and energy density (1825.7 W h L^{-1}) than Gr (361.4 mA h cm^{-3} and 1376.3 W h L^{-1}).[258] In Si nanotube-Gr composites (SiNTs), the Si internal pores prevented expansion and allowed 42% Si loading, which is 13–14% greater than the volumetric capacity of the anode of 978 mA h cc^{-1}.[279] Two-step ball milling produced a nanostructured P-doped Si/Gr composite that transported Li-ions and electrons for conductivity. The stable SEI film inhibited Si volume growth. The 50/50 Gr/p-doped Si composite anodes exhibited a capacity of 883.4 mA h g^{-1} over 200 cycles at 200 mA g^{-1}.[280] High-energy ball mills turned micrometer-sized Si and Gr into nanostructured Si/Gr composite building blocks encased in a thin carbon covering and partially etched them to create specific gaps. This tailored nanostructure increased the electrochemical performance over SiNP batteries with a specific discharge capacity of ~1800 mA h g^{-1} in the first cycle, 580 mA h g^{-1} after 40 cycles, and 350 mA h g^{-1} after 300 cycles.[281]

The framework of Si NPs contained in rGO bubble films was anchored in a 3D rGO macroporous network (encapsulated Si@rGO) for LIB anodes utilizing a simple self-assembly technique (Fig. 11e). The Si@rGO anode, enclosed within a protective layer, exhibited exceptional durability in many cycles when subjected to a high current density of 2.5 A g^{-1}. Prior to this, an activation process was conducted at 0.5 A g^{-1} for the initial 3 cycles. Throughout 1000 cycles, the composite anode demonstrated a consistently high average capacity of 1045 mA h g^{-1}, which is more than three-times that of the conventional graphite anode (Fig. 11f).[282] Systematic and scalable self-assembly produced micro nanostructured Gr/Si/rGO composites (SGG). SiNPs were uniformly self-assembled *via* Gr–GO by H-bonds, solving the incompatibility of SiNP-microsized Gr. The SGG anodes (Si

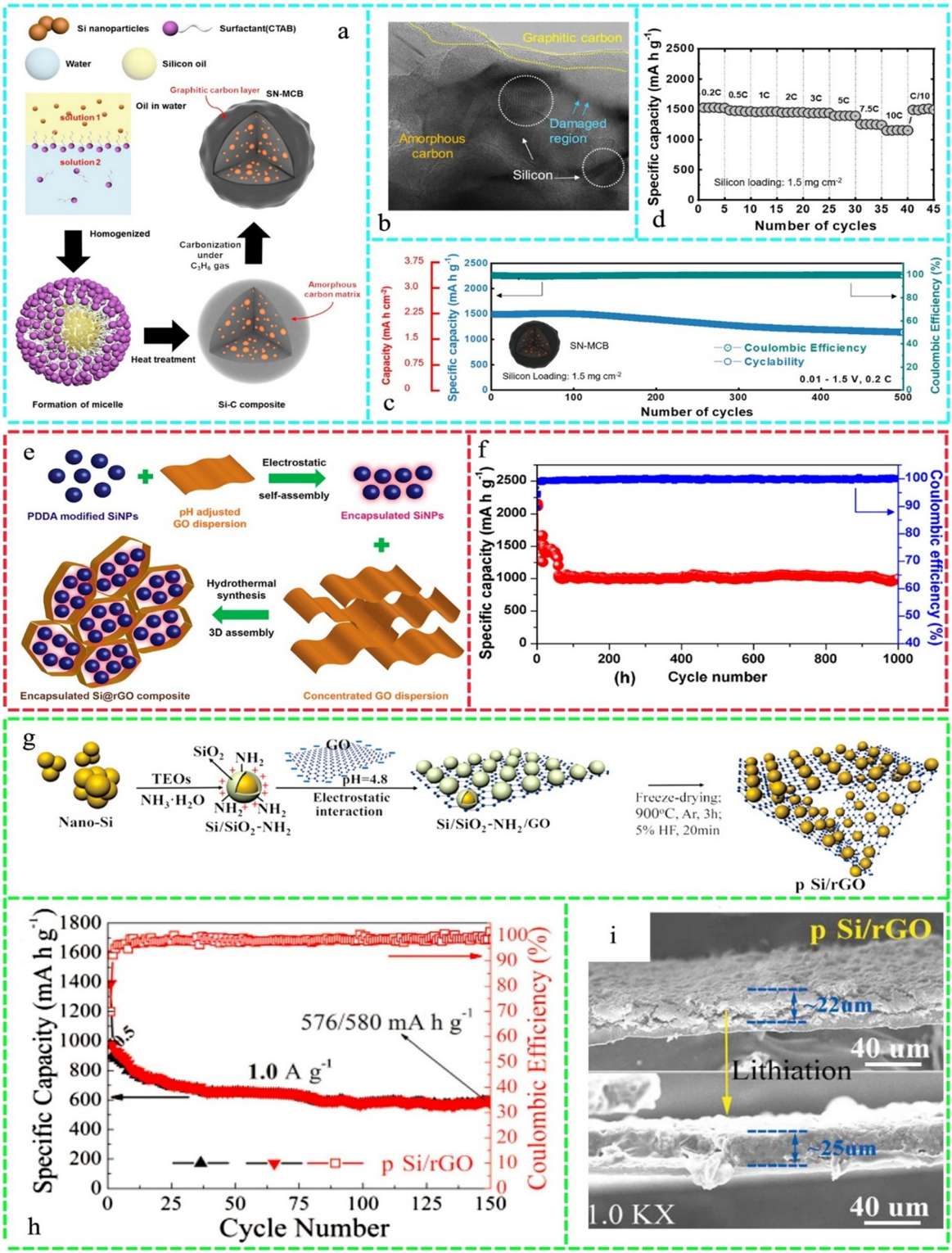

Fig. 11 (a) Schematic illustration of the synthesis of the proposed Si–C hybrid composite material. (b) STEM images of the SN-MCB electrode after 500 cycles. (c) Long-term cycling stability at 0.2 C. (d) Rate capability test. Reproduced with permission from ref. 276 Copyright 2019, the American Chemical Society. (e) Schematic Illustrating the assembly of encapsulated Si@rGO composite and (f) the long-term cycling performance of encapsulated Si@rGO at 0.5 A g^{-1} for 3 cycles and then at 2.5 A g^{-1} for 1000 cycles. Reproduced with permission from ref. 282 Copyright 2020, the American Chemical Society. (g) Schematic illustration of the preparation of p-Si/rGO and Si/rGO. (h) Cycling performance of p Si/ rGO 1.0 A g^{-1} in the potential range of 0.01–1.5 V *vs.* Li/Li^+ and (i) (top) fresh anodes and (bottom) lithiated anodes after 10 discharge/charge cycles at 1.0 A g^{-1}. Reproduced with permission from ref. 286 Copyright 2020, the American Chemical Society.

8%) exhibited reversible Li-storage capacities of 572 mA h g^{-1} at 0.2C, 502.2 mA h g^{-1} over 600 cycles at 0.8C, and 64% even at 10C. Due to their robust structure and 3D conducting network, Gr and graphene sheets can survive the considerable volume change of Si, maintain conductive connections and structural stability, and reduce the side reactions in the electrolyte.[283]

Electrostatic self-assembly and spray drying of spherical Gr/Si/graphene oxides/carbon (Gr/Si/GO/C) composites helped to maintain a high discharge capacity of 1212.0 mA h g^{-1} at 200 mA g^{-1}, 80.4% ICE, and 81.7% capacity retention after 100 cycles. The as-prepared spherical Gr/Si/GO/C composites could buffer the Si volume expansion, preserve the structural integrity of the electrode, minimize Si aggregation, boost the electric and ionic conductivity, and retain Li.[284] Two-step *in situ* carbon coating created a multicomponent carbon-based Si-based composite. The Si@C@RGO composite enhanced the LIB anode performance, with 74.57% ICE and charge capacity of 1474.9 mA h g^{-1}.[285] A nano-Si/rGO porous composite (p Si/rGO) was fabricated by electrostatic self-assembly using SiO_2 as the sacrificial template (Fig. 11g). p-Si/rGO exhibited greater electronic conductivity than the mechanically coupled nano-Si and rGO (Si/rGO) because SiNPs were more uniformly dispersed across the rGO sheets. The cycling performance of p Si/rGO was investigated at a current density of 1.0 A g^{-1}, where its initial charge specific capacity was 971 mA h g^{-1}, with a CE of 69.8%. After 150 cycles, its capacity remained constant at 580 mA h g^{-1}, while its columbic efficiency remained consistently high at around 98.5% in each cycle (Fig. 11h). The p Si/rGO electrode did not undergo significant volume expansion, as seen by the slight increase in thickness from approximately 22 μm before lithiation to approximately 25 μm after lithiation. The visual observation demonstrated that rGO could efficiently accommodate the increased volume of Si due to the presence of pores with a uniform distribution (Fig. 11i).[286]

4.2.2 Metal oxide-based composites. Several metals are utilized as composite anodes, resulting in better conductivity and mechanical properties as well as enhanced electrochemical performance. Transition metal oxides, such as Mn, Fe, Co, Ni, and Cu, can be employed as anode materials. Recent research has focused on using nanoscale metal to activate anodes to increase the ICE during the first lithiation and keep its reversible capacity. Overall, a metal matrix with high electrical conductivity enhances the structural integrity of Si-based anodes.

Using mechanical ball-milling and tunable phase transition, spatially constrained Si-based composites can be easily created by metallic vanadium oxide ($VO_{0.9}$) boundaries. In both SiOx and Si, the scalability of the interface design permits the expansion of transportation channels, while preserving their structural integrity. After 400 cycles, the resulting Ni-doped SiOx anode paired with a manganese oxide cathode still retained 82% of its original capacity and showed an excellent ICE of 84%. Similar results were seen when a mixture of SiO, Ni, and rGO was produced *via* hydrothermal mixing and sintering.[287] The commercially available SiOx and V_2O_5 were used in the synthesis of SiOx@$VO_{0.9}$, as shown in Fig. 12a. The optimal Si-based composite electrodes exhibited an extraordinary Li storage performance, with a high specific capacity of 1249 mA h g^{-1} at 500 mA g^{-1} after 100 cycles (Fig. 12b). The rate performance of these composites was enhanced as the current density increased stepwise from 200 to 5000 mA g^{-1}, while the enhanced capacity observed in the presence of metallic N–$VO_{0.9}$ was attributed to the enhanced electrochemical activity resulting from its inclusion compared to pristine SiOx (Fig. 12c).[288] Using a straightforward electroless plating technique paired with ultrasonication, an SiO/Cu/expanded Gr composite was produced, resulting in a dramatically enhanced reversible capacity and cycling stability.[289] The synthesis of the SiO/Cu/C composites involved Cu deposition in combination with carbon coating (Fig. 12d). The composite SiO/C and SiO/Cu anodes exhibited faster capacity fading, with 24% and 25% capacity loss over 50 cycles and specific capacities of 751 and 694 mA h g^{-1} over 100 cycles, respectively. In contrast, SiO/Cu/C exhibited a superior cycling performance, achieving 1006 mA h g^{-1} over 150 cycles (Fig. 12e). After 150 cycles, the SiO/Cu/C anode material was unchanged and showed a stable stability (Fig. 12f).[290] To speed up the slow kinetics of the electrochemical interactions between SiOx and Li, Kwon *et al.*[291] recently produced vanadium-doped SiOx composites *via* a selective alcoholysis technique, which showed the outstanding reversible capacity of 1305 mA h g^{-1} at 100 mA g^{-1}. Electrochemically active metals can also be incorporated in SiOx to improve the Li-storage efficiency. By milling nanoscale Sn particles with SiO, it was found that the resulting hybrid exhibited a significantly increased specific capacity by 50% and improved ICE from 66.5% to 85.5%.[292] A schematic diagram of the two-step ball-milling technique used to create the composite material consisting of few-layered graphene-wrapped and Fe_3O_4-pillared SiOx (SiOx@Fe_3O_4@FLG) is shown in Fig. 12g. It provided a reversible specific capacity of 833.4 mA h g^{-1} with a high ICE of 84.9% and a capacity retention of 81.8% even after 500 cycles at a current density of 500 mA g^{-1} (Fig. 12h).[293]

4.2.3 MXene-based composites. MXenes exhibit a perfect blend of graphene oxide and graphene characteristics compared to graphene. MXenes are superior to solution-processed graphene membranes in terms of electronic conductivity, making them a promising anode choice for LIBs. Among the MXenes, Ti_3C_2Tx is the most researched due to its strong electric conductivity, negative surface charge, lower ion diffusion barrier, two-dimensional nature, lower operating voltage, mechanical flexibility, and environmental friendliness. Also, it can be easily manufactured into flexible, additive-free films with good electrochemical performance. Thus, two-dimensional MXenes have been employed as flexible freestanding substrates for energy storage due to their characteristics.

In an approach to create flexible and freestanding Si/MXene paper, MXene (Ti_3C_2Tx) was created by selectively etching Al layers of the precursor (MAX, Ti_3AlC_2) with LiF/HCl, and then delaminating them into a dark colloidal solution in deionized water (Fig. 13a). This resulted in

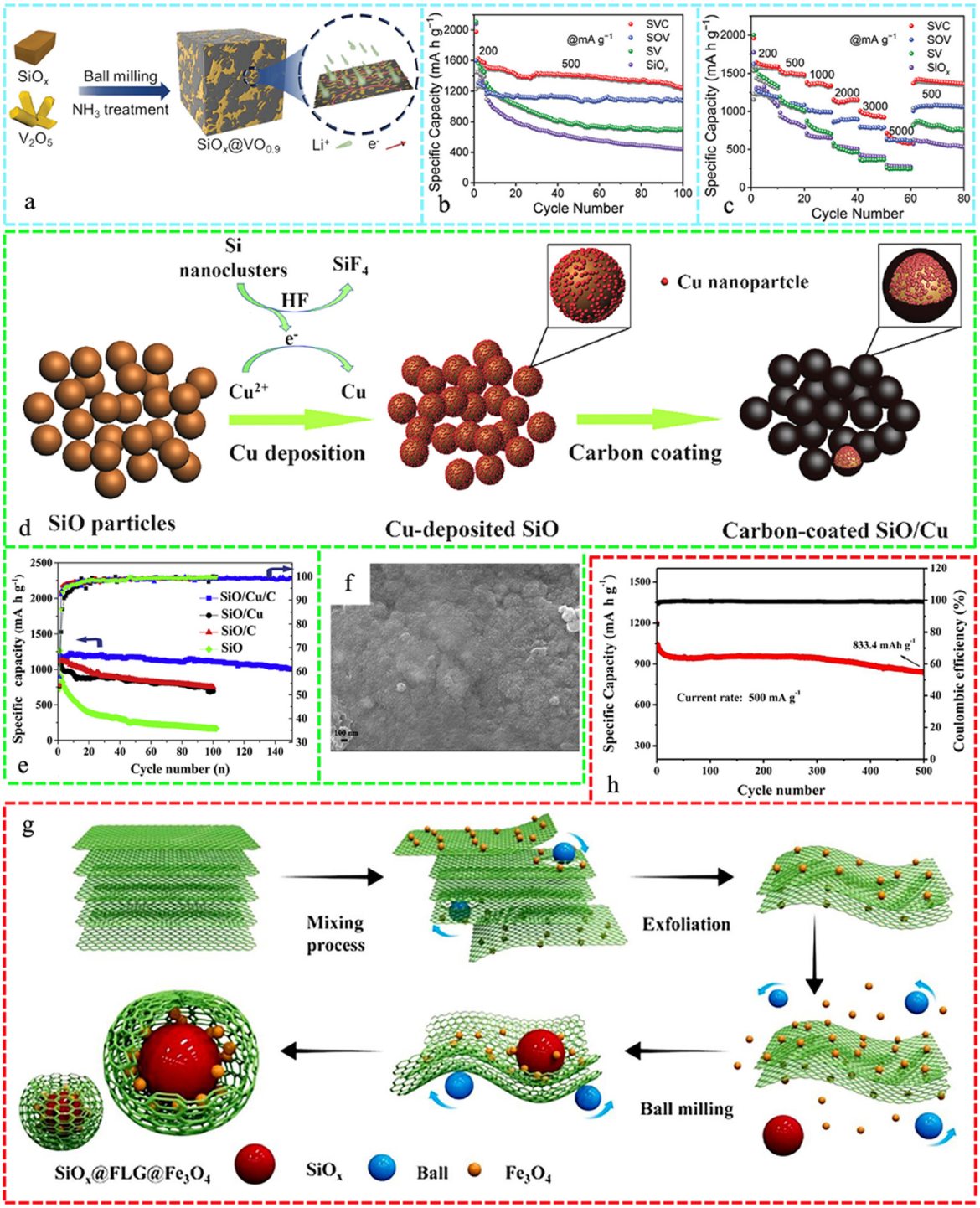

Fig. 12 (a) Schematic illustration of the fabrication of metallic vanadium oxide-confined Si-based composites. (b) Cycling stability at the current density of 500 mA g^{-1}. (c) Rate capabilities at various current densities. Reproduced with permission from ref. 288 Copyright 2022, WILEY-VCH. (d) Schematic illustration of the preparation of SiO/Cu/C composite. (e) Cycling performances of electrodes at a current density of 50 mA g^{-1} for the first cycle and 100 mA g^{-1} for the following cycles. (f) SiO/Cu/C electrodes after 150 cycles. Reproduced with permission from ref. 290 Copyright 2018, Elsevier. (g) Schematic diagram of the two-step ball-milling method for FLG (few-layered graphene)-wrapped and Fe_3O_4-pillared SiOx composites. (h) Cycling performance and corresponding coulombic efficiencies of SiOx@Fe_3O_4@FLG composite electrode at a current density of 500 mA g^{-1}. Reproduced with permission from ref. 293 Copyright 2019, Elsevier.

superior electrochemical behavior with a large capacity of 2118 mA h g^{-1} at a current density of 200 mA g^{-1} after 100 cycles, a stable cycling capacity of 1672 mA h g^{-1} at 1000 mA g^{-1} after 200 cycles, and rate performance of 890 mA h g^{-1} at 5000 mA g^{-1} (Fig. 13b and c). This structure enhanced the conductivity of Si/MXene, prevented sheet restacking,

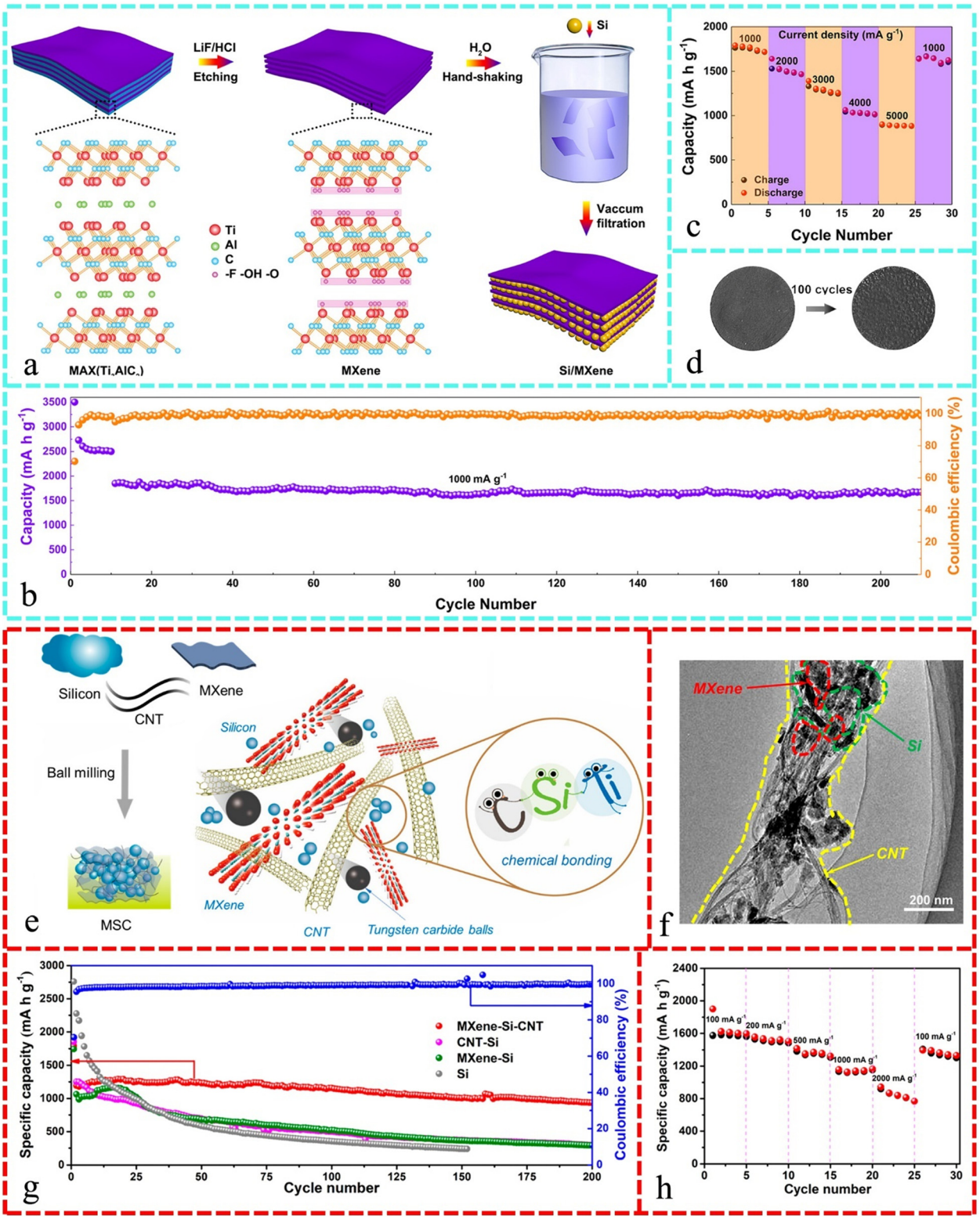

Fig. 13 (a) Schematic diagram of the preparation of Si/MXene composite paper. (b) Long-term cycling capability of Si/MXene anodes at 1000 mA h g^{-1}. (c) Rate ability at varying current densities from 1000 to 5000 mA g^{-1}. (d) Optical photographs before cycling and after 100 cycling. Reproduced with permission from ref. 294 Copyright 2019, the American Chemical Society. (e) Illustration of the synthesis of MSC composites. (f) TEM images of the MSC-60 composite consisting of MXene, Si, and CNT, (g) cycling capabilities and Coulombic efficiency of different anodes and (h) rate performance at different current densities in the same cutoff voltage. Reproduced with permission from ref. 295 Copyright 2019, WILEY-VCH.

provided more active sites, and facilitated efficient ion transport during lithiation. This arrangement could reduce the volume change, as shown by the optical photos of the Si/MXene anodes after 100 cycles (Fig. 13d).[294]

After implementing electrodes at 200 mA g^{-1} for the initial cycle and 500 mA g^{-1} for the subsequent cycles (Fig. 13g), MSC anodes showed a good electrochemical performance. Among them, MSC-60 exhibited the highest initial reversible capacity (1260 mA h g^{-1}), specific capacity (~1000 mA h g^{-1}), and about 80% capacity retention after 200 cycles. The exceptional rate capabilities of the MSC-60 composite were clearly evident, as depicted in Fig. 13h.[260] Dual-bond restricted MXene-Si-CNT composite anodes exhibited good electrochemical properties. The dual-bonding and multidimensional architecture improved the cycle stability of the ball-milled composite. The MXene-Si-CNT composite with 60% Si performed the best with 80% capacity preserved after 200 cycles. Elevated anode materials reduce the detrimental effects of Si.[295] Ultrasonic mixing of commercial nanosized Si and Ti_3C_2 MXene was performed to create Si@Ti_3C_2 NC. The electrochemical tests showed that the NC retained 188 mA h g^{-1} at 0.2 A g^{-1} after 150 cycles, which was better than pure Si. Also, Ti_3C_2 could lower the aggregation of SiNP and the Si–Ti_3C_2 electrical connection could enhance the cycling stability and pace.[296]

4.2.4 Other composites

4.2.4.1 SiO_x-based composites. Si kerf loss slurry was combined with quartz sand waste to form Si/SiO_2 composite LIB anodes, which after 400 cycles at 0.5 A g^{-1}, retained a capacity of 992.8 mA h g^{-1}. The pre-lithiated Si/SiO_2 composites exhibited an improved ICE of >90% by compensating for the irreversible capacity loss in the first cycle. The pre-lithiated Si/SiO_2 composites with $LiCoO_2$ anodes exhibited a greater energy density (459.4 W h kg^{-1}) than Gr anodes.[297] Spray pyrolysis of SiNPs, CA, and sodium hydroxide (NaOH) in water resulted in the formation of an Si–SiOx composite, while NaOH etching of SiNPs produced $[SiO_4]^{4-}$ in the precursor solution. During spray pyrolysis, NaOH catalyzed $[SiO_4]^{4-}$ to form the SiOx matrix and CA to form the C-based surface layer. The best composite structure in terms of Si domain size and Si-to-O ratio achieved 1561.9 mA h g^{-1} at 0.06C rate, 80.2% ICE, and 87.9% capacity retention after 100 cycles at 1C rate.[298] The cheap Al–Si alloy produced double-layer-constrained micron-sized porous Si/SiO_2/C. Primary Si, eutectic Si rods, and Al formed a 3D coral-like porous Si framework with void space and equally conducting sites. The outer C layer improved the mechanical and electrical conductivity. After 100 cycles, the porous Si1/SiO_2/C composite discharged and charged 933.3 and 929.2 mA h g^{-1} at 0.1 A g^{-1}, respectively. The porous Si1/SiO_2/C loops exhibited 0.08% charge attenuation and an Li-ion diffusion coefficient of 4.20×10^{-12} cm^2 $s^{-1/2}$.[99]

Si@SiOx/C NC electrodes with tunable surface oxide layers of 1–10 nm and SiNPs were analyzed. It was found that the oxidation temperature and time determined the surface oxide thickness, Si structure, and valence. SiNP lithiation/delithiation affected the electrochemical performance. Experimental and modeling research showed a suitable surface oxide layer thickness of 5 nm for SiNPs, enabling high capacity and extended cycle stability in Si@SiOx/C NC anodes. Also, surface oxide affects Si/C NC electrodes.[299] After 100 cycles, nanodiamond (ND)-supported carbon nanosheet and SiO_x (SiO_x/ND-C) NC anode LIBs exhibited a capacity of 1182 mA h g^{-1} at 100 mA g^{-1}. After 750 cycles, the current was boosted to 1000 mA g^{-1}, and a high specific capacity of 622 mA h g^{-1} was produced, suggesting improved long-term cycle stability. The nanodiamond buffered Li^+, improving the cycle stability and specific capacity.[300] The Si/v-SC composite electrode exhibited a reversible capacity of 664 mA h g^{-1} in 300 cycles at 0.4 A g^{-1} and a high capacity of 537 mA h g^{-1} at 10 A g^{-1}.[301]

Three-dimensional SiO_2/NGA aerogels were generated *via* the hydrothermal method. In these special aerogels, surface and interface engineering increased their capacity and their 3D architecture accommodated the volume expansion of silica. The SiO_2/NGA NC LIB anodes produced a capacity of over 1000 mA h g^{-1} at 100 mA g^{-1} with cycle life stability. The rate performance tests showed high-capacity reversibility. The SiO_2/pseudocapacitive NGA behavior and enhanced capacitive charge mechanism were discovered.[302] A new simple composition and electrode design technique improved the ICE and cyclability of SiO-based anodes by creating an SiO–Sn–Co/Gr anode. Tiny milled SiO–Sn–Co particles provided a unique structure between two Gr layers. Sn–Co alloys facilitated Li^+ extraction, and the complete reversibility of SiO and Gr increased the electrical conductivity in this hybrid electrode. The SiO–Sn–Co/G electrode had 77.6% aggregate ICE and 640 mA h g^{-1} reversible capacity at 800 mA g^{-1}. Compared to SiO at 55.3% and 50%, its capacity retention was above 98% after 100 cycles.[153] The hierarchical mesoporous/macroporous architecture of Si-based composite materials possesses porosity channel and surface including dual carbon protection layers generated by vacuum adsorption. Due to the regulated mesoporous/macroporous structure and dual carbon protection layers, the LIB cycle stability of the Si/SiO_2@C composite anode material increased. After 200 electrochemical cycles, the hierarchical mesoporous/macroporous Si/SiO_2@C composite material with 13% carbon showed 99.5% capacity retention and reversible capacity of 534.3 mA h g^{-1} at 500 mA g^{-1}.[303]

4.2.4.2 Derivatives. The results for the MSN@C@void@N–C composite revealed that integrating a double carbon layer and intermediate cavity can protect the Si core from electrolyte corrosion, increase the Si-based material electron network throughput, and allow Si volume expansion without destroying the electrode structure. Electrochemically, the MSN@C@void@N–C composites maintained 54.9% of their 2499 mA h g^{-1} discharge-specific capacity after 150 cycles.[151] A preceramic polymer was pyrolyzed to Sn NPs in SiOC. Sn and Si originated from Sn 2-ethyl-hexanoate ($Sn(Oct)_2$) and poly(methylhydrosiloxane). Polymers compatible with $Sn(Oct)_2$ have polar divinyl benzene sidechains. Using this

approach, 5–30 nm Sn NPs were uniformly dispersed in SiOC. The SiOC/Sn NC anodes exhibited capacities of 644 mA h g^{-1} and 553 mA h g^{-1} at a current density of 74.4 with 2232 mA g^{-1} (C/5 and 6C rates for Gr), respectively, and better rate capability with 14% capacity deterioration at higher currents.[304]

In situ polymerizing polyaniline on Si particles, carbonizing, and steam activating produced Si/PANI-AC composites. Activation formed 1–2 nm micropores in the C layer and maintained the Si particle crystal structure and shape. The Si/PANI-AC composites discharged 1000 mA h g^{-1} at 1.5 A g^{-1}, 1692 mA h g^{-1} at 0.2 A g^{-1}, and 1453 mA h g^{-1} after 70 cycles.[305] Etching Al_2O_3 with diluted HCl created void space in the external nitrogen-doped carbon (NC) shell generated by CVD using a pyridine precursor and the interior porous Si nanorods (p-Si NRs) synthesized by magnesiothermic reduction of ordered mesoporous silica nanorods. The p-Si NRs@void@ NC composite exhibited an initial discharge capacity of 3161 mA h g^{-1} at 0.5 A g^{-1}, excellent cycling characteristics up to 300 cycles, and super rate performance.[93] Two-step thermal reduction of commercial wheat flour yielded a carbon-encapsulated Si composite, which exhibited a stable gravimetric capacity of 1500 mA h g^{-1} Si (700 mA h g^{-1} composite mass) after 90 galvanostatic cycles at C/20. The multi-rate cycling displayed that the Si/C hybrid has a stable gravimetric capacity of 830 mA h g^{-1} at C/10 and 300 mA h g^{-1} at 1C. After continuous cycling, the C/Si hybrid exhibited greater mechanical and electrochemical durability than the unencapsulated Si anode, *i.e.*, stronger composite conductivity (4-times larger after complete lithiation), inferior anode deformation, and less SEI growth.[306]

Nano-Si@NG with pyrrolic type N doping exhibited a reversible capacity of 950 mA h g^{-1} over 100 cycles in LIB performance testing, well surpassing SiNPs. Density functional theory (DFT) simulations demonstrated that pyrrolic type N-doped graphene has the lowest energy blockade for Li-ion transport in the NC structure. This results in a high-capacity nano-Si-based LIB architecture.[307] One-step selective dealloying of the SiTiAl ternary alloy under mild conditions yielded core–shell nanoporous Si@TiO_2 composites. The as-prepared composites possessed a bimodal Si network skeleton core and an interconnected TiO_2 nanosponge shell. The nanoporous TiO_2 outer protective layer decreased the electrode material volume change for stable cycling and shortened the Li^+ diffusion paths for high-rate capabilities. The internal bimodal porous Si had an open bicontinuous system topology, providing enough space and a resilient pillar to relax the composite volume dissimilarity and ensure adequate electrode–electrolyte contact area. After 120 and 100 cycles of continuous testing, the enhanced nanoporous Si@TiO_2 composite exhibited a reversible capacity of 1338.1 mA h g^{-1} (after 200 cycles), 1174.4 mA h g^{-1} (after 120 cycles) and 1000 mA h g^{-1} after 100 cycles.[308]

Si-incorporated SnO_2 with graphene NC anodes (STOG) were prepared by hydrolysis, equally distributing ultrafine Si-incorporated SnO_2 (STO) NPs over graphene sheets. Si increased the Si–O–Sn bonding in the SnO_2 matrix and Sn–O–C bonding in STO-graphene. These advantages increased the structural stiffness and electron/ion transport in STOG NC, enabling Sn–SnO_2 conversion. After 100 cycles at 0.1 A g^{-1}, this STOG material retained 92.5% of its second capacity at 1117.8 mA h g^{-1} and 683.9 mA h g^{-1} at 1 A g^{-1}.[309] Polyurethane (PU)/Cu/Si NC films were easily manufactured using increased layer-by-layer self-assembly. This method minimized the particle aggregation in the NCs and efficiently combined the normal properties of the three construction components, *i.e.*, Li storage of Si, electro-conductivity of Cu, and stretchability of PU. The multifunctional films were ideal anodes for Si volumetric change and electrochemical cycles due to their mechanical flexibility (electro-conductivity of 8 S cm^{-1} and tensile strength of 8.2 MPa with 125.1% strain). After 300 cycles at 1C, the NC film electrodes exhibited a capacity of 574 mA h g^{-1} and 99.2–99.8% CE.[310]

4.3 Adopting liquid electrolytes

Several electrolytes have been used over the years to enhance the outputs such as the cyclic durability of Si-based anodes.[127,128,311,312] Regardless of the Si-based electrode material, the role of the electrolyte in ion transport and interphase creation is similar. Thus, rather than reviewing these considerations, we discuss the research on the involvement of the electrolyte in LIBs.[157,313,314] The mechanical properties of Si-based anodes are vulnerable to the formation of a solid SEI. In this section, several liquid electrolytes (2017–2022) are discussed (Table 2) and divided into the respective subsections. Among the various studied electrolytes such as conventional liquids, ionic liquids, and solid electrolytes, hybrid electrolytes are not considered here due to their intrinsic variation in chemical, physical, and electrochemical characteristics.

4.3.1 Solvents/cosolvents. The main function of the electrolyte solvent is to speed up the ion transportation and enable complete salt dissociation. Single compounds typically only permit one of these two requirements, and thus mixed solvents are frequently utilized as an interim solution.

4.3.1.1 Organic carbonate-based solvents. FEC, propylene carbonate (PC), and vinylene carbonate (VC) are the main organic carbonate-based solvents studied to date. Using $LiPF_6$ in FEC and VC as the electrolyte formulation, solid-state nuclear magnetic resonance (NMR) was used to explore Si NW electrodes. The achieved cycling performance was improved among the electrolytes considered, even that using FEC in the first 50 charge/discharge cycles. The SEI in the unadulterated solvents was abundant in branching or cross-linked poly(ethylene oxide) (PEO), close to the SEI found in electrolytes that have FEC additive, but different to the predominantly linear PEO initiated in the electrolytes that do not contain FEC additives according to scientists.[315] In the case when FEC was not used as an additive, it is typically used as a substitute for EC. This substitution results in an

Table 2 Summary of liquid electrolytes utilized in recent years

Electrolyte category	Added as	Electrolyte name	Anodic Si type	Insight into performance	Authors (year)/ref.
Organic carbonate	Solvents/cosolvents	FEC	Si NW	Cycling performance was superior	Jin *et al.* (2018)[315]
	Solvents/cosolvents	FEC	SiOx-Gr	Increased cycling performance	Kong *et al.* (2020)[317]
	Solvents/cosolvents	FEC	Si/Gr	Improved cycling performance	Zhao *et al.* (2021)[316]
	Solvents/cosolvents	FEC	SiNPs-MWCNTs	Consisting of significant portions of reduced SEI	Yao *et al.* (2018)[318]
Ethar based solvents	Solvents/cosolvents	BTFE	Si–Gr	Showed increased cycling performance	Jia *et al.* (2019)[319]
	Solvents/cosolvents	BTFE	Si–Gr	Less SEI formation	Jia *et al.* (2020)[320]
	Solvents/cosolvents	MTHF	Microsized Si	Outstanding cycling performance	Chen *et al.* (2020)[321]
Sulfur-based organic solvent	Solvents/cosolvents	Dimethyl sulfite (DMS) and diethyl sulfite (DES)	Gr–Si	Significant improvement in cycling performance	Liu *et al.* (2021)[322]
Sulfonimide-based salts	Conducting salts	LiTFSI	Gr–Si	Significant improvement in cycling performance	Liu *et al.* (2021)[322]
	Conducting salts	LiTFSI	Thick Si film (100 nm)	Non-uniform SEI development	Haruta *et al.* (2018)[323]
Organic salts	Conducting salts	LiBOB	Si–Gr	Showed better performance at lower currents and higher temperature	Hernández *et al.* (2020)[324]
	Conducting salts	LiTDI	Si–C	Better performance than with marketable $LiPF_6$-based electrolytes	Niedzicki *et al.* (2017)[325]
Organic carbonate-based additives	Functional additives	FEC and VC	Si NW	FEC reduction by studying the formed SEI	Jin *et al.* (2017)[326]
	Functional additives	MEC	Si–Gr	Improve the cycling performance like FEC	Nguyen *et al.* (2018)[327]
	Functional additives	DMVC-OTMS	Si–C	Pointedly increases flexibility and avoids particle fracture	Park *et al.* (2021)[328]
	Functional additives	TFPC	Si NW	10% of TFPC resulted in higher performance than 10% FEC	Hu *et al.* (2019)[329]
	Functional additives	DFEC	SiO_x/C	Significantly improved cycling performance when 2% of DFEC was used	Shen *et al.* (2019)[330]
Carbonyl-based additives	Functional additives	CO_2	Si thin film	SEI formed in CO_2-containing electrolytes is thinner and electronically insulating, resulting in an improved CE	Hopkins *et al.* (2021)[331]
Li salts	Functional additives	LiBOB	Si NW	Strange unstable performance in the cycling observed for VEC	Kennedy *et al.* (2017)[332]
Phosphorus-based additives	Functional additives	TMSPi	Si/C	Significantly enhanced the cycling performance	Liu *et al.* (2020)[333]

enhanced cycling efficacy for diverse Si-based anodes in contrast to the traditional organic carbonate-based electrolytes.[316]

4.3.1.2 Ether-based solvents. 1,1,2,2-Tetrafluoroethyl-2,2,3,3-tetrafluoropropyl ether (TTE), bis(2,2,2-trifluoroethyl)ether (BTFE), dimethoxyethane (DME), tetrahydrofuran (THF), 1-methyltetrahydrofuran (MTHF), and 1,3-dioxolane (DOL) are the ether-based solvents utilized for Si-based anodes in LIBs to date.

Yang and colleagues reported the preparation of an LiFSI-based electrolyte utilizing DME together with TTE solvents. Their findings indicated that this electrolyte outperforms the current state-of-the-art organic carbonate-based alternative when used on Si thin film electrodes. According to the experiment, the SEI exhibited a layered composition, wherein the inner layer was characterized by a high concentration of silicates, LiF, and sulfites, whereas the exterior deposit was predominantly composed of polyethers. The enhanced galvanostatic cycling performance was ascribed to the distinctive SEI architecture, which facilitates structural modifications, while preserving the pliable polyether SEI-forming layer.[334]

A significant enhancement in cycling performance was observed when comparing TTE-containing electrolytes to electrolytes without TTEs. Yang *et al.* discovered that glyme-constructed electrolytes containing higher TTE contents exhibited reduced interface resistance and substantially reduced SEI breakage.[334] Another study attributed the enhanced cycling performance in their phosphate-containing electrolyte to the more robust involvement of LiFSI in the development of the SEI induced by TTE. This was achieved by the modification of the coordination of Li^+ in the bulk electrolyte.[335] TTE in conjunction with dimethyl carbonate (DMC), sulfolane, and FEC in an $LiPF_6$ electrolytic solution

was employed by Kong and colleagues. Nonetheless, the absence of a comparative analysis with alternative compositions precludes a definitive determination of the precise influence of TTE on the interphase chemistry in this instance.[336]

4.3.1.3 Phosphate-based organic solvents. Yang *et al.* used 2-(2,2,2-trifluoroethoxy)-1,3,2-dioxaphospholane-2-oxide (TFEP) as a cosolvent in an LiFSI-based non-flammable electrolyte with SiO-based electrodes. It was shown that the cycle performance using the organic carbonate-based FEC-free electrolyte was superior. In addition to polyphosphoesters produced by TFEP decomposition, the authors discovered the formation of a thin SEI composed of inorganic chemicals. The experiment indicated that the presence of the polyphosphoesters improved the flexibility of the SEI, which was the cause of the excellent performance.[335]

4.3.2 Conducting salts. To ensure the proper functioning of rechargeable LIBs, it is necessary for the utilized electrolyte salt to satisfy certain fundamental criteria, as follows: (i) the solute must exhibit complete dissociation in the respective solvent, (ii) the anion must be withstand electrochemical breakdown on the electrodes and (iii) the anion must possess the ability to ensure the extended durability of various cellular constituents, either through its inert nature or by creating a protection layer, such as in the case of protecting the aluminum current collector.[337] This section is focused on the literature prioritizing Li salts besides $LiPF_6$, which is the primary electrolyte salt. Also, the inclusion of minor quantities of additional salts in the electrolyte in the last few years is considered as additives and will be addressed in the relevant section.

4.3.2.1 Sulfonimide-based salts. LiTFSI was employed in sulfite-based electrolytes by Liu *et al.* for the Si/Gr composite electrode operated at a low temperature of −20 °C. However, LiTFSI was not only the sulfur source and no evaluation was made comparing it with $LiPF_6$-based electrolytes, and thus it is impossible to infer the specific impact of LiTFSI.[322]

Haruta *et al.* employed LiTFSI as a replacement for $LiPF_6$ in an EC/DEC solvent blend with the aim of protecting the employed *in situ* atomic force microscopy (AFM) arrangement from HF. The non-uniform formation of an SEI was discovered on Si thin film anodes, which was linked to the suboptimal cycling performance. However, a direct comparison with the electrolyte based on $LiPF_6$ was not conducted.[323]

In their study, Jia and colleagues employed previously reported non-flammable electrolytes based on lithium bis(fluorosulfonyl)imide (LiFSI), BTFE, and TEP. These electrolytes were paired with Si–Gr composite electrodes, resulting in a noteworthy enhancement in the cycling performance of full cells at a high temperature (45 °C). This improvement was observed in comparison to an $LiPF_6$-based organic carbonate electrolyte that contained FEC as an additive. The observed enhancement was ascribed to the creation of an SEI that is rich in LiF, which is a result of the electrochemical decomposition of LiFSI.[319]

4.3.2.2 Organic salts. Hernandéz *et al.* performed an experiment to inspect the impact of fluorine-free electrolytes on Si–Gr composite anodes in a full-cell configuration, with the aim of developing electrolytes that are more environmentally sustainable. The inclusion of lithium bis(oxalato)borate (LiBOB) as the electrolyte salt resulted in the production of an SEI rich in oxygen-containing compounds, in contrast to the SEI rich in LiF observed with $LiPF_6$. Although the electrolyte without fluorine did not exhibit a superior performance compared to the electrolyte containing $LiPF_6$ during standard cycling conditions, it demonstrated improved efficacy at elevated temperatures and lower currents.[324] Subsequently, the lithium 4,5-dicyano-2-(trifluoromethyl)imidazolide (LiTDI) electrolyte formulation was augmented by Niedzicki *et al.* to realize an inclusive better performance than viable $LiPF_6$-based electrolytes.[325]

4.3.3 Functional additives. Various methods have been proposed for modifying the specific properties of LIBs, including cycling performance, shelf life, and flammability. Among them, the most straightforward, cost-effective, and scalable method involves the incorporation of electrolyte additives. These compounds are added in small quantities (such as ≤10% in volume, weight, or moles) to the electrolyte solution.[338] In contrast to solvents and conducting salts, functional additives may have less stringent requirements for their properties. This is because certain additives are intentionally included in the electrolyte for the purpose of decomposition on the electrodes. Consequently, the desirable characteristics of additives are dependent on their designated role in the battery.[339]

4.3.3.1 Organic carbonate. Jin *et al.* conducted a comprehensive investigation utilizing both liquid and NMR spectroscopy in conjunction with ^{13}C-labelled FEC. The objective was to further comprehend the method of FEC decomposition by analyzing the electrolyte and SEI formed during various stages of cycling.[326] Nguyen and Lucht conducted a study on the usage of methylene ethylene carbonate (MEC) as an electrolyte additive in various Si-based anodes. When incorporated at a concentration of 10% in the traditional electrolyte for Si/C composite anodes, MEC exhibited a comparable enhancement in the cycling performance to FEC. The researchers observed the development of poly(MEC) on the surface of the anode, whereas the cathode remained largely unaffected by the additive.[327]

Park *et al.* synthesized two additives, DMVC-OCF_3 and DMVC-OTMS, derived from VC. These additives were utilized in a minimal quantity of 0.5 wt% in combination with VC in a traditional electrolyte and used in NMC811||Si/C-based cells. This study revealed that the utilization of additives resulted in the modification of the VC-based SEI, leading to a considerable enhancement in its pliability, thereby mitigating the occurrence of particle fragmentation. Elevated quantities of LiF were detected, together with reduced $LiPF_6$ decomposition. In addition, it was observed that the trimethylsilyl functional groups in the oxol-2-one (DMVC-

OTMS) compound acted as an HF scavenger, resulting in a decrease in transition metal dissolution, and ultimately an improved cycling performance.[328]

Hu *et al.* utilized trifluoropropylene carbonate (TFPC) in place of an additive in a traditional electrolyte with Si NW electrodes, in which 10% TFPC outperformed 10% FEC. The formation of a strong SEI that could withstand breakage helped to protect the electrode. According to the authors, the enhanced performance was caused by the good polyolefin to LiF ratio, which produced an instinctively robust SEI that efficiently impeded solvent and salt breakdown.[329] In their study, Shen *et al.* utilized 1,2-difluoroethylene carbonate (DFEC) at a concentration of 2% in a traditional electrolyte for NCA||SiOx/C-based cells. Their study revealed a noteworthy enhancement in cycling performance with the administration of 2% DFEC, while a substantial decrement in cycling performance was detected when 3% DFEC was utilized. The XPS findings suggested that DFEC as the cathode electrolyte plays a significant part in the development of an SEI film, leading to an increase in the concentration of carbon–fluorine (C–F) compounds and Li_2CO_3 on the surface of the anode. Based on the diminished Si–O and SiOx signals, it was inferred by the authors that DFEC has the ability to stabilize the Si particles and impede their deterioration.[330]

4.3.3.2 Carbonyl-based functional additives. Later, Hopkins *et al.* added precisely 2.00 mL CO_2 gas to the studied cells utilizing a unique pouch cell setup with a standard electrolyte, Si thin film anodes, and Li counter electrodes. They showed that the existence of CO_2 caused the creation of supplementary PEO-identical species, which were individually weakly adhered to the external surface, and then removed when the anodes were washed. They demonstrated that the insoluble portion of the SEI is formed by a thinner, much more LiF-rich electrolyte compared to the CO_2-free electrolyte. The SEI produced in the electrolytes covering CO_2 was generally thinner and more electrically insulating, leading to an enhanced CE.[331] To combine the advantages of two additives, one of which was lactide (LAC), Nölle *et al.* created a new additive (lacOCA and DEDC). Poly(lactic acid) (PLA), a product of LAC, allowed the formation of useful layers. It was shown to greatly enhance the cycling performance of NMC111||Si thin film cells after its addition in a content of 2 wt% to a traditional electrolyte. However, the analysis of the generated SEI showed that LAC was only partially effective in preventing the degradation of EC on the Si-based electrode. Additionally, the ratio of Li fluorophosphate to LiF in the SEI increased as a result of the addition of LAC.[340]

4.3.3.3 Li salts as functional additives. In the study by Rezqita *et al.*, they incorporated 5% LiBOB in a traditional electrolyte for Si/C-based anodes. Initially, the capacity achieved with this electrolyte was the lowest among the electrolytes considered. However, after continuous cycling, the capacity increased, and eventually developed to the second highest after 100 charge/discharge cycles. The findings of the XPS investigation were determined to be consistent with previously reported results.[341] High-capacity NMC811||SiOx cells were used in several distinct additive studies conducted by An *et al.* An ordinary $LiPF_6$/organic carbonate-based electrolyte including lithium difluoro(oxalato)borate (LiDFOB) served as the basic electrolyte in the experiment. However, because the B species was not examined, it was impossible to regulate the precise consequence of LiDFOB given the existence of many other additives.[342]

5 Conclusion and outlook

The utilization of Si-based anodes has attracted considerable interest for the advancement of LIBs owing to their elevated theoretical specific capacity, which exceeds that of conventional graphite anodes by around tenfold. Also, significant breakthroughs have been achieved by researchers and corporations in tackling the issues associated with Si-based anode technology (Table 3).

The utilization of Si-carbon composite anodes involves the integration of Si with conductive carbon materials, such as graphene and carbon nanotubes. This amalgamation serves the purpose of preserving favorable electronic conductivity, even in the presence of volumetric fluctuations experienced by the Si component. This phenomenon results in enhanced

Table 3 Low-cost, facile manufacturing Si-based anode performance

Structure	Technique	Challenges overcome	Cyclic performance	Current density	Cost	Ref.
$AlSi_6P$ with graphite	Mechanical ball milling	Superior reaction kinetics, higher metallic conductivity	1058 mA h g^{-1} after 500 cycles	2000 mA g^{-1}	Simple and low cost	343
Ternary layered BiSbSi	Mechanical ball milling	High electronic conductivity and faster Li-ionic diffusion capability	561 mA h g^{-1} after 1000 cycles	2 A g^{-1}	Low cost	344
SiSMPs@TA-PAA	—	Excellent cycle stability and rate performance	2002 mA h g^{-1} after 100 cycles	2 A g^{-1}	Simple, green, and cheap	68
3-Layer graded Si	Three-step casting process	Higher capacity and capacity retention, higher coulombic efficiency, and higher effective mass loading	1299 mA h g^{-1} after 50 cycles	0.5C	Facile and low cost	56
Urchin-like hierarchical Si/CNTs anode	CVD	Superior conductivity and conspicuous rate capacity	20 mA h g^{-1} beyond 100 cycles	100 mA g^{-1}	Facile and low cost	345

performance and improved cycling stability. The performance of Si-based anodes can be influenced by the selection of the electrolyte. The incorporation of additives or the utilization of unique formulations in electrolytes has the potential to enhance the interaction between the electrolyte and the electrode, hence mitigating the production of SEI layers that may hinder the performance of batteries.

Numerous firms and research groups have been actively engaged in the development of Si-based anode technology for LIBs. Certain individuals or groups have made advancements in the expansion of production capabilities and the attainment of increased energy densities in battery products intended for commercial use. In addition to LIBs, researchers are investigating the potential of Si-based anodes in emerging battery technologies, including solid-state batteries and lithium–sulfur batteries. These anodes provide notable benefits due to their elevated capacity and ability to accommodate alternate chemical compositions.

Research in recent years shows that several chemical modifications (binders, composite materials, and electrolytes) provide superior stability and enhance the electrochemical performance of Si-based anodes in LIBs. Thus far, several different chemical interactions and structural alterations in Si-based anode materials have been attempted to enhance the Li^+ kinetics, structural stability, and volume development control throughout the delithiation/lithiation process.

1. In the case of binders, the impact of the binder on Si-based anodes is insignificant. In the development of new types of binders, it is expected that the half-cell will be expanded to full cells in LIBs to disclose their impact properly. Given that full-cell LIBs have less excess Li-ions, this can be a new prospect to enrich the performance of LIBs. Then, the synthesis of current binders is complicated, hindering their commercial application and further improvement. Additionally, the performance of both ICE and reversible capacity should be high for new binders compared to traditional binders. Moreover, new binders should be adaptable with not only Si-based anodes but also Gr-based anodes.

2. The formation of hybrid composites by doping Si with other materials can be a viable option to enhance the conductivity, ensure sufficient structural integrity, enhance the trap density and areal capacity, and finally stabilize the formed SEI. During the preparation of hybrid composites, their morphology, particle dimension, and coating should be considered to achieve the requirements.

3. Electrolytes, in comparison to the commonly used liquid electrolytes, show great promise to enhance the outcomes in Si-based anodes. Together with the newly designed liquid electrolytes, solid-state electrolytes should have proper physical and electrochemical properties as well as low cost, energy and non-combustible safety. Hence, they are attractive in the field of Si-based anode LIBs. Presently, it is necessary to make safety measures a priority during the development of new materials.

4. Together with experiments, some computation software such as COMSOL Multiphysics and ANSYS simulation for theoretical analysis may be a beneficial addition for the development of effective Si-based anodes in LIBs. Based on experimental data, we can analyze many optimizations to get the proper configuration of binders, composites, and electrolytes with a variation in configuration.

Despite the significant advancements, the development of Si and Si-based electrodes is still in its infancy and still far from finding widespread practical use. Si anodes face some difficulties, including substantial volume increase, low ICE, and limited areal capacity. Thus, approaches including material engineering, surface/interface engineering, and binder/electrolyte optimization can be used to address these drawbacks.

1. The mass production of Si-based anodes is considerably hindered by the high cost for the fabrication of Si-based materials. A commercialized anode with 5–10 wt% Si/graphite costs roughly double the price of synthetic graphite. If Si/graphite composites can be made with ease and at low cost using techniques such as ball milling and spray-drying/spray pyrolysis, their future commercialization will be more feasible.

2. Existing LIB approaches cannot satisfy the rising demand for power/energy densities greater than 300 W h kg^{-1} due to the inherent tension between superior efficiency and cycling reliability. The available Si-containing LIBs typically have a low Si ratio (10 wt%). However, there would be issues with reliability and instability of the cycling if the Si ratio was increased, offsetting any gains in energy density that may be achieved. Therefore, there is an immediate problem that needs to be solved, *i.e.*, achieving a compromise among the Si ratio, superior efficiency, and cycle reliability.

3. Safety concerns are widely acknowledged and one of the most essential criteria to use when comparing the effectiveness of various types of batteries is the issue of safety. In LIBs, the considerable volume expansion, unstable SEI formation, and electrolyte decomposition can trigger severe development of Li dendrites, which can culminate in a cell explosion together with a short circuit. Specifically, these factors can cause severe Li dendrite formation.

4. Mechanism of operation: more research into the reaction processes in Si-based anodes is required. Examining the *in situ* reactions of Li and Si during lithiation and delithiation with SEM, TEM, XRD, and cryo-electron microscopy is crucial. However, more sophisticated characterization techniques (for instance *in situ* neutron diffraction, *in situ* X-ray absorption fine structure, *in situ* atomic force microscopy, *in situ* FTIR, and *in situ* scanning tunnelling microscopy) should be merged with traditional techniques to clarify the more recognized interactions with the chemical responses on the surface of Si materials.

Finally, Si-based LIBs need to have evaluation criteria developed for their property–performance relationships. Considering that higher-capacity Si-based anodes will receive increasing research attention, it is important to account for all indexes in the evaluation together with that correlated with the composition (such as the Si surface oxide categories,

the compositional distribution of solid bulk, thickness, and the components of the SEI layer, as well as during cycling the electrolyte products) and the infrastructure (such as mass together with volumetric density).

List of abbreviations

Alg	Alginate
C	Carbon
CA	Citric acid
CE	Coulombic efficiency
CMC	Carboxymethyl cellulose
CNT	Carbon nanotube
CS	Chitosan
Cu	Copper
CVD	Chemical vapor deposition
EC	Ethylene carbonate
ICE	Initial coulombic efficiency
IL	Ionic-liquid
LAC	Lactide
Li	Lithium
Li_2CO_3	Lithium carbonate
LiBOB	Li-bis(oxalato)borate
LIBs	Lithium-ion batteries
$LiPF_6$	Lithium hexafluorophosphate
ND	Nanodiamond
NW	Nanowire
PAA	Polyacrylic acid
PTP	Potassium triphosphate
PVA	Polyvinyl alcohol
PVDF	Polyvinylidene fluoride
SEI	Solid electrolyte interface
Si	Silicon
Si NPs	Silicon nanoparticles
Si NW	Silicon nanowire
TEOSCN	2-(Cyanoethyl) triethoxysilane
TFPC	Trifluoro propylene carbonate
VC	Vinylene carbonate
HPAM	Hydrolyzed polyacrylamide
rGO	Reduced graphene oxide
SA	Sodium alginate
PDA	Polydopamine
GA	Glycinamide
PEI	Poly(ethylene imine)
PEG	Polyethylene glycol
PEU	Poly(ether urethane)
3D	Three-dimensional
DFT	Density functional theory
SA	Sodium alginate
PMDOPA	Poly(*N*-methacryloyl-3,4-dihydroxy-L-phenylalanine)
P	Phosphorous
FEC	Fluoroethylene carbonate
Gr	Graphite
XPS	X-ray photoelectron spectroscopy
CFG	Furan-modified corn viscose branching arabinoxylan
LiF	Lithium fluoride
NC	Nanocomposite
DEC	Diethyl carbonate
PVP	Polyvinyl pyrrolidone
PANI	Polyaniline
PU	Polyurethane
EGO	Exfoliated graphite oxide
–OH	Hydroxyl group
–COOH	Carboxyl group
PPy-*b*-PB	Poly(1-pyrene methyl methacrylate) and polybutadiene
B	Boron
TDI	4,5-Dicyano-2-trifluoromethane imidazole
NC	Nitrogen-doped carbon
SA	Succinic anhydride

Conflicts of interest

There are no conflicts to declare.

Acknowledgements

This work was supported by the Fundamental Research Funds for the Central Universities (No. 2232023D-02, 2232023Y-01, and 2232021A-02), and the National Natural Science Foundation of China (No. 52202361, No. 92163121, and No. 52122312).

References

1 B. Scrosati, History of lithium batteries, *J. Solid State Electrochem.*, 2011, **15**, 1623–1630.
2 E. C. Self, F. M. Delnick, R. E. Ruther, S. Allu and J. Nanda, High-capacity organic radical mediated phosphorus anode for sodium-based redox flow batteries, *ACS Energy Lett.*, 2019, **4**, 2593–2600.
3 S. Wu, C. Han, J. Iocozzia, M. Lu, R. Ge, R. Xu and Z. Lin, Germanium-based nanomaterials for rechargeable batteries, *Angew. Chem., Int. Ed.*, 2016, **55**, 7898–7922.
4 D. Ma, Y. Li, H. Mi, S. Luo, P. Zhang, Z. Lin, J. Li and H. Zhang, Robust SnO_{2-x} nanoparticle-impregnated carbon nanofibers with outstanding electrochemical performance for advanced sodium-ion batteries, *Angew. Chem.*, 2018, **130**, 9039–9043.
5 J. Asenbauer, T. Eisenmann, M. Kuenzel, A. Kazzazi, Z. Chen and D. Bresser, The success story of graphite as a lithium-ion anode material – fundamentals, remaining challenges, and recent developments including silicon (oxide) composites, *Sustainable Energy Fuels*, 2020, **4**, 5387–5416.
6 X.-Q. Chen, S.-J. Fan, C. Han, T. Wu, L.-J. Wang, W. Jiang, W. Dai and J.-P. Yang, Multiscale architectures boosting thermoelectric performance of copper sulfide compound, *Rare Met.*, 2021, **40**, 2017–2025.
7 M. E. Biresselioglu, M. Demirbag Kaplan and B. K. Yilmaz, Electric mobility in Europe: A comprehensive review of motivators and barriers in decision making processes, *Transp. Res. A*, 2018, **109**, 1–13.

8 N. Scarlat, J.-F. Dallemand and F. Fahl, Biogas: Developments and perspectives in Europe, *Renewable Energy*, 2018, **129**, 457–472.
9 X.-Y. Yu, L. Yu and X. W. D. Lou, Metal sulfide hollow nanostructures for electrochemical energy storage, *Adv. Energy Mater.*, 2016, **6**, 1501333.
10 L. Shen, L. Yu, H. Bin Wu, X.-Y. Yu, X. Zhang and X. W. Lou, Formation of nickel cobalt sulfide ball-in-ball hollow spheres with enhanced electrochemical pseudocapacitive properties, *Nat. Commun.*, 2015, **6**, 6694.
11 M. Ge, C. Cao, G. M. Biesold, C. D. Sewell, S. Hao, J. Huang, W. Zhang, Y. Lai and Z. Lin, Recent advances in silicon-based electrodes: From fundamental research toward practical applications, *Adv. Mater.*, 2021, **33**, 2004577.
12 B. Scrosati, J. Hassoun and Y.-K. Sun, Lithium-ion batteries. A look into the future, *Energy Environ. Sci.*, 2011, **4**, 3287.
13 X. Guo, B. Sun, D. Su, X. Liu, H. Liu, Y. Wang and G. Wang, Recent developments of aprotic lithium-oxygen batteries: functional materials determine the electrochemical performance, *Sci. Bull*, 2017, **62**, 442–452.
14 J.-M. Peng, Z.-Q. Chen, Y. Li, S.-J. Hu, Q.-C. Pan, F.-H. Zheng, H.-Q. Wang and Q.-Y. Li, Conducting network interface modulated rate performance in $LiFePO_4$/C cathode materials, *Rare Met.*, 2022, **41**, 951–959.
15 Y. Xing, L. Zhang, S. Mao, X. Wang, H. Wenren, X. Xia, C. Gu and J. Tu, Core-shell structure of porous silicon with nitrogen-doped carbon layer for lithium-ion batteries, *Mater. Res. Bull.*, 2018, **108**, 170–175.
16 M.-S. Wang, G.-L. Wang, S. Wang, J. Zhang, J. Wang, W. Zhong, F. Tang, Z.-L. Yang, J. Zheng and X. Li, In situ catalytic growth 3D multi-layers graphene sheets coated nano-silicon anode for high performance lithium-ion batteries, *Chem. Eng. J.*, 2019, **356**, 895–903.
17 F. Xin and M. S. Whittingham, Challenges and development of tin-based anode with high volumetric capacity for Li-ion batteries, *Electrochem. Energy Rev.*, 2020, **3**, 643–655.
18 J. C. Jiang, Q. N. Fan, S. L. Chou, Z. P. Guo, K. Konstantinov, H. K. Liu and J. Z. Wang, Li_2S-based Li-ion sulfur batteries: Progress and prospects, *Small*, 2021, **17**, 1903934.
19 T. Shen, Z. Yao, X. Xia, X. Wang, C. Gu and J. Tu, Rationally designed silicon nanostructures as anode material for lithium-ion batteries, *Adv. Eng. Mater.*, 2018, **20**, 1700591.
20 K. Feng, M. Li, W. Liu, A. G. Kashkooli, X. Xiao, M. Cai and Z. Chen, Silicon-based anodes for lithium-ion batteries: From fundamentals to practical applications, *Small*, 2018, **14**, 1702737.
21 L. Sun, Y. Liu, R. Shao, J. Wu, R. Jiang and Z. Jin, Recent progress and future perspective on practical silicon anode-based lithium ion batteries, *Energy Storage Mater.*, 2022, **46**, 482–502.
22 K.-J. Park, M.-J. Choi, F. Maglia, S.-J. Kim, K.-H. Kim, C. S. Yoon and Y.-K. Sun, High-capacity concentration gradient $Li[Ni_{0.865}Co_{0.120}Al_{0.015}]O_2$ cathode for lithium-ion batteries, *Adv. Energy Mater.*, 2018, **8**, 1703612.
23 J. Yang, Y. Wang, W. Li, L. Wang, Y. Fan, W. Jiang, W. Luo, Y. Wang, B. Kong, C. Selomulya, H. K. Liu, S. X. Dou and D. Zhao, Amorphous TiO_2 shells: A vital elastic buffering layer on silicon nanoparticles for high-performance and safe lithium storage, *Adv. Mater.*, 2017, **29**, 1700523.
24 W. Luo, Y. Wang, L. Wang, W. Jiang, S.-L. Chou, S. X. Dou, H. K. Liu and J. Yang, Silicon/mesoporous carbon/crystalline TiO_2 nanoparticles for highly stable lithium storage, *ACS Nano*, 2016, **10**, 10524–10532.
25 W. Luo, D. Shen, R. Zhang, B. Zhang, Y. Wang, S. X. Dou, H. K. Liu and J. Yang, Germanium nanograin decoration on carbon shell: Boosting lithium-storage properties of silicon nanoparticles, *Adv. Funct. Mater.*, 2016, **26**, 7800–7806.
26 X. Qiao, X.-B. Yang, N. Zhang, X.-L. Wang, Y.-Y. Song, Y.-Q. Zhai, D. Li and H.-Q. Wang, One-step in situ encapsulation of Ge nanoparticles into porous carbon network with enhanced electron/ion conductivity for lithium storage, *Rare Met.*, 2021, **40**, 2432–2439.
27 X. Ma, Z.-J. Zhang, J.-M. Wang, S.-H. Sun, S.-F. Zhang, S. Yuan, Z.-J. Qiao, Z.-Y. Yu, J.-L. Kang and W.-J. Li, Tuning dual three-dimensional porous copper/graphite composite to achieve diversified utilization of copper current collector for lithium storage, *Rare Met.*, 2021, **40**, 2802–2809.
28 M. H. Parekh, V. P. Parikh, P. J. Kim, S. Misra, Z. Qi, H. Wang and V. G. Pol, Encapsulation and networking of silicon nanoparticles using amorphous carbon and graphite for high performance Li-ion batteries, *Carbon*, 2019, **148**, 36–43.
29 K. Xiao, Q. Tang, Z. Liu, A. Hu, S. Zhang, W. Deng and X. Chen, 3D interconnected mesoporous Si/SiO_2 coated with CVD derived carbon as an advanced anode material of Li-ion batteries, *Ceram. Int.*, 2018, **44**, 3548–3555.
30 X. Zhou, Y. Liu, C. Du, Y. Ren, T. Mu, P. Zuo, G. Yin, Y. Ma, X. Cheng and Y. Gao, Polyaniline-encapsulated silicon on three-dimensional carbon nanotubes foam with enhanced electrochemical performance for lithium-ion batteries, *J. Power Sources*, 2018, **381**, 156–163.
31 A. Mukanova, A. Nurpeissova, A. Urazbayev, S.-S. Kim, M. Myronov and Z. Bakenov, Silicon thin film on graphene coated nickel foam as an anode for Li-ion batteries, *Electrochim. Acta*, 2017, **258**, 800–806.
32 X.-Y. Han, D.-L. Zhao, W.-J. Meng, H.-X. Yang, M. Zhao, Y.-J. Duan and X.-M. Tian, Graphene caging silicon nanoparticles anchored on graphene sheets for high performance Li-ion batteries, *Appl. Surf. Sci.*, 2019, **484**, 11–20.
33 Y. Yu, G. Li, S. Zhou, X. Chen, H.-W. Lee and W. Yang, Self–adaptive Si/reduced graphene oxide scrolls for high–performance Li–ion battery anodes, *Carbon*, 2017, **120**, 397–404.
34 I. Kang, J. Jang, K.-W. Yi and Y. W. Cho, Porous nanocomposite anodes of silicon/iron silicide/3D carbon network for lithium-ion batteries, *J. Alloys Compd.*, 2019, **770**, 369–376.
35 T. Mu, P. Zuo, S. Lou, Q. Pan, H. Zhang, C. Du, Y. Gao, X. Cheng, Y. Ma, H. Huo and G. Yin, A three-dimensional

silicon/nitrogen-doped graphitized carbon composite as high-performance anode material for lithium ion batteries, *J. Alloys Compd.*, 2019, **777**, 190–197.

36 L. Zhu, Y. Chen, C. Wu, R. Chu, J. Zhang, H. Jiang, Y. Zeng, Y. Zhang and H. Guo, Double-carbon protected silicon anode for high performance lithium-ion batteries, *J. Alloys Compd.*, 2020, **812**, 151848.

37 B. Lu, B. Ma, X. Deng, B. Wu, Z. Wu, J. Luo, X. Wang and G. Chen, Dual stabilized architecture of hollow Si@TiO_2@C nanospheres as anode of high-performance Li-ion battery, *Chem. Eng. J.*, 2018, **351**, 269–279.

38 X. Guo, W. Li, Q. Zhang, Y. Liu, G. Yuan, P. Braunstein and H. Pang, Ultrasmall metal (Fe, Co, Ni) nanoparticles strengthen silicon oxide embedded nitrogen-doped carbon superstructures for long-cycle-life Li-ion-battery anodes, *Chem. Eng. J.*, 2022, **432**, 134413.

39 Q. Xu, J.-K. Sun, J.-Y. Li, Y.-X. Yin and Y.-G. Guo, Scalable synthesis of spherical Si/C granules with 3D conducting networks as ultrahigh loading anodes in lithium-ion batteries, *Energy Storage Mater.*, 2018, **12**, 54–60.

40 J. Yu, C. Zhang, W. Wu, Y. Cai and Y. Zhang, Nodes-connected silicon-carbon nanofibrous hybrids anodes for lithium-ion batteries, *Appl. Surf. Sci.*, 2021, **548**, 148944.

41 Z. Yi, N. Lin, Y. Zhao, W. Wang, Y. Qian, Y. Zhu and Y. Qian, A flexible micro/nanostructured Si microsphere cross-linked by highly-elastic carbon nanotubes toward enhanced lithium ion battery anodes, *Energy Storage Mater.*, 2019, **17**, 93–100.

42 D. Yang, J. Shi, J. Shi and H. Yang, Simple synthesis of Si/Sn@C-G anodes with enhanced electrochemical properties for Li-ion batteries, *Electrochim. Acta*, 2018, **259**, 1081–1088.

43 J. Cui, J. Yang, J. Man, S. Li, J. Yin, L. Ma, W. He, J. Sun and J. Hu, Porous Al/Al_2O_3 two-phase nanonetwork to improve electrochemical properties of porous C/SiO_2 as anode for Li-ion batteries, *Electrochim. Acta*, 2019, **300**, 470–481.

44 Y. Dong, W. Wei, X. Lv, B. Huang and Y. Dai, Semimetallic Si_3C as a high capacity anode material for advanced lithium ion batteries, *Appl. Surf. Sci.*, 2019, **479**, 519–524.

45 J. Y. Woo, A. Y. Kim, M. K. Kim, S. H. Lee, Y. K. Sun, G. Liu and J. K. Lee, Cu3Si-doped porous-silicon particles prepared by simplified chemical vapor deposition method as anode material for high-rate and long-cycle lithium-ion batteries, *J. Alloys Compd.*, 2017, **701**, 425–432.

46 J. Liu, S. Wang, Y. Qie, J. Yu and Q. Sun, A new porous metallic silicon dicarbide for highly efficient Li-ion battery anode identified by targeted structure search, *Carbon*, 2018, **140**, 680–687.

47 X. Zhou, K. Han, H. Jiang, Z. Liu, Z. Zhang, H. Ye and Y. Liu, High-rate and long-cycle silicon/porous nitrogen-doped carbon anode via a low-cost facile pre-template-coating approach for Li-ion batteries, *Electrochim. Acta*, 2017, **245**, 14–24.

48 K. H. Kim, J. Shon, H. Jeong, H. Park, S. J. Lim and J. S. Heo, Improving the cyclability of silicon anodes for lithium-ion batteries using a simple pre-lithiation method, *J. Power Sources*, 2020, **459**, 228066.

49 L. Wu, H. Zhou, J. Yang, X. Zhou, Y. Ren, Y. Nie and S. Chen, Carbon coated mesoporous Si anode prepared by a partial magnesiothermic reduction for lithium-ion batteries, *J. Alloys Compd.*, 2017, **716**, 204–209.

50 Q. Pan, P. Zuo, S. Lou, T. Mu, C. Du, X. Cheng, Y. Ma, Y. Gao and G. Yin, Micro-sized spherical silicon@carbon@graphene prepared by spray drying as anode material for lithium-ion batteries, *J. Alloys Compd.*, 2017, **723**, 434–440.

51 T. Mu, P. Zuo, S. Lou, Q. Pan, H. Zhang, C. Du, Y. Gao, X. Cheng, Y. Ma, H. Huo and G. Yin, A three-dimensional silicon/nitrogen-doped graphitized carbon composite as high-performance anode material for lithium ion batteries, *J. Alloys Compd.*, 2019, **777**, 190–197.

52 L. Zhu, Y. Chen, C. Wu, R. Chu, J. Zhang, H. Jiang, Y. Zeng, Y. Zhang and H. Guo, Double-carbon protected silicon anode for high performance lithium-ion batteries, *J. Alloys Compd.*, 2020, **812**, 151848.

53 Y. Jiang, Y. Zhang, X. Yan, M. Tian, W. Xiao and H. Tang, A sustainable route from fly ash to silicon nanorods for high performance lithium ion batteries, *Chem. Eng. J.*, 2017, **330**, 1052–1059.

54 N. Sun, X. Wang, X. Dong, H. Huang and M. Qi, PVP-grafted synthesis for uniform electrospinning silica@carbon nanofibers as flexible free-standing anode for Li-ion batteries, *Solid State Ionics*, 2022, **374**, 115817.

55 S. Liu, W. Xu, C. Ding, J. Yu, D. Fang, Y. Ding and H. Hou, Boosting electrochemical performance of electrospun silicon-based anode materials for lithium-ion battery by surface coating a second layer of carbon, *Appl. Surf. Sci.*, 2019, **494**, 94–100.

56 Z. Guo, L. Zhou and H. Yao, Improving the electrochemical performance of Si-based anode via gradient Si concentration, *Mater. Des.*, 2019, **177**, 107851.

57 H. Shi, A. Yuan and J. Xu, Tailored synthesis of monodispersed nano/submicron porous silicon oxycarbide (SiOC) spheres with improved Li-storage performance as an anode material for Li-ion batteries, *J. Power Sources*, 2017, **364**, 288–298.

58 X.-Y. Yue, A. Abulikemu, X.-L. Li, Q.-Q. Qiu, F. Wang, X.-J. Wu and Y.-N. Zhou, Vermiculite derived porous silicon nanosheet as a scalable and low cost anode material for lithium-ion batteries, *J. Power Sources*, 2019, **410–411**, 132–136.

59 K. Pan, F. Zou, M. Canova, Y. Zhu and J. H. Kim, Systematic electrochemical characterizations of Si and SiO anodes for high-capacity Li-Ion batteries, *J. Power Sources*, 2019, **413**, 20–28.

60 Z. Wang, X. Zhang, X. Liu, Y. Wang, Y. Zhang, Y. Li, W. Zhao, C. Qin, A. Mukanova and Z. Bakenov, Bimodal nanoporous NiO@Ni–Si network prepared by dealloying method for stable Li-ion storage, *J. Power Sources*, 2020, **449**, 227550.

61 A. Münzer, L. Xiao, Y. H. Sehlleier, C. Schulz and H. Wiggers, All gas-phase synthesis of graphene: Characterization and its utilization for silicon-based lithium-ion batteries, *Electrochim. Acta*, 2018, **272**, 52–59.

62 J. Cui, J. Yang, J. Man, S. Li, J. Yin, L. Ma, W. He, J. Sun and J. Hu, Porous Al/Al_2O_3 two-phase nanonetwork to improve electrochemical properties of porous C/SiO_2 as anode for Li-ion batteries, *Electrochim. Acta*, 2019, **300**, 470–481.

63 J. Yang, L. Zhang, T. Zhang, X. Wang, Y. Gao and Q. Fang, Self-healing strategy for Si nanoparticles towards practical application as anode materials for Li-ion batteries, *Electrochem. Commun.*, 2018, **87**, 22–26.

64 R. Shao, J. Niu, F. Zhu, M. Dou, Z. Zhang and F. Wang, A facile and versatile strategy towards high-performance Si anodes for Li-ion capacitors: Concomitant conductive network construction and dual-interfacial engineering, *Nano Energy*, 2019, **63**, 103824.

65 Y. Zhou, Y. Yang, G. Hou, D. Yi, B. Zhou, S. Chen, T. D. Lam, F. Yuan, D. Golberg and X. Wang, Stress-relieving defects enable ultra-stable silicon anode for Li-ion storage, *Nano Energy*, 2020, **70**, 104568.

66 Q. Meng, G. Li, J. Yue, Q. Xu, Y.-X. Yin and Y.-G. Guo, High-performance lithiated SiOx anode obtained by a controllable and efficient prelithiation strategy, *ACS Appl. Mater. Interfaces*, 2019, **11**, 32062–32068.

67 W. Wang, Z. Favors, C. Li, C. Liu, R. Ye, C. Fu, K. Bozhilov, J. Guo, M. Ozkan and C. S. Ozkan, Silicon and carbon nanocomposite spheres with enhanced electrochemical performance for full cell lithium ion batteries, *Sci. Rep.*, 2017, **7**, 44838.

68 M. Tian and P. Wu, Nature plant polyphenol coating silicon submicroparticle conjugated with polyacrylic acid for achieving a high-performance anode of lithium-ion battery, *ACS Appl. Energy Mater.*, 2019, **2**, 5066–5073.

69 M. Ruttert, V. Siozios, M. Winter and T. Placke, Mechanochemical synthesis of Fe–Si-based anode materials for high-energy lithium ion full-cells, *ACS Appl. Energy Mater.*, 2020, **3**, 743–758.

70 F. Xi, Z. Zhang, X. Wan, S. Li, W. Ma, X. Chen, R. Chen, B. Luo and L. Wang, High-performance porous silicon/nanosilver anodes from industrial low-grade silicon for lithium-ion batteries, *ACS Appl. Mater. Interfaces*, 2020, **12**, 49080–49089.

71 B. Lu, B. Ma, X. Deng, W. Li, Z. Wu, H. Shu and X. Wang, Cornlike ordered mesoporous silicon particles modified by nitrogen-doped carbon layer for the application of Li-ion battery, *ACS Appl. Mater. Interfaces*, 2017, **9**, 32829–32839.

72 W. Luo, Y. Wang, S. Chou, Y. Xu, W. Li, B. Kong, S. X. Dou, H. K. Liu and J. Yang, Critical thickness of phenolic resin-based carbon interfacial layer for improving long cycling stability of silicon nanoparticle anodes, *Nano Energy*, 2016, **27**, 255–264.

73 R. Li, J. Li, K. Qi, X. Ge, Q. Zhang and B. Zhang, One-step synthesis of 3D sulfur/nitrogen dual-doped graphene supported nano silicon as anode for Li-ion batteries, *Appl. Surf. Sci.*, 2018, **433**, 367–373.

74 D. Qu, X. You, X. Feng, J. Wu, D. Liu, D. Zheng, Z. Xie, D. Qu, J. Li and H. Tang, Lithium ion supercapacitor composed by Si-based anode and hierarchal porous carbon cathode with super long cycle life, *Appl. Surf. Sci.*, 2019, **463**, 879–888.

75 K. Hirata, Y. Morita, T. Kawase and Y. Sumida, Electrochemical performance of an ethylene carbonate-free electrolyte based on lithium bis(fluorosulfonyl)imide and sulfolane, *J. Power Sources*, 2018, **395**, 163–170.

76 F. Men, Y. Yang, Y. Shang, H. Zhang, Z. Song, Y. Zhou, X. Zhou and H. Zhan, Fluorine-substituted ionic liquid for Si anode in Li-ion battery, *J. Power Sources*, 2018, **401**, 354–361.

77 Y. Xu, E. Swaans, S. Chen, S. Basak, P. P. R. M. L. Harks, B. Peng, H. W. Zandbergen, D. M. Borsa and F. M. Mulder, A high-performance Li-ion anode from direct deposition of Si nanoparticles, *Nano Energy*, 2017, **38**, 477–485.

78 R. Fu, K. Zhang, R. P. Zaccaria, H. Huang, Y. Xia and Z. Liu, Two-dimensional silicon suboxides nanostructures with Si nanodomains confined in amorphous SiO_2 derived from siloxene as high performance anode for Li-ion batteries, *Nano Energy*, 2017, **39**, 546–553.

79 Q. Xu, J. Sun, Z. Yu, Y. Yin, S. Xin, S. Yu and Y. Guo, SiOx encapsulated in graphene bubble film: An ultrastable Li-ion battery anode, *Adv. Mater.*, 2018, **30**, 1707430.

80 H. S. Sitinamaluwa, H. Li, K. C. Wasalathilake, A. Wolff, T. Tesfamichael, S. Zhang and C. Yan, Nanoporous SiO coated amorphous silicon anode material with robust mechanical behavior for high-performance rechargeable Li-ion batteries, *Nano Mater. Sci.*, 2019, **1**, 70–76.

81 J. Wu, F. Ma, X. Liu, X. Fan, L. Shen, Z. Wu, X. Ding, X. Han, Y. Deng, W. Hu and C. Zhong, Recent progress in advanced characterization methods for silicon-based lithium-ion batteries, *Small Methods*, 2019, **3**, 1900158.

82 L. C. Loaiza, L. Monconduit and V. Seznec, Si and Ge-based anode materials for Li-, Na-, and K-ion batteries: A perspective from structure to electrochemical mechanism, *Small*, 2020, **16**, 1905260.

83 G. Zhu, W. Luo, L. Wang, W. Jiang and J. Yang, Silicon: Toward eco-friendly reduction techniques for lithium-ion battery applications, *J. Mater. Chem. A*, 2019, **7**, 24715–24737.

84 J. Piątek, S. Afyon, T. M. Budnyak, S. Budnyk, M. H. Sipponen and A. Slabon, Sustainable Li-Ion batteries: Chemistry and recycling, *Adv. Energy Mater.*, 2021, **11**, 2003456.

85 R. Zafar Abbas Manj, F. Zhang, W. Ur Rehman, W. Luo and J. Yang, Toward understanding the interaction within Silicon-based anodes for stable lithium storage, *Chem. Eng. J.*, 2020, **385**, 123821.

86 W. Luo, X. Chen, Y. Xia, M. Chen, L. Wang, Q. Wang, W. Li and J. Yang, Surface and interface engineering of silicon-based anode materials for lithium-ion batteries, *Adv. Energy Mater.*, 2017, **7**, 1701083.

87 M. Li, J. Lu, Z. Chen and K. Amine, 30 years of lithium-ion batteries, *Adv. Mater.*, 2018, **30**, 1800561.

88 M. Jiang, J. Chen, Y. Zhang, N. Song, W. Jiang and J. Yang, Assembly: A key enabler for the construction of superior silicon-based anodes, *Adv. Sci.*, 2022, **9**, 2203162.

89 M. Jiang, Y. Ma, J. Chen, W. Jiang and J. Yang, Regulating the carbon distribution of anode materials in lithium-ion batteries, *Nanoscale*, 2021, **13**, 3937–3947.

90 F. Zhang, W. Luo and J. Yang, Interface heteroatom-doping: Emerging solutions to silicon-based anodes, *Chem. – Asian J.*, 2020, **15**, 1394–1404.
91 R. Sujith, J. Gangadhar, M. Greenough, R. K. Bordia and D. K. Panda, A review of silicon oxycarbide ceramics as next generation anode materials for lithium-ion batteries and other electrochemical applications, *J. Mater. Chem. A*, 2023, **11**, 20324–20348.
92 X. Ma, G. Hou, Q. Ai, L. Zhang, P. Si, J. Feng and L. Ci, A heart-coronary arteries structure of carbon nanofibers/graphene/silicon composite anode for high performance lithium ion batteries, *Sci. Rep.*, 2017, **7**, 9642.
93 F.-H. Du, Y. Ni, Y. Wang, D. Wang, Q. Ge, S. Chen and H. Y. Yang, Green fabrication of silkworm cocoon-like silicon-based composite for high-performance Li-ion batteries, *ACS Nano*, 2017, **11**, 8628–8635.
94 Y. Ma, H. Qu, W. Wang, Y. Yu, X. Zhang, B. Li and L. Wang, Si/SiO_2 @graphene superstructures for high-performance lithium-ion batteries, *Adv. Funct. Mater.*, 2023, **33**, 2211648.
95 H. Su, X. Li, C. Liu, Y. Shang and H. Liu, Scalable synthesis of micrometer-sized porous silicon/carbon composites for high-stability lithium-ion battery anodes, *Chem. Eng. J.*, 2023, **451**, 138394.
96 Z. Yan, S. Yi, X. Li, J. Jiang, D. Yang and N. Du, A scalable silicon/graphite anode with high silicon content for high-energy lithium-ion batteries, *Mater. Today Energy*, 2023, **31**, 101225.
97 M. Sohn, D. G. Lee, H.-I. Park, C. Park, J.-H. Choi and H. Kim, Microstructure controlled porous silicon particles as a high capacity lithium storage material via dual step pore engineering, *Adv. Funct. Mater.*, 2018, **28**, 1800855.
98 C. Xiao, P. He, J. Ren, M. Yue, Y. Huang and X. He, Walnut-structure Si–G/C materials with high coulombic efficiency for long-life lithium ion batteries, *RSC Adv.*, 2018, **8**, 27580–27586.
99 K. Wang, Y. Tan, P. Li, B. Xue and J. Sun, Facile synthesis of double-layer-constrained micron-sized porous $Si/SiO_2/C$ composites for lithium-ion battery anodes, *ACS Appl. Mater. Interfaces*, 2019, **11**, 37732–37740.
100 L. Hu, B. Luo, C. Wu, P. Hu, L. Wang and H. Zhang, Yolk-shell Si/C composites with multiple Si nanoparticles encapsulated into double carbon shells as lithium-ion battery anodes, *J. Energy Chem.*, 2019, **32**, 124–130.
101 J. Wang, W. Huang, Y. S. Kim, Y. K. Jeong, S. C. Kim, J. Heo, H. K. Lee, B. Liu, J. Nah and Y. Cui, Scalable synthesis of nanoporous silicon microparticles for highly cyclable lithium-ion batteries, *Nano Res.*, 2020, **13**, 1558–1563.
102 W. Zhang, Y. Weng, W. Shen, R. Lv, F. Kang and Z.-H. Huang, Scalable synthesis of lotus-seed-pod-like Si/SiOx@CNF: Applications in freestanding electrode and flexible full lithium-ion batteries, *Carbon*, 2020, **158**, 163–171.
103 Z. Yang, C. Wu, S. Li, L. Qiu, Z. Yang, Y. Zhong, B. Zhong, Y. Song, G. Wang, Y. Liu, Z. Wu and X. Guo, A unique structure of highly stable interphase and self-consistent stress distribution radial-gradient porous for silicon anode, *Adv. Funct. Mater.*, 2022, **32**, 2107897.
104 J. Wang, C. Gao, Z. Yang, M. Zhang, Z. Li and H. Zhao, Carbon-coated mesoporous silicon shell-encapsulated silicon nano-grains for high performance lithium-ion batteries anode, *Carbon*, 2022, **192**, 277–284.
105 W. Wang, Y. Wang, L. Yuan, C. You, J. Wu, L. Liu, J. Ye, Y. Wu and L. Fu, Recent advances in modification strategies of silicon-based lithium-ion batteries, *Nano Res.*, 2023, **16**(3), 3781–3803.
106 B. A. Nuhu, O. Bamisile, H. Adun, U. O. Abu and D. Cai, Effects of transition metals for silicon-based lithium-ion battery anodes: A comparative study in electrochemical applications, *J. Alloys Compd.*, 2023, **933**, 167737.
107 M. Lavigne Philippot, D. Costa, G. Cardellini, L. De Sutter, J. Smekens, J. Van Mierlo and M. Messagie, Life cycle assessment of a lithium-ion battery with a silicon anode for electric vehicles, *J. Energy Storage*, 2023, **60**, 106635.
108 F. Zhang and J. Yang, Boosting initial coulombic efficiency of Si-based anodes: A review, *Emergent Mater.*, 2020, **3**, 369–380.
109 W. U. Rehman, H. Wang, R. Z. A. Manj, W. Luo and J. Yang, When silicon materials meet natural sources: Opportunities and challenges for low-cost lithium storage, *Small*, 2021, **17**, 1904508.
110 Z. Zhao, J. Han, F. Chen, J. Xiao, Y. Zhao, Y. Zhang, D. Kong, Z. Weng, S. Wu and Q. Yang, Liquid metal remedies silicon microparticulates toward highly stable and superior volumetric lithium storage, *Adv. Energy Mater.*, 2022, **12**, 2103565.
111 G. Zhu, R. Guo, W. Luo, H. K. Liu, W. Jiang, S. X. Dou and J. Yang, Boron doping-induced interconnected assembly approach for mesoporous silicon oxycarbide architecture, *Natl. Sci. Rev.*, 2021, **8**, 112O.
112 S. Cho, W. Jung, G. Jung and K. Eom, High-performance boron-doped silicon micron-rod anode fabricated using a mass-producible lithography method for a lithium ion battery, *J. Power Sources*, 2020, **454**, 227931.
113 M. S. Kang, I. Heo, S. Kim, J. Yang, J. Kim, S.-J. Min, J. Chae and W. C. Yoo, High-areal-capacity of micron-sized silicon anodes in lithium-ion batteries by using wrinkled-multilayered-graphenes, *Energy Storage Mater.*, 2022, **50**, 234–242.
114 L. Yu, J. Liu, S. He, C. Huang, L. Gan, Z. Gong and M. Long, A novel high-performance 3D polymer binder for silicon anode in lithium-ion batteries, *J. Phys. Chem. Solids*, 2019, **135**, 109113.
115 G. C. Shivaraju, C. Sudakar and A. S. Prakash, High-rate and long-cycle life performance of nano-porous nano-silicon derived from mesoporous MCM-41 as an anode for lithium-ion battery, *Electrochim. Acta*, 2019, **294**, 357–364.
116 N. Hamzelui, G. G. Eshetu and E. Figgemeier, Customizing active materials and polymeric binders: Stern requirements to realize silicon-graphite anode based lithium-ion batteries, *J. Energy Storage*, 2021, **35**, 102098.
117 G. Liu, M. Xia, J. Gao, Y. Cheng, M. Wang, W. Hong, Y. Yang and J. Zheng, Dual-salt localized high-concentration electrolyte for long cycle life silicon-based lithium-ion batteries, *ACS Appl. Mater. Interfaces*, 2023, **15**, 3586–3598.
118 X. Ren, T. Huang and A. Yu, Carboxymethylated tamarind polysaccharide gum as a green binder for silicon-based

lithium-ion battery anodes, *Electrochem. Commun.*, 2022, **136**, 107241.

119 J. Kim, Y. K. Park, H. Kim and I. H. Jung, Ambidextrous Polymeric binder for silicon anodes in lithium-ion batteries, *Chem. Mater.*, 2022, **34**, 5791–5798.

120 Z. Xu, X. Chu, K. Wang, H. Zhang, Z. He, Y. Xie and W. Yang, Stress-dissipated conductive polymer binders for high-stability silicon anode in lithium-ion batteries, *J. Mater.*, 2023, **9**, 378–386.

121 S. Gao, F. Sun, A. Brady, Y. Pan, A. Erwin, D. Yang, V. Tsukruk, A. G. Stack, T. Saito, H. Yang and P.-F. Cao, Ultra-efficient polymer binder for silicon anode in high-capacity lithium-ion batteries, *Nano Energy*, 2020, **73**, 104804.

122 A. M. Haregewoin, L. Terborg, L. Zhang, S. Jurng, B. L. Lucht, J. Guo, P. N. Ross and R. Kostecki, The electrochemical behavior of poly 1-pyrenemethyl methacrylate binder and its effect on the interfacial chemistry of a silicon electrode, *J. Power Sources*, 2018, **376**, 152–160.

123 L.-H. Huang and C.-C. Li, Effects of interactions between binders and different-sized silicons on dispersion homogeneity of anodes and electrochemistry of lithium-silicon batteries, *J. Power Sources*, 2019, **409**, 38–47.

124 A. Ladam, N. Bibent, C. Cénac-Morthé, L. Aldon, J. Olivier-Fourcade, J.-C. Jumas and P.-E. Lippens, One-pot ball-milling synthesis of a Ni-Ti-Si based composite as anode material for Li-ion batteries, *Electrochim. Acta*, 2017, **245**, 497–504.

125 Q. Li, R. Yi, Y. Xu, X. Cao, C. Wang, W. Xu and J.-G. Zhang, Failure analysis and design principles of silicon-based lithium-ion batteries using micron-sized porous silicon/carbon composite, *J. Power Sources*, 2022, **548**, 232063.

126 F. Wang, S. Lin, X. Lu, R. Hong and H. Liu, Poly-dopamine carbon-coated stable silicon/graphene/CNT composite as anode for lithium ion batteries, *Electrochim. Acta*, 2022, **404**, 139708.

127 H. Liu, Q. Sun, H. Zhang, J. Cheng, Y. Li, Z. Zeng, S. Zhang, X. Xu, F. Ji, D. Li, J. Lu and L. Ci, The application road of silicon-based anode in lithium-ion batteries: From liquid electrolyte to solid-state electrolyte, *Energy Storage Mater.*, 2023, **55**, 244–263.

128 A. Ghaur, C. Peschel, I. Dienwiebel, L. Haneke, L. Du, L. Profanter, A. Gomez-Martin, M. Winter, S. Nowak and T. Placke, Effective SEI Formation via phosphazene-based electrolyte additives for stabilizing silicon-based lithium-ion batteries, *Adv. Energy Mater.*, 2023, 2203503.

129 Y. Liang, J. H. K. Pfisterer, D. McLaughlin, C. Csoklich, L. Seidl, A. S. Bandarenka and O. Schneider, Electrochemical scanning probe microscopies in electrocatalysis, *Small Methods*, 2019, **3**, 1800387.

130 B. Breitung, N. Aguiló-Aguayo, T. Bechtold, H. Hahn, J. Janek and T. Brezesinski, Embroidered copper microwire current collector for improved cycling performance of silicon anodes in lithium-ion batteries, *Sci. Rep.*, 2017, **7**, 13010.

131 S. Chae, S. Choi, N. Kim, J. Sung and J. Cho, Integration of graphite and silicon anodes for the commercialization of high-energy lithium-ion batteries, *Angew. Chem., Int. Ed.*, 2020, **59**, 110–135.

132 H. Jung, M. Park, Y. G. Yoon, G. B. Kim and S. K. Joo, Amorphous silicon anode for lithium-ion rechargeable batteries, *J. Power Sources*, 2003, **115**, 346–351.

133 M. N. Obrovac and L. Christensen, Structural changes in silicon anodes during lithium insertion/extraction, *Electrochem. Solid-State Lett.*, 2004, **7**, A93.

134 M. W. Verbrugge, D. R. Baker, X. Xiao, Q. Zhang and Y.-T. Cheng, Experimental and theoretical characterization of electrode materials that undergo large volume changes and application to the lithium–silicon system, *J. Phys. Chem. C*, 2015, **119**, 5341–5349.

135 B. Liang, Y. Liu and Y. Xu, Silicon-based materials as high capacity anodes for next generation lithium ion batteries, *J. Power Sources*, 2014, **267**, 469–490.

136 M. Nie, D. P. Abraham, Y. Chen, A. Bose and B. L. Lucht, Silicon solid electrolyte interphase (SEI) of lithium ion battery characterized by microscopy and spectroscopy, *J. Phys. Chem. C*, 2013, **117**, 13403–13412.

137 F. Chen, J. Han, D. Kong, Y. Yuan, J. Xiao, S. Wu, D.-M. Tang, Y. Deng, W. Lv, J. Lu, F. Kang and Q.-H. Yang, 1000 Wh L^{-1} lithium-ion batteries enabled by crosslink-shrunk tough carbon encapsulated silicon microparticle anodes, *Natl. Sci. Rev.*, 2021, **8**, nwab012.

138 C. Yang, Y. Zhang, J. Zhou, C. Lin, F. Lv, K. Wang, J. Feng, Z. Xu, J. Li and S. Guo, Hollow Si/SiOx nanosphere/nitrogen-doped carbon superstructure with a double shell and void for high-rate and long-life lithium-ion storage, *J. Mater. Chem. A*, 2018, **6**, 8039–8046.

139 Y. Zhou, H. Guo, Z. Wang, X. Li, R. Zhou and W. Peng, Improved electrochemical performance of Si/C material based on the interface stability, *J. Alloys Compd.*, 2017, **725**, 1304–1312.

140 F. Luo, B. Liu, J. Zheng, G. Chu, K. Zhong, H. Li, X. Huang and L. Chen, Review—nano-silicon/carbon composite anode materials towards practical application for next generation Li-Ion batteries, *J. Electrochem. Soc.*, 2015, **162**, A2509–A2528.

141 V. L. Chevrier, L. Liu, D. B. Le, J. Lund, B. Molla, K. Reimer, L. J. Krause, L. D. Jensen, E. Figgemeier and K. W. Eberman, Evaluating Si-based materials for Li-Ion batteries in commercially relevant negative electrodes, *J. Electrochem. Soc.*, 2014, **161**, A783–A791.

142 C. Kim, M. Ko, S. Yoo, S. Chae, S. Choi, E.-H. Lee, S. Ko, S.-Y. Lee, J. Cho and S. Park, Novel design of ultra-fast Si anodes for Li-ion batteries: Crystalline Si@amorphous Si encapsulating hard carbon, *Nanoscale*, 2014, **6**, 10604–10610.

143 J. Yang, Y.-X. Wang, S.-L. Chou, R. Zhang, Y. Xu, J. Fan, W. Zhang, H. Kun Liu, D. Zhao and S. Xue Dou, Yolk-shell silicon-mesoporous carbon anode with compact solid electrolyte interphase film for superior lithium-ion batteries, *Nano Energy*, 2015, **18**, 133–142.

144 D. Shen, C. Huang, L. Gan, J. Liu, Z. Gong and M. Long, Rational design of $Si@SiO_2$/C composites using sustainable

cellulose as a carbon resource for anodes in lithium-ion batteries, *ACS Appl. Mater. Interfaces*, 2018, **10**, 7946–7954.

145 J. Kaspar, M. Graczyk-Zajac, S. Choudhury and R. Riedel, Impact of the electrical conductivity on the lithium capacity of polymer-derived silicon oxycarbide (SiOC) ceramics, *Electrochim. Acta*, 2016, **216**, 196–202.

146 S. S. Zhang, A review on electrolyte additives for lithium-ion batteries, *J. Power Sources*, 2006, **162**, 1379–1394.

147 Y. He, X. Yu, Y. Wang, H. Li and X. Huang, Alumina-coated patterned amorphous silicon as the anode for a lithium-ion battery with high coulombic efficiency, *Adv. Mater.*, 2011, **23**, 4938–4941.

148 B. Krüner, C. Odenwald, N. Jäckel, A. Tolosa, G. Kickelbick and V. Presser, Silicon oxycarbide beads from continuously produced polysilsesquioxane as stable anode material for lithium-ion batteries, *ACS Appl. Energy Mater.*, 2018, **1**, 2961–2970.

149 Y. Ren, M. Wang, J. Wang and Y. Cui, Tris (trimethylsilyl) phosphate as electrolyte additive for lithium-Ion batteries with graphite anode at elevated temperature, *Int. J. Electrochem. Sci.*, 2018, **13**, 664–674.

150 Y. Li, K. Leung and Y. Qi, Computational Exploration of the Li-Electrode|Electrolyte Interface in the Presence of a Nanometer Thick Solid-Electrolyte Interphase Layer, *Acc. Chem. Res.*, 2016, **49**, 2363–2370.

151 J. Luo, B. Ma, J. Peng, Z. Wu, Z. Luo and X. Wang, Modified chestnut-like structure silicon carbon composite as anode material for lithium-ion batteries, *ACS Sustainable Chem. Eng.*, 2019, **7**, 10415–10424.

152 X. Li, Z. Chen, A. Li, Y. Yu, X. Chen and H. Song, Three-dimensional hierarchical porous structures constructed by two-stage MXene-wrapped Si nanoparticles for Li-Ion batteries, *ACS Appl. Mater. Interfaces*, 2020, **12**, 48718–48728.

153 X. Du, H. Zhang, X. Lan, B. Yuan and R. Hu, Sn alloy and graphite addition to enhance initial coulombic efficiency and cycling stability of SiO anodes for Li-Ion batteries, *Energy Environ. Mater.*, 2022, **5**, 353–359.

154 X. Wan, C. Kang, T. Mu, J. Zhu, P. Zuo, C. Du and G. Yin, A multilevel buffered binder network for high-performance silicon anodes, *ACS Energy Lett.*, 2022, **7**, 3572–3580.

155 K. Minnici, Y. H. Kwon, L. M. Housel, G. D. Renderos, J. F. Ponder, C. Buckley, J. R. Reynolds, K. J. Takeuchi, E. S. Takeuchi, A. C. Marschilok and E. Reichmanis, Tuning conjugated polymers for binder applications in high-capacity magnetite anodes, *ACS Appl. Energy Mater.*, 2019, **2**, 7584–7593.

156 J.-M. Yuan, W.-F. Ren, K. Wang, T.-T. Su, G.-J. Jiao, C.-Y. Shao, L.-P. Xiao and R.-C. Sun, Ultrahighly elastic lignin-based copolymers as an effective binder for silicon anodes of lithium-ion batteries, *ACS Sustainable Chem. Eng.*, 2022, **10**, 166–176.

157 C. Wölke, B. A. Sadeghi, G. G. Eshetu, E. Figgemeier, M. Winter and I. Cekic-Laskovic, Interfacing Si-based electrodes: Impact of liquid electrolyte and its components, *Adv. Mater. Interfaces*, 2022, **9**, 2101898.

158 D. Li, Y. Wang, J. Hu, B. Lu, D. Dang, J. Zhang and Y.-T. Cheng, Role of polymeric binders on mechanical behavior and cracking resistance of silicon composite electrodes during electrochemical cycling, *J. Power Sources*, 2018, **387**, 9–15.

159 H. Xu, Y. Wang, R. Chen, Y. Bai, T. Li, H. Jin, J. Wang and H. Xia, A green-synthetic spiderweb-like Si@Graphene-oxide anode material with multifunctional citric acid binder for high energy-density Li-ion batteries, *Carbon*, 2020, **157**, 330–339.

160 Y. Wang, D. Dang, D. Li, J. Hu, X. Zhan and Y.-T. Cheng, Effects of polymeric binders on the cracking behavior of silicon composite electrodes during electrochemical cycling, *J. Power Sources*, 2019, **438**, 226938.

161 M. Zheng, Y. Wang, J. Reeve, H. Souzandeh and W.-H. Zhong, A polymer-alloy binder for structures-properties control of battery electrodes, *Energy Storage Mater.*, 2018, **14**, 149–158.

162 D. Bo, H. Xuanning, C. Zhenfei, M. Yangzhou, S. Guangsheng, Y. Weidong and W. Cuie, Effects of binders on electrochemical properties of high capacity silicon composite anodes, *Inorg. Chem. Commun.*, 2020, **113**, 107771.

163 Y. Liu, R. Shao, R. Jiang, X. Song, Z. Jin and L. Sun, A review of existing and emerging binders for silicon anodic Li-ion, *Nano Res.*, 2023, **16**, 6736–6752.

164 X. Zhang, W.-L. Song, H.-S. Chen and D. Fang, Role of the binder in the mechanical integrity of micro-sized crystalline silicon anodes for Li-Ion batteries, *J. Power Sources*, 2020, **465**, 228290.

165 T. Munaoka, X. Yan, J. Lopez, J. W. F. To, J. Park, J. B.-H. Tok, Y. Cui and Z. Bao, Ionically conductive self-healing binder for low cost Si microparticles anodes in Li-ion batteries, *Adv. Energy Mater.*, 2018, **8**, 1703138.

166 E. Zhao, Z. Guo, J. Liu, Q. Zhang, Z. Guo, Y. Yang, H. Wang and L. Wang, A low-cost and eco-friendly network binder coupling stiffness and softness for high-performance Li-ion batteries, *Electrochim. Acta*, 2021, **387**, 138491.

167 S. N. S. Hapuarachchi, K. C. Wasalathilake, J. Y. Nerkar, E. Jaatinen, A. P. O'Mullane and C. Yan, Mechanically Robust tapioca starch composite binder with improved ionic conductivity for sustainable lithium-ion batteries, *ACS Sustainable Chem. Eng.*, 2020, **8**, 9857–9865.

168 O. S. Taskin, N. Yuca, J. Papavasiliou and G. Avgouropoulos, Interconnected conductive gel binder for high capacity silicon anode for Li-ion batteries, *Mater. Lett.*, 2020, **273**, 127918.

169 W. Zeng, L. Wang, X. Peng, T. Liu, Y. Jiang, F. Qin, L. Hu, P. K. Chu, K. Huo and Y. Zhou, Enhanced ion conductivity in conducting polymer binder for high-performance silicon anodes in advanced lithium-ion batteries, *Adv. Energy Mater.*, 2018, **8**, 1702314.

170 X. Zhao, C.-H. Yim, N. Du and Y. Abu-Lebdeh, Crosslinked chitosan networks as binders for silicon/graphite composite electrodes in Li-Ion batteries, *J. Electrochem. Soc.*, 2018, **165**, A1110–A1121.

171 L. Ma, J. Meng, Y. Pan, Y.-J. Cheng, Q. Ji, X. Zuo, X. Wang, J. Zhu and Y. Xia, Microporous binder for the silicon-based lithium-ion battery anode with exceptional rate capability and improved cyclic performance, *Langmuir*, 2020, **36**, 2003–2011.

172 P. Mandal, K. Stokes, G. Hernández, D. Brandell and J. Mindemark, Influence of binder crystallinity on the performance of Si electrodes with poly(vinyl alcohol) binders, *ACS Appl. Energy Mater.*, 2021, **4**, 3008–3016.

173 L. Wang, T. Liu, X. Peng, W. Zeng, Z. Jin, W. Tian, B. Gao, Y. Zhou, P. K. Chu and K. Huo, Highly stretchable conductive glue for high-performance silicon anodes in advanced lithium-ion batteries, *Adv. Funct. Mater.*, 2018, **28**, 1704858.

174 S. Choi, T. Kwon, A. Coskun and J. W. Choi, Highly elastic binders integrating polyrotaxanes for silicon microparticle anodes in lithium ion batteries, *Science*, 2017, **357**, 279–283.

175 L. Lü, H. Lou, Y. Xiao, G. Zhang, C. Wang and Y. Deng, Synthesis of triblock copolymer polydopamine-polyacrylic-polyoxyethylene with excellent performance as a binder for silicon anode lithium-ion batteries, *RSC Adv.*, 2018, **8**, 4604–4609.

176 S. Guo, H. Li, Y. Li, Y. Han, K. Chen, G. Xu, Y. Zhu and X. Hu, SiO2-enhanced structural stability and strong adhesion with a new binder of konjac glucomannan enables stable cycling of silicon anodes for lithium-ion batteries, *Adv. Energy Mater.*, 2018, **8**, 1800434.

177 X. Zhu, F. Zhang, L. Zhang, L. Zhang, Y. Song, T. Jiang, S. Sayed, C. Lu, X. Wang, J. Sun and Z. Liu, A highly stretchable cross-linked polyacrylamide hydrogel as an effective binder for silicon and sulfur electrodes toward durable lithium-ion storage, *Adv. Funct. Mater.*, 2018, **28**, 1705015.

178 G. Zhang, Y. Yang, Y. Chen, J. Huang, T. Zhang, H. Zeng, C. Wang, G. Liu and Y. Deng, A quadruple-hydrogen-bonded supramolecular binder for high-performance silicon anodes in lithium-ion batteries, *Small*, 2018, **14**, 1801189.

179 N. Yuca, M. E. Cetintasoglu, M. F. Dogdu, H. Akbulut, S. Tabanli, U. Colak and O. S. Taskin, Highly efficient poly(fluorene phenylene) copolymer as a new class of binder for high-capacity silicon anode in lithium-ion batteries, *Int. J. Energy Res.*, 2018, **42**, 1148–1157.

180 H. Zhao, Y. Wei, C. Wang, R. Qiao, W. Yang, P. B. Messersmith and G. Liu, Mussel-inspired conductive polymer binder for Si-alloy anode in lithium-ion batteries, *ACS Appl. Mater. Interfaces*, 2018, **10**, 5440–5446.

181 C.-H. Jung, K.-H. Kim and S.-H. Hong, Stable silicon anode for lithium-ion batteries through covalent bond formation with a binder via esterification, *ACS Appl. Mater. Interfaces*, 2019, **11**, 26753–26763.

182 P. Li, G. Chen, Y. Lin, F. Chen, L. Chen, N. Zhang, Y. Cao, R. Ma and X. Liu, 3D network binder via in situ cross-linking on silicon anodes with improved stability for lithium-ion batteries, *Macromol. Chem. Phys.*, 2020, **221**, 1900414.

183 P.-F. Cao, G. Yang, B. Li, Y. Zhang, S. Zhao, S. Zhang, A. Erwin, Z. Zhang, A. P. Sokolov, J. Nanda and T. Saito, Rational design of a multifunctional binder for high-capacity silicon-based anodes, *ACS Energy Lett.*, 2019, **4**, 1171–1180.

184 T.-C. Kuo, C.-Y. Chiou, C.-C. Li and J.-T. Lee, In situ cross-linked poly(ether urethane) elastomer as a binder for high-performance Si anodes of lithium-ion batteries, *Electrochim. Acta*, 2019, **327**, 135011.

185 Y. K. Jeong and J. W. Choi, Mussel-inspired self-healing metallopolymers for silicon nanoparticle anodes, *ACS Nano*, 2019, **13**, 8364–8373.

186 J. Wang, C. Wan and J. Hong, Polymer blends of pectin/poly(acrylic acid) as efficient binders for silicon anodes in lithium-ion batteries, *ChemElectroChem*, 2020, **7**, 3106–3115.

187 Z. Li, Y. Zhang, T. Liu, X. Gao, S. Li, M. Ling, C. Liang, J. Zheng and Z. Lin, Silicon anode with high initial coulombic efficiency by modulated trifunctional binder for high-areal-capacity lithium-ion batteries, *Adv. Energy Mater.*, 2020, **10**, 1903110.

188 X. Liu, J. Zai, A. Iqbal, M. Chen, N. Ali, R. Qi and X. Qian, Glycerol-crosslinked PEDOT:PSS as bifunctional binder for Si anodes: Improved interfacial compatibility and conductivity, *J. Colloid Interface Sci.*, 2020, **565**, 270–277.

189 J. Nam, E. Kim, R. K. K., Y. Kim and T.-H. Kim, A conductive self healing polymeric binder using hydrogen bonding for Si anodes in lithium ion batteries, *Sci. Rep.*, 2020, **10**, 14966.

190 H. Woo, B. Gil, J. Kim, K. Park, A. J. Yun, J. Kim, S. Nam and B. Park, Metal-coordination mediated polyacrylate for high performance silicon microparticle anode, *Batteries Supercaps*, 2020, **3**, 1287–1295.

191 J. Nam, W. Jang, K. K. Rajeev, J.-H. Lee, Y. Kim and T.-H. Kim, Ion-conductive self-healing polymer network based on reversible imine bonding for Si electrodes, *J. Power Sources*, 2021, **499**, 229968.

192 L. Hu, X. Zhang, P. Zhao, H. Fan, Z. Zhang, J. Deng, G. Ungar and J. Song, Gradient H-bonding binder enables stable high-areal-capacity Si-based anodes in pouch cells, *Adv. Mater.*, 2021, **33**, 2104416.

193 Z. Dong, W. Du, H. Gu, Y. Long, C. Zhang, G. Chen, Z. Feng, W. Sun, Y. Jiang, Y. Liu, Y. Yang, J. Gan, M. Gao and H. Pan, A unique structural highly compacted binder-free silicon-based anode with high electronic conductivity for high-performance lithium-ion batteries, *Small Struct.*, 2022, **3**, 2100174.

194 C. Luo, X. Wu, T. Zhang, S. Chi, Z. Liu, J. Wang, C. Wang and Y. Deng, A Four-armed polyacrylic acid homopolymer binder with enhanced performance for SiOx/graphite anode, *Macromol. Mater. Eng.*, 2021, **306**, 2000525.

195 Z. Wang, X. Xu, C. Chen, T. Huang and A. Yu, Natural sesbania gum as an efficient biopolymer binder for high-performance Si-based anodes in lithium-ion batteries, *J. Power Sources*, 2022, **539**, 231604.

196 Z. Song, T. Zhang, L. Wang, Y. Zhao, Z. Li, M. Zhang, K. Wang, S. Xue, J. Fang, Y. Ji, F. Pan and L. Yang, Bio-

inspired binder design for a robust conductive network in silicon-based anodes, *Small Methods*, 2022, **6**, 2101591.

197 M.-J. Guo, C.-C. Xiang, Y.-Y. Hu, L. Deng, S.-Y. Pan, C. Lv, S.-X. Chen, H.-T. Deng, C.-D. Sun, J.-T. Li, Y. Zhou and S.-G. Sun, A dual force cross-linked γ-PGA-PAA binder enhancing the cycle stability of silicon-based anodes for lithium-ion batteries, *Electrochim. Acta*, 2022, **425**, 140704.

198 S. Zhang, X. Xu, J. Tu, F. Chen, J. Xie, T. Zhu and X. Zhao, Cross-linked binder enables reversible volume changes of Si-based anodes from sustainable photovoltaic waste silicon, *Mater. Today Sustain.*, 2022, **19**, 100178.

199 T. Zheng, T. Zhang, M. S. de la Fuente and G. Liu, Aqueous emulsion of conductive polymer binders for Si anode materials in lithium ion batteries, *Eur. Polym. J.*, 2019, **114**, 265–270.

200 Z. Karkar, D. Guyomard, L. Roué and B. Lestriez, A comparative study of polyacrylic acid (PAA) and carboxymethyl cellulose (CMC) binders for Si-based electrodes, *Electrochim. Acta*, 2017, **258**, 453–466.

201 J. Feng, D. Wang, Q. Zhang, J. Liu, Y. Wu and L. Wang, Stabilizing a Si anode via an inorganic oligomer binder enabled by robust polar interfacial interactions, *ACS Appl. Mater. Interfaces*, 2021, **13**, 44312–44320.

202 H. Cho, K. Kim, C.-M. Park and G. Jeong, In situ fabrication of nanohybrid carbon/polyamide film providing robust binding and conductive network in silicon anode for lithium-ion battery, *J. Power Sources*, 2019, **410–411**, 25–30.

203 A. Miranda, X. Li, A. M. Haregewoin, K. Sarang, J. Lutkenhaus, R. Kostecki and R. Verduzco, A comprehensive study of hydrolyzed polyacrylamide as a binder for silicon anodes, *ACS Appl. Mater. Interfaces*, 2019, **11**, 44090–44100.

204 S. Hu, Z. Cai, T. Huang, H. Zhang and A. Yu, A modified natural polysaccharide as a high-performance binder for silicon anodes in lithium-ion batteries, *ACS Appl. Mater. Interfaces*, 2019, **11**, 4311–4317.

205 B. Hu, S. Jiang, I. A. Shkrob, J. Zhang, S. E. Trask, B. J. Polzin, A. Jansen, W. Chen, C. Liao, Z. Zhang and L. Zhang, Understanding of pre-lithiation of poly(acrylic acid) binder: Striking the balances between the cycling performance and slurry stability for silicon-graphite composite electrodes in Li-ion batteries, *J. Power Sources*, 2019, **416**, 125–131.

206 P.-F. Cao, M. Naguib, Z. Du, E. Stacy, B. Li, T. Hong, K. Xing, D. N. Voylov, J. Li, D. L. Wood, A. P. Sokolov, J. Nanda and T. Saito, Effect of Binder Architecture on the Performance of Silicon/Graphite Composite Anodes for Lithium Ion Batteries, *ACS Appl. Mater. Interfaces*, 2018, **10**, 3470–3478.

207 D. Yao, J. Feng, J. Wang, Y. Deng and C. Wang, Synthesis of silicon anode binders with ultra-high content of catechol groups and the effect of molecular weight on battery performance, *J. Power Sources*, 2020, **463**, 228188.

208 S. Jiang, B. Hu, Z. Shi, W. Chen, Z. Zhang and L. Zhang, Re-engineering poly(acrylic acid) binder toward optimized electrochemical performance for silicon lithium-ion batteries: branching architecture leads to balanced properties of polymeric binders, *Adv. Funct. Mater.*, 2020, **30**, 1908558.

209 Q. Zhang, C. Zhang, W. Luo, L. Cui, Y. Wang, T. Jian, X. Li, Q. Yan, H. Liu, C. Ouyang, Y. Chen, C. Chen and J. Zhang, Sequence-defined peptoids with -OH and -COOH groups as binders to reduce cracks of Si nanoparticles of lithium-ion batteries, *Adv. Sci.*, 2020, **7**, 2000749.

210 J. Song, Z. Feng, Y. Wang, X. Zhou, X. Zhang, K. Wang and J. Xie, Suppressed volume variation of optimized SiOx/C anodes with PAA-based binders for advanced lithium-ion pouch cells, *Solid State Ionics*, 2019, **343**, 115070.

211 Y. Zhang, X. Wang, L. Ma, R. Tang, X. Zheng, F. Zhao, G. Tang, Y. Wang, A. Pang, W. Li and L. Wei, Polydopamine blended with polyacrylic acid for silicon anode binder with high electrochemical performance, *Powder Technol.*, 2021, **388**, 393–400.

212 S. Kim, Y. K. Jeong, Y. Wang, H. Lee and J. W. Choi, A "Sticky" mucin-inspired DNA-polysaccharide binder for silicon and silicon-graphite blended anodes in lithium-ion batteries, *Adv. Mater.*, 2018, **30**, 1707594.

213 B. Hu, I. A. Shkrob, S. Zhang, L. Zhang, J. Zhang, Y. Li, C. Liao, Z. Zhang, W. Lu and L. Zhang, The existence of optimal molecular weight for poly(acrylic acid) binders in silicon/graphite composite anode for lithium-ion batteries, *J. Power Sources*, 2018, **378**, 671–676.

214 J. Li, G. Zhang, Y. Yang, D. Yao, Z. Lei, S. Li, Y. Deng and C. Wang, Glycinamide modified polyacrylic acid as high-performance binder for silicon anodes in lithium-ion batteries, *J. Power Sources*, 2018, **406**, 102–109.

215 S.-Y. Lee, Y. Choi, K.-S. Hong, J. K. Lee, J.-Y. Kim, J.-S. Bae and E. D. Jeong, Influence of EDTA in poly(acrylic acid) binder for enhancing electrochemical performance and thermal stability of silicon anode, *Appl. Surf. Sci.*, 2018, **447**, 442–451.

216 J. He and L. Zhang, Polyvinyl alcohol grafted poly (acrylic acid) as water-soluble binder with enhanced adhesion capability and electrochemical performances for Si anode, *J. Alloys Compd.*, 2018, **763**, 228–240.

217 Y. Gao, X. Qiu, X. Wang, A. Gu, L. Zhang, X. Chen, J. Li and Z. Yu, Chitosan-g-poly(acrylic acid) copolymer and its sodium salt as stabilized aqueous binders for silicon anodes in lithium-ion batteries, *ACS Sustainable Chem. Eng.*, 2019, **7**, 16274–16283.

218 D. Lee, H. Park, A. Goliaszewski, Y. Byeun, T. Song and U. Paik, In situ cross-linked carboxymethyl cellulose-polyethylene glycol binder for improving the long-term cycle life of silicon anodes in Li ion batteries, *Ind. Eng. Chem. Res.*, 2019, **58**, 8123–8130.

219 L. Zhang, Y. Ding and J. Song, Crosslinked carboxymethyl cellulose-sodium borate hybrid binder for advanced silicon anodes in lithium-ion batteries, *Chin. Chem. Lett.*, 2018, **29**, 1773–1776.

220 J. Ryu, S. Kim, J. Kim, S. Park, S. Lee, S. Yoo, J. Kim, N. Choi, J. Ryu and S. Park, Room-temperature crosslinkable natural polymer binder for high-rate and stable silicon anodes, *Adv. Funct. Mater.*, 2020, **30**, 1908433.

221 S. Lim, K. Lee, I. Shin, A. Tron, J. Mun, T. Yim and T.-H. Kim, Physically cross-linked polymer binder based on

poly(acrylic acid) and ion-conducting poly(ethylene glycol-co-benzimidazole) for silicon anodes, *J. Power Sources*, 2017, **360**, 585–592.

222 C. Chen, F. Chen, L. Liu, J. Zhao and F. Wang, Cross-linked hyperbranched polyethylenimine as an efficient multidimensional binder for silicon anodes in lithium-ion batteries, *Electrochim. Acta*, 2019, **326**, 134964.

223 L. Zhu, F. Du, Y. Zhuang, H. Dai, H. Cao, J. Adkins, Q. Zhou and J. Zheng, Effect of crosslinking binders on Li-storage behavior of silicon particles as anodes for lithium ion batteries, *J. Electroanal. Chem.*, 2019, **845**, 22–30.

224 S. Wang, Q. Duan, J. Lei and D. Y. W. Yu, Slime-inspired polyacrylic acid-borax crosslinked binder for high-capacity bulk silicon anodes in lithium-ion batteries, *J. Power Sources*, 2020, **468**, 228365.

225 Y.-P. Chuang, Y.-L. Lin, C.-C. Wang and J.-L. Hong, Dual cross-linked polymer networks derived from the hyperbranched poly(ethyleneimine) and poly(acrylic acid) as efficient binders for silicon anodes in lithium-ion batteries, *ACS Appl. Energy Mater.*, 2021, **4**, 1583–1592.

226 S. Chen, H. Y. Ling, H. Chen, S. Zhang, A. Du and C. Yan, Development of cross-linked dextrin as aqueous binders for silicon based anodes, *J. Power Sources*, 2020, **450**, 227671.

227 R. Rohan, T.-C. Kuo, C.-Y. Chiou, Y.-L. Chang, C.-C. Li and J.-T. Lee, Low-cost and sustainable corn starch as a high-performance aqueous binder in silicon anodes via in situ cross-linking, *J. Power Sources*, 2018, **396**, 459–466.

228 Z. Shi, Q. Liu, Z. Yang, L. A. Robertson, S. R. Bheemireddy, Y. Zhao, Z. Zhang and L. Zhang, A chemical switch enabled autonomous two-stage crosslinking polymeric binder for high performance silicon anodes, *J. Mater. Chem. A*, 2022, **10**, 1380–1389.

229 Z. Li, Z. Wan, X. Zeng, S. Zhang, L. Yan, J. Ji, H. Wang, Q. Ma, T. Liu, Z. Lin, M. Ling and C. Liang, A robust network binder via localized linking by small molecules for high-areal-capacity silicon anodes in lithium-ion batteries, *Nano Energy*, 2021, **79**, 105430.

230 X. Wang, S. Liu, Y. Zhang, H. Wang, A. A. Aboalhassan, G. Li, G. Xu, C. Xue, J. Yu, J. Yan and B. Ding, Highly elastic block copolymer binders for silicon anodes in lithium-ion batteries, *ACS Appl. Mater. Interfaces*, 2020, **12**, 38132–38139.

231 W. Wang, Y. Li, Y. Wang, W. Huang, L. Lv, G. Zhu, Q. Qu, Y. Liang, W. Zheng and H. Zheng, A novel covalently grafted binder through in-situ polymerization for high-performance Si-based lithium-ion batteries, *Electrochim. Acta*, 2021, **400**, 139442.

232 Z. Zheng, H. Gao, C. Ke, M. Li, Y. Cheng, D.-L. Peng, Q. Zhang and M.-S. Wang, Constructing robust cross-linked binder networks for silicon anodes with improved lithium storage performance, *ACS Appl. Mater. Interfaces*, 2021, **13**, 53818–53828.

233 D. Yao, Y. Yang, Y. Deng and C. Wang, Flexible polyimides through one-pot synthesis as water-soluble binders for silicon anodes in lithium ion batteries, *J. Power Sources*, 2018, **379**, 26–32.

234 H. Liao, W. He, N. Liu, D. Luo, H. Dou and X. Zhang, Facile in situ cross-linked robust three-dimensional binder for high-performance SiOx anodes in lithium-ion batteries, *ACS Appl. Mater. Interfaces*, 2021, **13**, 49313–49321.

235 Z. Cai, S. Hu, Y. Wei, T. Huang, A. Yu and H. Zhang, In situ room-temperature cross-linked highly branched biopolymeric binder based on the diels–alder reaction for high-performance silicon anodes in lithium-ion batteries, *ACS Appl. Mater. Interfaces*, 2021, **13**, 56095–56108.

236 Y. Gu, S. Yang, G. Zhu, Y. Yuan, Q. Qu, Y. Wang and H. Zheng, The effects of cross-linking cations on the electrochemical behavior of silicon anodes with alginate binder, *Electrochim. Acta*, 2018, **269**, 405–414.

237 F. De Giorgio, A. La Monaca, A. Dinter, M. Frankenberger, K.-H. Pettinger and C. Arbizzani, Water-processable $Li_4Ti_5O_{12}$ electrodes featuring eco-friendly sodium alginate binder, *Electrochim. Acta*, 2018, **289**, 112–119.

238 B. Gendensuren and E.-S. Oh, Dual-crosslinked network binder of alginate with polyacrylamide for silicon/graphite anodes of lithium ion battery, *J. Power Sources*, 2018, **384**, 379–386.

239 K. K. Rajeev, E. Kim, J. Nam, S. Lee, J. Mun and T.-H. Kim, Chitosan-grafted-polyaniline copolymer as an electrically conductive and mechanically stable binder for high-performance Si anodes in Li-ion batteries, *Electrochim. Acta*, 2020, **333**, 135532.

240 H. Chen, Z. Wu, Z. Su, S. Chen, C. Yan, M. Al-Mamun, Y. Tang and S. Zhang, A mechanically robust self-healing binder for silicon anode in lithium ion batteries, *Nano Energy*, 2021, **81**, 105654.

241 L. Deng, S.-S. Deng, S.-Y. Pan, Z.-Y. Wu, Y.-Y. Hu, K. Li, Y. Zhou, J.-T. Li, L. Huang and S.-G. Sun, Multivalent amide-hydrogen-bond supramolecular binder enhances the cyclic stability of silicon-based anodes for lithium-ion batteries, *ACS Appl. Mater. Interfaces*, 2021, **13**, 22567–22576.

242 D. Mazouzi, R. Grissa, M. Paris, Z. Karkar, L. Huet, D. Guyomard, L. Roué, T. Devic and B. Lestriez, CMC-citric acid Cu(II) cross-linked binder approach to improve the electrochemical performance of Si-based electrodes, *Electrochim. Acta*, 2019, **304**, 495–504.

243 Z. Xu, J. Yang, T. Zhang, Y. Nuli, J. Wang and S. Hirano, Silicon microparticle anodes with self-healing multiple network binder, *Joule*, 2018, **2**, 950–961.

244 H. Huang, R. Chen, S. Yang, W. Zhang, Y. Fang, L. Li, Y. Liu and J. Huang, High-performance Si flexible anode with rGO substrate and Ca^{2+} crosslinked sodium alginate binder for lithium ion battery, *Synth. Met.*, 2019, **247**, 212–218.

245 Z.-Y. Wu, L. Deng, J.-T. Li, Q.-S. Huang, Y.-Q. Lu, J. Liu, T. Zhang, L. Huang and S.-G. Sun, Multiple hydrogel alginate binders for Si anodes of lithium-ion battery, *Electrochim. Acta*, 2017, **245**, 371–378.

246 T. Zhu and G. Liu, Communication—functional conductive polymer binder for practical Si-based electrodes, *J. Electrochem. Soc.*, 2021, **168**, 050533.

247 M. Zheng, C. Wang, Y. Xu, K. Li and D. Liu, A water-soluble binary conductive binder for Si anode lithium ion battery, *Electrochim. Acta*, 2019, **305**, 555–562.

248 C. Zhang, Q. Chen, X. Ai, X. Li, Q. Xie, Y. Cheng, H. Kong, W. Xu, L. Wang, M.-S. Wang, H. Yang and D.-L. Peng, Conductive polyaniline doped with phytic acid as a binder and conductive additive for a commercial silicon anode with enhanced lithium storage properties, *J. Mater. Chem. A*, 2020, **8**, 16323–16331.

249 C.-Y. Tsai and Y.-L. Liu, 2,2-Dimethyl-1,3-dioxane-4,6-dione functionalized poly(ethylene oxide)-based polyurethanes as multi-functional binders for silicon anodes of lithium ion batteries, *Electrochim. Acta*, 2021, **379**, 138180.

250 F. Wang, X. Zhang, R. Hong, X. Lu, Y. Zhu and Y. Zheng, High-performance anode of lithium ion batteries with plasma-prepared silicon nanoparticles and a three-component binder, *Electrochim. Acta*, 2021, **390**, 138809.

251 K. Lee and T.-H. Kim, Poly(aniline-co-anthranilic acid) as an electrically conductive and mechanically stable binder for high-performance silicon anodes, *Electrochim. Acta*, 2018, **283**, 260–268.

252 A. Mery, P. Bernard, A. Valero, J. P. Alper, N. Herlin-Boime, C. Haon, F. Duclairoir and S. Sadki, A polyisoindigo derivative as novel n-type conductive binder inside Si@C nanoparticle electrodes for Li-ion battery applications, *J. Power Sources*, 2019, **420**, 9–14.

253 Y. Zhao, L. Yang, Y. Zuo, Z. Song, F. Liu, K. Li and F. Pan, Conductive binder for Si anode with boosted charge transfer capability via n-type doping, *ACS Appl. Mater. Interfaces*, 2018, **10**, 27795–27800.

254 Q. Ye, P. Zheng, X. Ao, D. Yao, Z. Lei, Y. Deng and C. Wang, Novel multi-block conductive binder with polybutadiene for Si anodes in lithium-ion batteries, *Electrochim. Acta*, 2019, **315**, 58–66.

255 L. Li, Z. Zuo, H. Shang, F. Wang and Y. Li, In-situ constructing 3D graphdiyne as all-carbon binder for high-performance silicon anode, *Nano Energy*, 2018, **53**, 135–143.

256 D. Liu, Y. Zhao, R. Tan, L.-L. Tian, Y. Liu, H. Chen and F. Pan, Novel conductive binder for high-performance silicon anodes in lithium ion batteries, *Nano Energy*, 2017, **36**, 206–212.

257 B. F. Song, A. Dhanabalan and S. L. Biswal, Evaluating the capacity ratio and prelithiation strategies for extending cyclability in porous silicon composite anodes and lithium iron phosphate cathodes for high capacity lithium-ion batteries, *J. Energy Storage*, 2020, **28**, 101268.

258 J. Ma, J. Sung, J. Hong, S. Chae, N. Kim, S.-H. Choi, G. Nam, Y. Son, S. Y. Kim, M. Ko and J. Cho, Towards maximized volumetric capacity via pore-coordinated design for large-volume-change lithium-ion battery anodes, *Nat. Commun.*, 2019, **10**, 475.

259 J. Xiao, J. Han, D. Kong, H. Shi, X. Du, Z. Zhao, F. Chen, P. Lan, S. Wu, Y. Zhang and Q.-H. Yang, "Nano-spring" confined in a shrinkable graphene cage towards self-adaptable high-capacity anodes, *Energy Storage Mater.*, 2022, **50**, 554–562.

260 X. Hui, R. Zhao, P. Zhang, C. Li, C. Wang and L. Yin, Low-temperature reduction strategy synthesized Si/Ti_3C_2 MXene composite anodes for high-performance Li-ion batteries, *Adv. Energy Mater.*, 2019, **9**, 1901065.

261 M. Jiang, M. Jiang, H. Gao, J. Chen, W. Liu, Y. Ma, W. Luo and J. Yang, Comparison of additives in anode: The Case of graphene, MXene, CNTs integration with silicon inside carbon nanofibers, *Acta Metall. Sin.*, 2021, **34**, 337–346.

262 M. Jiang, F. Zhang, G. Zhu, Y. Ma, W. Luo, T. Zhou and J. Yang, Interface-amorphized Ti_3C_2 @Si/SiOx @TiO_2 anodes with sandwiched structures and stable lithium storage, *ACS Appl. Mater. Interfaces*, 2020, **12**, 24796–24805.

263 G. Zhu, F. Zhang, X. Li, W. Luo, L. Li, H. Zhang, L. Wang, Y. Wang, W. Jiang, H. K. Liu, S. X. Dou and J. Yang, Engineering the distribution of carbon in silicon oxide nanospheres at the atomic level for highly stable anodes, *Angew. Chem., Int. Ed.*, 2019, **58**, 6669–6673.

264 F.-Z. Zhang, Y.-Y. Ma, M.-M. Jiang, W. Luo and J.-P. Yang, Boron heteroatom-doped silicon–carbon peanut-like composites enables long life lithium-ion batteries, *Rare Met.*, 2022, **41**, 1276–1283.

265 Y. Zheng, J. Ma, X. He, Y. Gan, J. Zhang, Y. Xia, W. Zhang and H. Huang, Fe_3O_4 contribution to core–shell structured Si@C nanospheres as high-performance anodes for lithium-ion batteries, *J. Electron. Mater.*, 2023, **52**, 1730–1739.

266 B.-H. Zhang, W.-X. Wen, H.-Y. Wang, Y.-L. Hou, J.-Z. Chen and D.-L. Zhao, Core-shell structured Si@Cu_3Si-Cu nanoparticles coated by N-doped carbon as an enhanced capacity and high-rate anode for lithium-ion batteries, *J. Electroanal. Chem.*, 2022, **927**, 116973.

267 H. Su, A. A. Barragan, L. Geng, D. Long, L. Ling, K. N. Bozhilov, L. Mangolini and J. Guo, Colloidal Synthesis of silicon–carbon composite material for lithium-ion batteries, *Angew. Chem.*, 2017, **129**, 10920–10925.

268 T. Yang, X. Tian, X. Li, Y. Song, Z. Liu and Q. Guo, Preparation of Si-based composite encapsulated by an incomplete multifunction-coating for lithium storage, *Electrochim. Acta*, 2019, **295**, 75–81.

269 G. Liang, X. Qin, J. Zou, L. Luo, Y. Wang, M. Wu, H. Zhu, G. Chen, F. Kang and B. Li, Electrosprayed silicon-embedded porous carbon microspheres as lithium-ion battery anodes with exceptional rate capacities, *Carbon*, 2018, **127**, 424–431.

270 H. Wang, S. Fan, Y. Cao, H. Yang, X. Ai and F. Zhong, Building a cycle-stable Fe–Si alloy/carbon nanocomposite anode for Li-ion batteries through a covalent-bonding method, *ACS Appl. Mater. Interfaces*, 2020, **12**, 30503–30509.

271 M. Chen, Q.-S. Jing, H.-B. Sun, J.-Q. Xu, Z.-Y. Yuan, J.-T. Ren, A.-X. Ding, Z.-Y. Huang and M.-Y. Dong, Engineering the core–shell-structured NCNTs-Ni_2Si@porous Si composite with robust Ni–Si interfacial bonding for high-performance Li-ion batteries, *Langmuir*, 2019, **35**, 6321–6332.

272 C. Yu, X. Chen, Z. Xiao, C. Lei, C. Zhang, X. Lin, B. Shen, R. Zhang and F. Wei, Silicon carbide as a protective layer to stabilize Si-based anodes by inhibiting chemical reactions, *Nano Lett.*, 2019, **19**, 5124–5132.

273 P. Li, J.-Y. Hwang and Y.-K. Sun, Nano/microstructured silicon–graphite composite anode for high-energy-density Li-ion battery, *ACS Nano*, 2019, **13**, 2624–2633.

274 J. Fu, H. Liu, L. Liao, P. Fan, Z. Wang, Y. Wu, Z. Zhang, Y. Hai, G. Lv, L. Mei, H. Hao, J. Xing and J. Dong, Ultrathin Si/CNTs paper-like composite for flexible Li-ion battery anode with high volumetric capacity, *Front. Chem.*, 2018, **6**, 624.

275 L. Deng, Z.-Y. Wu, Z.-W. Yin, Y.-Q. Lu, Z.-G. Huang, J.-H. You, J.-T. Li, L. Huang and S.-G. Sun, High-performance Si Mn/C composite anodes with integrating inactive Mn_4Si_7 alloy for lithium-ion batteries, *Electrochim. Acta*, 2018, **260**, 830–837.

276 H. J. Kwon, J.-Y. Hwang, H.-J. Shin, M.-G. Jeong, K. Y. Chung, Y.-K. Sun and H.-G. Jung, Nano/microstructured silicon–carbon hybrid composite particles fabricated with corn starch biowaste as anode materials for Li-ion batteries, *Nano Lett.*, 2020, **20**, 625–635.

277 X. Yi, W.-J. Yu, M. A. Tsiamtsouri, F. Zhang, W. He, Q. Dai, S. Hu, H. Tong, J. Zheng, B. Zhang and J. Liao, Highly conductive C-Si@G nanocomposite as a high-performance anode material for Li-ion batteries, *Electrochim. Acta*, 2019, **295**, 719–725.

278 X. Li, X. Tian, T. Yang, W. Wang, Y. Song, Q. Guo and Z. Liu, Silylated functionalized silicon-based composite as anode with excellent cyclic performance for lithium-ion battery, *J. Power Sources*, 2018, **385**, 84–90.

279 S. J. Yeom, C. Lee, S. Kang, T.-U. Wi, C. Lee, S. Chae, J. Cho, D. O. Shin, J. Ryu and H.-W. Lee, Native void space for maximum volumetric capacity in silicon-based anodes, *Nano Lett.*, 2019, **19**, 8793–8800.

280 S. Huang, L.-Z. Cheong, D. Wang and C. Shen, Nanostructured phosphorus doped silicon/graphite composite as anode for high-performance lithium-ion batteries, *ACS Appl. Mater. Interfaces*, 2017, **9**, 23672–23678.

281 M. Ashuri, Q. He, Y. Liu, S. Emani and L. L. Shaw, Synthesis and performance of nanostructured silicon/graphite composites with a thin carbon shell and engineered voids, *Electrochim. Acta*, 2017, **258**, 274–283.

282 K. C. Wasalathilake, S. N. S. Hapuarachchi, Y. Zhao, J. F. S. Fernando, H. Chen, J. Y. Nerkar, D. Golberg, S. Zhang and C. Yan, Unveiling the working mechanism of graphene bubble film/silicon composite anodes in Li-Ion batteries: From experiment to modeling, *ACS Appl. Energy Mater.*, 2020, **3**, 521–531.

283 N. Lin, T. Xu, T. Li, Y. Han and Y. Qian, Controllable self-assembly of micro-nanostructured Si-embedded graphite/graphene composite anode for high-performance Li-ion batteries, *ACS Appl. Mater. Interfaces*, 2017, **9**, 39318–39325.

284 Y. Huang, J. Peng, J. Luo, W. Li, Z. Wu, M. Shi, X. Li, N. Li, B. Chang and X. Wang, Spherical Gr/Si/GO/C composite as high-performance anode material for lithium-ion batteries, *Energy Fuels*, 2020, **34**, 7639–7647.

285 M. Su, H. Wan, Y. Liu, W. Xiao, A. Dou, Z. Wang and H. Guo, Multi-layered carbon coated Si-based composite as anode for lithium-ion batteries, *Powder Technol.*, 2018, **323**, 294–300.

286 M.-S. Wang, Z.-Q. Wang, R. Jia, Y. Yang, F.-Y. Zhu, Z.-L. Yang, Y. Huang, X. Li and W. Xu, Facile electrostatic self-assembly of silicon/reduced graphene oxide porous composite by silica assist as high performance anode for Li-ion battery, *Appl. Surf. Sci.*, 2018, **456**, 379–389.

287 Y. Liu, J. Huang, X. Zhang, J. Wu, A. Baker, H. Zhang, S. Chang and X. Zhang, A bm-SiO/Ni/rGO composite as an anode material for lithium-ion batteries, *J. Alloys Compd.*, 2018, **749**, 236–243.

288 A. Huang, X. Zhang, Q. Zhang, Y. Zhang, Z. Ma, H. Lin, X. Huang, K. Rui and J. Zhu, Stereoactive metallic vanadium oxide barriers to boost silicon-based lithium-ion storage, *Adv. Mater. Interfaces*, 2022, **9**, 2201246.

289 J. Zhang, J. Zhang, T. Bao, X. Xie and B. Xia, Electrochemical and stress characteristics of SiO/Cu/expanded graphite composite as anodes for lithium ion batteries, *J. Power Sources*, 2017, **348**, 16–20.

290 T. Xu, J. Zhang, C. Yang, H. Luo, B. Xia and X. Xie, Facile synthesis of carbon-coated SiO/Cu composite as superior anode for lithium-ion batteries, *J. Alloys Compd.*, 2018, **738**, 323–330.

291 M. J. Kwon, M. Maniyazagan, H. W. Yang, W. S. Kang and S. J. Kim, A facile synthesis of vanadium-doped SiOx composites for high-performance Li-ion battery anodes, *J. Alloys Compd.*, 2020, **842**, 155900.

292 R. Fu, Y. Wu, C. Fan, Z. Long, G. Shao and Z. Liu, Reactivating Li_2O with Nano-Sn to achieve ultrahigh initial coulombic efficiency SiO anodes for Li-Ion batteries, *ChemSusChem*, 2019, **12**, 3377–3382.

293 C. Liao and S. Wu, Pseudocapacitance behavior on Fe_3O_4-pillared SiOx microsphere wrapped by graphene as high performance anodes for lithium-ion batteries, *Chem. Eng. J.*, 2019, **355**, 805–814.

294 Y. Tian, Y. An and J. Feng, Flexible and freestanding silicon/MXene composite papers for high-performance lithium-ion batteries, *ACS Appl. Mater. Interfaces*, 2019, **11**, 10004–10011.

295 S. Liu, X. Zhang, P. Yan, R. Cheng, Y. Tang, M. Cui, B. Wang, L. Zhang, X. Wang, Y. Jiang, L. Wang and H. Yu, Dual bond enhanced multidimensional constructed composite silicon anode for high-performance lithium ion batteries, *ACS Nano*, 2019, **13**, 8854–8864.

296 F. Kong, X. He, Q. Liu, X. Qi, D. Sun, Y. Zheng, R. Wang and Y. Bai, Enhanced reversible Li-ion storage in $Si@Ti_3C_2$ MXene nanocomposite, *Electrochem. Commun.*, 2018, **97**, 16–21.

297 H. Wu, L. Zheng, J. Zhan, N. Du, W. Liu, J. Ma, L. Su and L. Wang, Recycling silicon-based industrial waste as sustainable sources of Si/SiO2 composites for high-performance Li-ion battery anodes, *J. Power Sources*, 2020, **449**, 227513.

298 S. J. Lee, H. J. Kim, T. H. Hwang, S. Choi, S. H. Park, E. Deniz, D. S. Jung and J. W. Choi, Delicate structural control of Si–SiO x –C composite via high-speed spray pyrolysis for Li-ion battery anodes, *Nano Lett.*, 2017, **17**, 1870–1876.

299 G. Zheng, Y. Xiang, L. Xu, H. Luo, B. Wang, Y. Liu, X. Han, W. Zhao, S. Chen, H. Chen, Q. Zhang, T. Zhu and Y. Yang, Controlling surface oxides in Si/C nanocomposite anodes

for high-performance Li-ion batteries, *Adv. Energy Mater.*, 2018, **8**, 1801718.

300 X. Gao, X. Sun, J. Liu, N. Gao and H. Li, A carbon-based anode combining with SiO and nanodiamond for high performance lithium ion battery, *J. Energy Storage*, 2019, **25**, 100901.

301 D. Shao, I. Smolianova, D. Tang and L. Zhang, Novel core–shell structured Si/S-doped-carbon composite with buffering voids as high performance anode for Li-ion batteries, *RSC Adv.*, 2017, **7**, 2407–2414.

302 X. Dong, X. Zheng, Y. Deng, L. Wang, H. Hong and Z. Ju, SiO_2/N-doped graphene aerogel composite anode for lithium-ion batteries, *J. Mater. Sci.*, 2020, **55**, 13023–13035.

303 M. Cui, L. Wang, X. Guo, E. Wang, Y. Yang, T. Wu, D. He, S. Liu and H. Yu, Designing of hierarchical mesoporous/macroporous silicon-based composite anode material for low-cost high-performance lithium-ion batteries, *J. Mater. Chem. A*, 2019, **7**, 3874–3881.

304 R. J.-C. Dubey, P. V. W. Sasikumar, F. Krumeich, G. Blugan, J. Kuebler, K. V. Kravchyk, T. Graule and M. V. Kovalenko, Silicon oxycarbide—Tin nanocomposite as a high-power-density anode for Li-ion batteries, *Adv. Sci.*, 2019, **6**, 1901220.

305 S. Zhao, C. Yao, L. Sun and X. Xian, Si/polyaniline-based porous carbon composites with an enhanced electrochemical performance as anode materials for Li-ion batteries, *Ionics*, 2018, **24**, 1039–1048.

306 J. Tang, A. D. Dysart, D. H. Kim, R. Saraswat, G. M. Shaver and V. G. Pol, Fabrication of carbon/silicon composite as lithium-ion anode with enhanced cycling stability, *Electrochim. Acta*, 2017, **247**, 626–633.

307 R. Na, Y. Liu, Z.-P. Wu, X. Cheng, Z. Shan, C.-J. Zhong and J. Tian, Nano-Silicon composite materials with N-doped graphene of controllable and optimal pyridinic-to-pyrrolic structural ratios for lithium ion battery, *Electrochim. Acta*, 2019, **321**, 134742.

308 J. Ye, Z. Chen, Q. Hao, C. Xu and J. Hou, One-step mild fabrication of porous core-shelled Si@TiO_2 nanocomposite as high performance anode for Li-ion batteries, *J. Colloid Interface Sci.*, 2019, **536**, 171–179.

309 X. Liang, J. Wang, S. Zhang, L. Wang, W. Wang, L. Li, H. Wang, D. Huang, W. Zhou and J. Guo, Fabrication of uniform Si-incorporated SnO_2 nanoparticles on graphene sheets as advanced anode for Li-ion batteries, *Appl. Surf. Sci.*, 2019, **476**, 28–35.

310 L. Liu, M. Li, L. Chu, B. Jiang and R. Lin, Facile fabrication of flexible Si-based nanocomposite films as high-rate anodes by layer-by-layer self-assembly, *Appl. Surf. Sci.*, 2019, **476**, 501–512.

311 T. Ma, X. Yu, X. Cheng, H. Li, W. Zhu and X. Qiu, Confined solid electrolyte interphase growth space with solid polymer electrolyte in hollow structured silicon anode for Li-ion batteries, *ACS Appl. Mater. Interfaces*, 2017, **9**, 13247–13254.

312 R. Nölle, A. J. Achazi, P. Kaghazchi, M. Winter and T. Placke, pentafluorophenyl isocyanate as an effective electrolyte additive for improved performance of silicon-based lithium-ion full cells, *ACS Appl. Mater. Interfaces*, 2018, **10**, 28187–28198.

313 I. Cekic-Laskovic, N. von Aspern, L. Imholt, S. Kaymaksiz, K. Oldiges, B. R. Rad and M. Winter, Synergistic Effect of Blended Components in Nonaqueous Electrolytes for Lithium Ion Batteries, *Top. Curr. Chem.*, 2017, **375**, 37.

314 E. Peled and S. Menkin, Review—SEI: Past, present and future, *J. Electrochem. Soc.*, 2017, **164**, A1703–A1719.

315 Y. Jin, N.-J. H. Kneusels, L. E. Marbella, E. Castillo-Martínez, P. C. M. M. Magusin, R. S. Weatherup, E. Jónsson, T. Liu, S. Paul and C. P. Grey, Understanding fluoroethylene carbonate and vinylene carbonate based electrolytes for Si anodes in lithium ion batteries with NMR spectroscopy, *J. Am. Chem. Soc.*, 2018, **140**, 9854–9867.

316 E. Zhao, Y. Gu, S. Fang, L. Yang and S. Hirano, Systematic investigation of electrochemical performances for lithium-ion batteries with Si/graphite anodes: Effect of electrolytes based on fluoroethylene carbonate and linear carbonates, *ACS Appl. Energy Mater.*, 2021, **4**, 2419–2429.

317 F. Kong and B. Xin, Three-dimensional and flexible carbon nanofiber mat by one-step electrospinning for efficient oil/water separation, *Colloids Surf., A*, 2022, **652**, 129824.

318 K. Yao, J. P. Zheng and R. Liang, Ethylene carbonate-free fluoroethylene carbonate-based electrolyte works better for freestanding Si-based composite paper anodes for Li-ion batteries, *J. Power Sources*, 2018, **381**, 164–170.

319 H. Jia, L. Zou, P. Gao, X. Cao, W. Zhao, Y. He, M. H. Engelhard, S. D. Burton, H. Wang, X. Ren, Q. Li, R. Yi, X. Zhang, C. Wang, Z. Xu, X. Li, J. Zhang and W. Xu, High-performance silicon anodes enabled by nonflammable localized high-concentration electrolytes, *Adv. Energy Mater.*, 2019, **9**, 1900784.

320 H. Jia, P. Gao, L. Zou, K. S. Han, M. H. Engelhard, Y. He, X. Zhang, W. Zhao, R. Yi, H. Wang, C. Wang, X. Li and J.-G. Zhang, Controlling ion coordination structure and diffusion kinetics for optimized electrode-electrolyte interphases and high-performance Si anodes, *Chem. Mater.*, 2020, **32**, 8956–8964.

321 J. Chen, X. Fan, Q. Li, H. Yang, M. R. Khoshi, Y. Xu, S. Hwang, L. Chen, X. Ji, C. Yang, H. He, C. Wang, E. Garfunkel, D. Su, O. Borodin and C. Wang, Electrolyte design for LiF-rich solid–electrolyte interfaces to enable high-performance microsized alloy anodes for batteries, *Nat. Energy*, 2020, **5**, 386–397.

322 X. Liu, X. Sun, X. Shi, D. Song, H. Zhang, C. Li, K.-Y. Wang, C. Xiao, X. Liu and L. Zhang, Low-temperature and high-performance Si/graphite composite anodes enabled by sulfite additive, *Chem. Eng. J.*, 2021, **421**, 127782.

323 M. Haruta, Y. Kijima, R. Hioki, T. Doi and M. Inaba, Artificial lithium fluoride surface coating on silicon negative electrodes for the inhibition of electrolyte decomposition in lithium-ion batteries: Visualization of a solid electrolyte interphase using in situ AFM, *Nanoscale*, 2018, **10**, 17257–17264.

324 G. Hernández, A. J. Naylor, Y.-C. Chien, D. Brandell, J. Mindemark and K. Edström, Elimination of fluorination: The

influence of fluorine-free electrolytes on the performance of $LiNi_{1/3}Mn_{1/3}Co_{1/3}$ O_2/silicon–graphite Li-ion battery cells, *ACS Sustainable Chem. Eng.*, 2020, **8**, 10041–10052.

325 L. Niedzicki, P. Oledzki, P. Wieczorek, M. Marcinek and W. Wieczorek, LiTDI based lithium-ion cells electrolyte compositions, *Synth. Met.*, 2017, **223**, 73–79.

326 Y. Jin, N.-J. H. Kneusels, P. C. M. M. Magusin, G. Kim, E. Castillo-Martínez, L. E. Marbella, R. N. Kerber, D. J. Howe, S. Paul, T. Liu and C. P. Grey, Identifying the structural basis for the increased stability of the solid electrolyte interphase formed on silicon with the additive fluoroethylene carbonate, *J. Am. Chem. Soc.*, 2017, **139**, 14992–15004.

327 C. C. Nguyen and B. L. Lucht, Development of electrolytes for Si-graphite composite electrodes, *J. Electrochem. Soc.*, 2018, **165**, A2154–A2161.

328 S. Park, S. Y. Jeong, T. K. Lee, M. W. Park, H. Y. Lim, J. Sung, J. Cho, S. K. Kwak, S. Y. Hong and N.-S. Choi, Replacing conventional battery electrolyte additives with dioxolone derivatives for high-energy-density lithium-ion batteries, *Nat. Commun.*, 2021, **12**, 838.

329 Z. Hu, L. Zhao, T. Jiang, J. Liu, A. Rashid, P. Sun, G. Wang, C. Yan and L. Zhang, Trifluoropropylene carbonate-driven interface regulation enabling greatly enhanced lithium storage durability of silicon-based anodes, *Adv. Funct. Mater.*, 2019, **29**, 1906548.

330 J. Shen, H. Chen, L. Yu, D. Huang and Z. Luo, 4, 5-difluoro-1, 3-dioxolan-2-one as an film forming additive on $LiNi_{0.8}Co_{0.15}Al_{0.05}O_2$/SiO@C full cells, *J. Electroanal. Chem.*, 2019, **834**, 1–7.

331 E. J. Hopkins, S. Frisco, R. T. Pekarek, C. Stetson, Z. Huey, S. Harvey, X. Li, B. Key, C. Fang, G. Liu, G. Yang, G. Teeter, N. R. Neale and G. M. Veith, Examining CO_2 as an additive for solid electrolyte interphase formation on silicon anodes, *J. Electrochem. Soc.*, 2021, **168**, 030534.

332 T. Kennedy, M. Brandon, F. Laffir and K. M. Ryan, Understanding the influence of electrolyte additives on the electrochemical performance and morphology evolution of silicon nanowire based lithium-ion battery anodes, *J. Power Sources*, 2017, **359**, 601–610.

333 H. Liu, A. J. Naylor, A. S. Menon, W. R. Brant, K. Edström and R. Younesi, Understanding the roles of tris(trimethylsilyl) phosphite (TMSPi) in $LiNi_{0.8}Mn_{0.1}Co_{0.1}O_2$ (NMC811)/silicon–graphite (Si–Gr) Lithium-ion batteries, *Adv. Mater. Interfaces*, 2020, **7**, 2000277.

334 G. Yang, S. Frisco, R. Tao, N. Philip, T. H. Bennett, C. Stetson, J.-G. Zhang, S.-D. Han, G. Teeter, S. P. Harvey, Y. Zhang, G. M. Veith and J. Nanda, Robust solid/electrolyte interphase (SEI) formation on Si anodes using glyme-based electrolytes, *ACS Energy Lett.*, 2021, **6**, 1684–1693.

335 S. Yang, Y. Zhang, Z. Li, N. Takenaka, Y. Liu, H. Zou, W. Chen, M. Du, X.-J. Hong, R. Shang, E. Nakamura, Y.-P. Cai, Y.-Q. Lan, Q. Zheng, Y. Yamada and A. Yamada, Rational electrolyte design to form inorganic–polymeric interphase on silicon-based anodes, *ACS Energy Lett.*, 2021, **6**, 1811–1820.

336 X. Kong, J. Liu, Y. Zhang, J. Zeng and J. Zhao, An effective electrolyte design to improve the high-voltage performance of high-capacity NCM811/SiOx-Gr batteries, *Electrochim. Acta*, 2020, **349**, 136356.

337 P. Meister, X. Qi, R. Kloepsch, E. Krämer, B. Streipert, M. Winter and T. Placke, Anodic behavior of the aluminum current collector in imide-based electrolytes: Influence of solvent, operating temperature, and native oxide-layer thickness, *ChemSusChem*, 2017, **10**, 804–814.

338 H. Zhao, X. Yu, J. Li, B. Li, H. Shao, L. Li and Y. Deng, Film-forming electrolyte additives for rechargeable lithium-ion batteries: progress and outlook, *J. Mater. Chem. A*, 2019, **7**, 8700–8722.

339 Y. Zhang, N. Du and D. Yang, Designing superior solid electrolyte interfaces on silicon anodes for high-performance lithium-ion batteries, *Nanoscale*, 2019, **11**, 19086–19104.

340 R. Nölle, J.-P. Schmiegel, M. Winter and T. Placke, Tailoring electrolyte additives with synergistic functional moieties for silicon negative electrode-based lithium ion batteries: A case study on lactic acid O -carboxyanhydride, *Chem. Mater.*, 2020, **32**, 173–185.

341 A. Rezqita, M. Sauer, A. Foelske, H. Kronberger and A. Trifonova, The effect of electrolyte additives on electrochemical performance of silicon/mesoporous carbon (Si/MC) for anode materials for lithium-ion batteries, *Electrochim. Acta*, 2017, **247**, 600–609.

342 F. An, H. Zhao, W. Zhou, Y. Ma and P. Li, S-containing and Si-containing compounds as highly effective electrolyte additives for SiOx -based anodes/NCM 811 cathodes in lithium ion cells, *Sci. Rep.*, 2019, **9**, 14108.

343 W. Li, Q. Ma, X. Liu, A. Chen, J.-H. Wang, D. H. Min, P. Xiong, M. Liu and H. S. Park, Enhanced reaction kinetics enabled by a bi-element co-doping strategy for high-performance ternary Si-based anodes of Li-ion batteries, *Chem. Eng. J.*, 2023, **453**, 139567.

344 Y. Zhao, X. Liu, H. Zhang, M. Liu and W. Li, BiSbSi: A new ternary layered Si-based anode for Li-ion batteries with high performance, *Electrochem. Commun.*, 2022, **141**, 107343.

345 P. Guan, W. Zhang, C. Li, N. Han, X. Wang, Q. Li, G. Song, Z. Peng, J. Li, L. Zhang and X. Zhu, Low-cost urchin-like silicon-based anode with superior conductivity for lithium storage applications, *J. Colloid Interface Sci.*, 2020, **575**, 150–157.